Goran Lovrić, BSc

Numerical Investigation of Strongly Correlated Electron and Electron-Phonon Systems

MASTER THESIS

For obtaining the academic degree
Diplom-Ingenieur

Master Programme of
Technical Physics

Graz University of Technology

Supervisor:

Univ.-Prof. Dr.rer.nat. Enrico Arrigoni

Institute of Theoretical and Computational Physics

in cooperation with:

Faculty of Physics and Electronic Technology - Hubei University

Graz, November 2010

Cover design: TU Graz
Typesetting and layout with LaTeX by Goran Lovrić

Abstract

Two relevant models of strongly correlated systems are studied with many-body schemes, in particular the Lanczos diagonalization method. The first one concerns individual carbon clusters and is motivated by recent reports stating that some of these clusters may show ferromagnetic characteristics. To study the magnetic properties of ten-atom clusters we apply an extended Hubbard model approach, which we think is more realistic. We show that the nearest neighbor interaction V "destroys" the ferromagnetic solutions in most cases. However for the so-called "iso-g," "iso-h" and "iso-i" isomers it has no negative effect, or even shows an enhancement of the ferromagnetic state. In the second part of this thesis we study the electron-phonon interaction in a one-dimensional chain of copper and oxygen atoms by modelling it with a three-band model with phonons Hilbert space truncation. This is motivated by recent studies showing a strong interplay between electron-phonon interaction and strong electronic correlations in high-T_c cuprates. We show that buckling phonons lead to a charge transfer from oxygen to copper sites inducing an enhancement of antiferromagnetic spin correlations, whereas for breathing phonons we mostly obtain opposite effects. In conclusion the (pair) binding energies of the two phonon modes are compared. The comparison suggests that buckling phonons might prevent pair binding while breathing phonons induce an enhancement.

Zusammenfassung

Zwei aktuelle Modelle stark korrelierter Systeme werden mit Hilfe der Viel-Teilchen-Theorie untersucht, insbesondere der Lanczos-Diagonalisierungsmethode. Das Erstere betrifft einzelne Kohlenstoffcluster und ist veranlasst durch jüngste Forschungsergebnisse, welche darauf schließen lassen, dass einige dieser Cluster ferromagnetische Eigenschaften aufweisen. Um die magnetischen Eigenschaften von zehnatomigen Clustern zu untersuchen, wenden wir das erweiterte Hubbard-Modell an, was nach unseren Überlegungen realistischer erscheint. Wir belegen, dass die zwischen benachbarten Atomen vermittelte Wechselwirkung V in den meisten Fällen die ferromagnetischen Lösungen "zerstört." Allerdings verursacht sie bei den so genannten "iso-g," "iso-h" und "iso-i" Isomeren keine negativen Effekte, bzw. führt sogar zu einer Verstärkung des ferromagnetischen Zustands. Im zweiten Teil dieser Arbeit untersuchen wir die Elektron-Phonon-Wechselwirkung in einer eindimensionalen Kette bestehend aus Kupfer- und Sauerstoffatomen indem wir das System mit einem Drei-Bänder-Modell mit phononischer Hilbertraumlimitierung modellieren. Dies ist motiviert durch jüngste Forschungsergebnisse, welche ein starkes Zusammenspiel von Elektron-Phonon-Wechselwirkungen mit starken Elektronenkorrelationen in Kuprat-Hochtemperatursupraleitern belegen. Wir zeigen, dass longitudinale ("buckling") Phononen zu einem Ladungstransfer von Sauerstoff- zu Kupferatomen hin führen und gleichzeitig eine Verstärkung der antiferromagnetischen Spinkorrelationen induzieren, wohingegen axiale ("breathing") Phononen im Grunde gegensätzliche Effekte bewirken. Abschließend werden die (Paar-)Bindungsenergien beider Phononenmoden miteinander verglichen. Der Vergleich suggeriert, dass longitudinale ("buckling") Phononen Paarbildung verhindern während axiale ("breathing") Phononen diese begünstigen.

Acknowledgments

First of all I would like to express my deepest thanks to Prof. Zhong-Bing Huang for his excellent supervision and support during my half-year stay at Hubei University in Wuhan (P.R. China). I owe my deepest gratitude to him for not only managing all "organizational affairs" like providing me with all necessary documents (for visa, scholarship, etc.), picking me up from the airport upon arrival, arranging a high-class accommodation for me and many (many) other things, but also for his great educational efforts and the vast amount of time he spent with me discussing all the stuff related to my Master thesis. It is also an honor for me that I had the opportunity to learn from his outstanding scientific knowledge.

The underlying thesis would not have ever been possible without my supervisor Prof. Enrico Arrigoni who made the first contact and recommended me to Prof. Huang. I would like to deeply thank him for accepting me as one of his students and giving me the opportunity and encouragement to go abroad. Especially all the support I experienced from Prof. Arrigoni before and after my educational journey to China was outstanding and made it possible for me to finish the project in the given time period. I am also grateful that I had the opportunity to learn from his excellent analytical knowledge when conducting final discussions about the correction of my thesis.

I am also indebted to my friends Guangkun Liu and Xiaojun Zheng for their inexhaustible everyday support at the office and for all the fertile discussions that helped me to understand physics as well as Chinese culture during my time in Wuhan. I would also like to thank Prof. Gao, Prof. Xia and Ms Deng for supporting me numerous times during my stay at Hubei University as well as to thank Prof. Gao's students Haowen Liu, Yang Lin and Guowen Jiang. It is due to all these people as well as to my other friends Yi Li and Yichao Tan that I will always keep positive memories about my half-year stay in Wuhan.

I am also thankful to my parents who encouraged me during all my working steps and supported me as much as possible.

Finally it is a pleasure to thank Dr. Renate Belaj for proofreading the underlying thesis and providing her great help at short notice.

The project was financed by the "foreign scholarship" of Austrian's Federal Ministry of Science and Research ("Auslandsstipendium der Studienbeihilfenbehörde") as well as the "Top-up scholarship for short time academic research and expert courses abroad" ("KUWI Stipendium") of TU Graz. Some additional paying was made possible by Prof. Huang from one of his national Chinese grants.

Contents

List of Figures

List of Tables

Chapter 1

Introduction

The theoretical description of many-body systems is still one of the most unexplored and in many spheres controversial fields of physics. Since the development of powerful computers and especially in the last decades this field has gained enormous interest, which is documented by a huge number of scientific publications. Computer science, on the other hand, has evolved into a "third way" of making science being a reasonable alternative to "bare" theory and experimental physics. After the discovery of "new" condensed matter properties such as heavy fermions and high-temperature superconductors, strongly-correlated systems have also gained much interest leading to a drastic development of new numerical methods and theoretical explanatory attempts.

In the present work we study two relevant examples of strongly correlated systems. In the first part we investigate magnetic properties of individual carbon clusters with ten atoms. This is motivated by recent reports stating that these materials may exhibit magnetic properties. In the second part we study the electron-phonon interaction in a one-dimensional chain of copper and oxygen atoms by means of novel approaches to correlated systems. The latter case is motivated by recent theory work on high-T_c superconductivity for studying distinctive properties of such materials. [1–5]

The thesis is organized as follows: First (Chapters 2 and 3), we introduce the main physical background as well as numerical methods, in the first place the Lanczos diagonalization method, by which we treat our problems of interest. We begin our calculations by studying a simplified 1D problem (Chapter 4) which we can compare with known results. In the following, the magnetic properties of individual carbon clusters (Chapter 5) and the electron-phonon interaction in a 1D Cu-O-chain (Chapter 6) are studied. The results are discussed at the end of each chapter as well as in the summary (Chapter 7). Finally, in the appendix, we present some additional material which we considered important. All used references are listed at the end of the thesis.

Chapter 2

Physical Background

2.1 Introduction to Many-Body Physics

The underlying chapter mainly follows the approaches to many-body physics given in [6–8], whereas detailed source references are given at the respective positions.

The interest in many-body systems and their evaluation mainly emerges because of two simple reasons. On the one hand, in real life we mostly deal with matter of macroscopic dimensions, and on the other hand correlation effects within a many-body system lead to completely new physical properties that we want to examine. Since many-body systems are composed of single quantum-mechanical particles, it is obvious to choose a quantum-mechanical approach when evaluating these systems. In the following we deal with solids which represent good examples for many-body systems. On contrary to free particles a solid can be seen as a system consisting of an interacting electron gas moving in a (approximately static) charge compensating background. For crystalline solids we can assume that this background has a perfectly periodic arrangement which is crucial for a theoretical (and computational) evaluation.

In a more detailed consideration we can describe each atom out of a solid consisting of three parts: the *nucleus*, the *core electrons* and the *valence electrons*. Further we refer to the nucleus with its tightly bound core electrons as *ion*. Thus a solid can be seen as *an interacting system of particles consisting of lattice ions and valence electrons* [see 6, p. 37]. In our discussion so far this classification is the first approximation we make because the distinction between core and valence electrons is not always unique. In particular it also depends on the chemical bond and element.

With this approximation and our preceding discussion we are finally able to formulate the

ab initio Hamiltonian for a solid consisting of five terms which are described subsequently:

$$\hat{H} = \underbrace{\sum_{i=1}^{N_{\text{el}}} \frac{\hat{\mathbf{p}}_i^2}{2m}}_{\text{(i)}} + \underbrace{\sum_{k=1}^{N_{\text{ion}}} \frac{\hat{\mathbf{P}}_k^2}{2M_k}}_{\text{(ii)}} + \underbrace{\sum_{i<j} V_{\text{el-el}}(\hat{\mathbf{r}}_j - \hat{\mathbf{r}}_i)}_{\text{(iii)}} + \underbrace{\sum_{k<l} V_{\text{ion-ion}}(\hat{\mathbf{R}}_l - \hat{\mathbf{R}}_k)}_{\text{(iv)}} + \underbrace{\sum_{i,k} V_{\text{el-ion}}(\hat{\mathbf{r}}_i - \hat{\mathbf{R}}_k)}_{\text{(v)}}. \quad (2.1)$$

Term (i): **kinetic energy of the electrons**

N_{el} ..... number of valence electrons
$\hat{\mathbf{p}}_i$ ..... momentum operator for electrons
m ..... electron mass

Term (ii): **kinetic energy of the ions**

N_{ion} ..... number of ions
$\hat{\mathbf{P}}_k$ ..... momentum operator for ions
M_k ..... ion masses

Term (iii): **interaction term for electrons among each other**

$V_{\text{el-el}}$ ..... interaction energy between two electrons
$\hat{\mathbf{r}}_i, \hat{\mathbf{r}}_j$ ..... position vectors (operators) of electrons

Term (iv): **interaction term for ions among each other**

$V_{\text{ion-ion}}$ ..... interaction energy between two ions
$\hat{\mathbf{R}}_k, \hat{\mathbf{R}}_l$ ..... position vectors (operators) of ions

Term (v): **interaction term for ions and valence electrons**

$V_{e,K}$ ..... interaction energy between nuclei and electrons

The main aim of many-body quantum mechanics is to evaluate the Schrödinger equation corresponding to the Hamiltonian written above. However, for the most part we are interested in the solution of the static Schrödinger equation, i. e. the quantum-mechanical eigenvalue problem

$$\hat{H}|x_i\rangle = \varepsilon_i|x_i\rangle, \quad (2.2)$$

where $|x_i\rangle$ denote the eigenstates (eigenvectors) with the eigenvalues (energies) ε_i.

The most obvious approach in this matter is to make several simplifications (starting with the Born-Oppenheimer approximation) of the Hamiltonian in Eq. (2.1) and adapt them to the mathematical problem of interest. Such considerations lead us e. g. to the *Jellium model* and are very useful for band structure calculations and the so-called mean-field theories (like the *Local density approximation*). Generally speaking, we can conclude that for *weakly correlated systems* this is a very good way to gain reasonable results.

However, in *strongly correlated systems* the interaction between electrons plays the most essential role and is responsible for a variety of physical effects. It is therefore obvious to resort to somewhat different models and approaches that take the electron-electron interaction explicitly into account. In the following we will first introduce the *second quantization* which is a very useful formalism for describing many-body systems and Hamiltonians. After that we will have a more closer look at the individual terms from Eq. (2.1) where we can apply the formalism of second quantization. In relation to these we will formulate (common) *model Hamiltonians*, used in the latter numerical treatment, as well as physical quantities being the main scope of all calculations.

2.2 Mathematical Apparatus

So far we have only introduced the *ab initio* Hamiltonian for solids together with the initial eigenvalue problem where the latter marks the beginning point for our further calculations. In the following we will describe the basic techniques of these calculations together with special aspects of quantum theory which have to be considered when treating many-body systems.

For (single-particle) quantum theory [see 9, p. 89-126] we already know that any state of a physical system is defined by a state vector $|\psi\rangle$ (ket) in the Hilbert space. All measurable physical quantities are described by Hermitian operators, called *observables*[1] that act on the same space. As parallel state vectors describe the same state, we mainly deal with normalized state vectors. All Hermitian operators have a defined number of eigenstates which are invariant by the action of the operator (except a scalar factor, the eigenvalue). Furthermore the set of all eigenvectors forms a complete basis of the Hilbert space and we can expand any state (vector) as a linear combination of these basis states by

$$|\psi\rangle = \sum_i c_i |x_i\rangle,$$

where $|x_i\rangle$ are the eigenvectors with expansion coefficients c_i.

The eigenvalue ε_i, corresponding to an arbitrary observable (e. g. $\hat{H}$) and one of its eigenstates $|x_i\rangle$, is the only possible result we can get when measuring a physical quantity. The probability $P(\varepsilon_i)$ of obtaining the (*non-degenerate*) eigenvalue ε_i when measuring the

[1] In the present work all observables are marked with a hat accent " ˆ " to distinguish them from other variables.

physical quantity $\hat{H}$ of a system described by the *normalized* state $|\psi\rangle$ is:

$$P(\varepsilon_i) = |\langle x_i|\psi\rangle|^2 = |c_i|^2. \tag{2.3}$$

The expansion to *degenerated* and *continuous* eigenvalues can be done in an analogue way. For further reading we refer to [9, p. 191–195].

The notation we used above is the so called *Dirac notation* for the *first quantization* and is a very useful formalism for the whole (single-particle) quantum theory. One of its main advantages is the fact that any state vector $|\psi\rangle$ can be described in an arbitrary chosen basis. Often we consider the so called *position basis*, representing a state (e. g. describing one particle without spin) in the three-dimensional real space:

$$\psi(\mathbf{r}) := \langle \mathbf{r}|\psi\rangle. \tag{2.4}$$

In such a case $\psi(\mathbf{r})$ from Eq. (2.4) is called *wave function* (corresponding to the state $|\psi\rangle$), which represents a complex-valued function in $\mathbb{C}^3$. Without going into further details we can state that the wave function marks the basic concept of quantum theory, as it contains all the information possible to obtain from a quantum-mechanical particle like an electron. It can also be interpreted as a *probability amplitude of the particle's presence* [see 9, p. 11] which makes it the most important quantity for the characterization of a quantum-mechanical state.

For our further discussion it is therefore important to derive a useful formalism for describing a many-body system by considering all principles written above. The most obvious approach in this matter is the expansion of the one-particle wave function to a N-particle wave function by

$$\psi(\mathbf{r}) \quad \longrightarrow \quad \psi(\mathbf{r}_1, \mathbf{r}_2, \ldots, \mathbf{r}_N), \tag{2.5}$$

which is now a complex-valued function in $\mathbb{C}^{3N}$. The above form suggests that one can construct the many-body wave function from individual single-particle wave functions which we will not treat in particular. At this point we want to note that most physical textbooks dealing with many-body theory widely treat this ansatz in their introducing chapters [see, e. g. 6, 7, 10]. Although this is not crucial for numerical calculations it represents a good didactic way for demonstrating the analogy between the one-particle and the many-particle quantum mechanics. Therefore we will skip explicit derivations based on Eq. (2.5), but describe the main ideas like the *indistinguishability* of quantum-mechanical particles which lead us directly to the *second quantization* formalism.

2.2.1 Identical Particles

In the transition from classical mechanics to quantum mechanics one of the most fundamental principles denotes that identical particles are *indistinguishable*. In classical mechanics each particle can be described by its mass and trajectory in the six-dimensional phase

space (i. e. by its position and impulse). Thus *classical* identical particles (e. g. same mass, charge, etc.) are always distinguishable at least by their phase space trajectory. However, we have learned from before that in quantum mechanics particles are described by their corresponding wave functions. Once brought together, their individual wave functions overlap, and subsequently we lose all information belonging to a certain particle. So to speak, we cannot *distinguish* the individual particles any more.

The most important consequence of this fact is that all measurable quantities within a many-body system are invariant under an exchange of particles.[2] Mathematically this implies that the expectation values of observables and thereby the scalar products of states remain the same if the particles quantum numbers are exchanged. However, the principle of indistinguishability by itself does not give an *a priori* mathematical description for the explicit states and operators. In order to derive the main mathematical properties following from the above statements, it is useful to introduce the so-called *Transposition operator* $\hat{P}_{ij}$ by

Definition 2.1 *The* Transposition operator $\hat{P}_{ij}$ *is defined by acting on a particular state* $|\psi\rangle$ *and exchanging the quantum numbers* $\mathbf{r}_i$ *and* $\mathbf{r}_j$ *corresponding to the particles* i *and* j*:*

$$\hat{P}_{ij}\psi(\mathbf{r}_1,\ldots,\mathbf{r}_i,\ldots,\mathbf{r}_j,\ldots,\mathbf{r}_N) = \psi(\mathbf{r}_1,\ldots,\mathbf{r}_j,\ldots,\mathbf{r}_i,\ldots,\mathbf{r}_N). \tag{2.6}$$

Without loss of generality the state $|\psi\rangle$ *in Eq. (2.6) is chosen to be represented in the* position space. *However the same operation can be described in any other state representation.*

It is now clear that we return to the same result when applying the Transposition operator twice:

$$\hat{P}_{ij}^2\psi(\mathbf{r}_1,\ldots,\mathbf{r}_i,\ldots,\mathbf{r}_j,\ldots,\mathbf{r}_N) = \psi(\mathbf{r}_1,\ldots,\mathbf{r}_i,\ldots,\mathbf{r}_j,\ldots,\mathbf{r}_N). \tag{2.7}$$

It follows that

$$\hat{P}_{ij}^2 = \mathbb{1} \quad \Longrightarrow \quad \hat{P}_{ij} = \hat{P}_{ij}^{-1},$$

and a trivial further derivation can show that $\hat{P}_{ij}$ is an *unitary* and *Hermitian* operator. On the other hand, Eq. (2.7) can also be interpreted as the eigenvalue equation for $\hat{P}_{ij}^2$ with its eigenvalue $\lambda = 1$. Thus we can state that $\hat{P}_{ij}$ has two possible eigenvalues (± 1) which do not depend on the particular state $|\psi\rangle$ and particle pair (i, j). Although we still have not introduced an explicit way for representing basis states of a many-body system (see next section), we are already able to summarize the most important mathematical properties.

In a system consisting of identical particles the exchange of two particles is not detectable in any way. The quantum-mechanical state (function) after an exchange is either

[2] More precisely: under an exchange of the particles quantum numbers.

symmetric or *antisymmetric*, and we can define two kinds of quantum-mechanical particles by the following:

$$\hat{P}_{ij}\psi(\mathbf{r}_1,\ldots,\mathbf{r}_i,\ldots,\mathbf{r}_j,\ldots,\mathbf{r}_N) = \begin{cases} +\psi(\mathbf{r}_1,\ldots,\mathbf{r}_i,\ldots,\mathbf{r}_j,\ldots,\mathbf{r}_N) & \textbf{bosons} \\ -\psi(\mathbf{r}_1,\ldots,\mathbf{r}_i,\ldots,\mathbf{r}_j,\ldots,\mathbf{r}_N) & \textbf{fermions}. \end{cases} \tag{2.8}$$

The antisymmetry of fermionic wave functions is equivalent to "Pauli's exclusion principle" which states that two identical fermions cannot occupy the same quantum-mechanical state simultaneously. It is worth mentioning that this principle is responsible for the characteristic composition of the periodic table of the chemical elements. Further properties, however, are treated in relativistic *quantum field theory* (QFT), which is beyond the scope of this work.

2.2.2 Second Quantization

We are now able to introduce a very useful mathematical formalism for many-body systems, often referred to as *second quantization* or *occupation number representation*. It represents a very convenient way for describing basis states and observables, especially in the later numerical treatment. However, it only describes a mathematical reformulation of the initial eigenvalue problem [introduced in Eq. (2.2)] and gives no indication for a solving approach.

The basic idea behind the second quantization is a basis transformation to a special Hilbert space, called *Fock space*. Although not shown in detail, we have already stated that it is possible to construct an arbitrary many-body basis out of one-particle basis states. On the other hand we can skip this part and immediately conclude that any arbitrary system of *identical particles* has a particular (or even infinite) number of orbitals. So we can construct a many-body basis in the way that we *arrange* all orbitals in a particular order and *assign a number* to each of them. Thus we only have to specify how many particles occupy a certain orbital and we can express an arbitrary basis state vector (ket) by

$$|k\rangle = |n_1, n_2, n_3, \ldots\rangle \qquad \text{with} \qquad \sum_i n_i = N, \tag{2.9}$$

where each n_i describes the number of particles occupying orbital i with N being the overall number of particles in the system. Thus the state $|k\rangle$ stands only for one particular combination of occupation numbers n_i.

Originally introduced by Vladimir Aleksandrovich Fock [see 11], the Fock space in the above context is spanned by all possible combinations of n_i with a finite number of particles up to N. In his work, Fock not only made clear the connection between single-particle Hilbert spaces and the many-body configuration space, but he also showed that the representation in Eq. (2.9) is unique if we specify the *particle statistics* we refer to (i. e. *bosonic* or *fermionic* statistics).

Following above way of basis representation we are already able to stress some basic principles. As we know from before, a quantum-mechanical state gets changed by the action

of an operator, e. g. the Hamiltonian. Hence it is clear that in terms of second quantization this means nothing more than a change of the occupation number's configuration. For the first step it is therefore obvious to introduce some kind of *fundamental operators* for changing (i. e. *increasing* or *decreasing*) the occupation number of a certain orbital. Thus it is possible to show that any general operator can be expressed by a sum of products of these fundamental operators.

In the following we will introduce these kinds of operators, called *creation* and *annihilation* operators, whereas right from the start we will treat the case for bosons and fermions separately.

Bosons

According to the *spin-statistics theorem* which depicts the difference between bosons and fermions and its theoretical explanation bosons are quantum-mechanical particles (either *elementary* or *composite*) with integer spin described by symmetric wave functions. Further, bosons are able to occupy arbitrary quantum-mechanical states in an arbitrary amount. We define bosonic creation and annihilation operators by their action on a state

$$\hat{b}_i^\dagger \,|\ldots, n_i, \ldots\rangle = B_+(n_i)\,|\ldots, n_i+1, \ldots\rangle$$
$$\hat{b}_i \,|\ldots, n_i, \ldots\rangle = B_-(n_i)\,|\ldots, n_i-1, \ldots\rangle$$

where the $\hat{b}_i^\dagger$, $\hat{b}_i$ are called *creation* and *annihilation operators* respectively, while $B_\pm$ represents a normalization constant. For the occupation numbers n_i, any non-negative integer is possible:

$$n_i = 0, 1, 2, \ldots, \infty.$$

A trivial derivation shows that $\hat{b}_i^\dagger$ and $\hat{b}_i$ behave like adjoint operators and we define that

$$\hat{b}_i \,|\ldots, n_i = 0, \ldots\rangle := 0$$

since the occupation number of an "empty" orbital cannot be lowered further. From this definition it follows that $\hat{b}_i^\dagger$ and $\hat{b}_i$ don't commute. By this fact and by taking the symmetry of bosonic wave functions into account we can define the fundamental commutation relations for bosonic operators:

$$\left[\hat{b}_i^\dagger, \hat{b}_j^\dagger\right] = 0 \qquad \left[\hat{b}_i, \hat{b}_j\right] = 0 \qquad \left[\hat{b}_i, \hat{b}_j^\dagger\right] = \delta_{i,j} \tag{2.10}$$

After having defined these relations we are able to determine the normalization constant $B_\pm$ as well as all other relations that are important for our further calculations. We will omit any explicit derivations but summarize the most important results in the following. A very good overview with all calculation steps can be found in [7, p. 10].

We define a new operator, called *occupation number operator*, by

$$\hat{n}_i := \hat{b}_i^\dagger \hat{b}_i$$

and it can be shown that the action of this operator yields the occupation number n_i for orbital i:

$$\hat{n}_i \,|\ldots, n_i, \ldots\rangle = n_i \,|\ldots, n_i, \ldots\rangle$$

Concerning the creation and annihilation operators from before we get

$$\hat{b}_i^\dagger |\ldots, n_i, \ldots\rangle = \sqrt{n_i + 1}\,|\ldots, n_i + 1, \ldots\rangle$$
$$\hat{b}_i \,|\ldots, n_i, \ldots\rangle = \quad \sqrt{n_i} \;|\ldots, n_i - 1, \ldots\rangle$$

and we are finally able to write down the expression for a general bosonic basis state with N being the total number of available orbitals:

$$|k\rangle = |n_1, \ldots, n_i, \ldots, n_N\rangle = \prod_{i=1}^{N} \frac{\left(\hat{b}_i^\dagger\right)^{n_i}}{\sqrt{n_i!}} |0\rangle \tag{2.11}$$

Fermions

Basically for fermions we can proceed in an analogue way by defining fundamental operators. However, we must somehow include the asymmetry for fermionic wave functions as well as Pauli's exclusion principle, stating that two identical fermions cannot occupy the same orbital. The latter one effects the possible values for the occupation numbers n_i, so we can write that

$$n_i = 0, 1. \tag{2.12}$$

Further on we define fermionic creation and annihilation operators naming them $\hat{c}_i^\dagger$ and $\hat{c}_i$ which is very common in popular textbooks:

$$\hat{c}_i^\dagger |\ldots, n_i, \ldots\rangle = C_+(n_i)\,|\ldots, n_i + 1, \ldots\rangle$$
$$\hat{c}_i \,|\ldots, n_i, \ldots\rangle = C_-(n_i)\,|\ldots, n_i - 1, \ldots\rangle.$$

Following all statements outlined above, we have to introduce two more definitions:

$$\hat{c}_i^\dagger |\ldots, n_i = 1, \ldots\rangle := 0 \qquad\qquad \hat{c}_i \,|\ldots, n_i = 0, \ldots\rangle := 0.$$

Finally we can take into account the antisymmetry for fermionic wave functions by considering a strict order of orbitals. We already know from Eq. (2.8) that

$$|\ldots, n_i = 1, \ldots, n_j = 1, \ldots\rangle = -|\ldots, n_j = 1, \ldots, n_i = 1, \ldots\rangle,$$

which makes it clear that the wave function's sign changes if we exchange two particles, i. e. if we change their order. However, from a mathematical point of view the ordering of orbitals is equivalent to the ordering of particles. This, on the other hand, can be expressed by choosing appropriate commutation relations for the fermionic fundamental operators. We define these relations like before whereas the only difference to bosonic operators is the sign change. Therefore we now use *anticommutators* (denoted by curly brackets)

$$\left\{\hat{c}_i^\dagger, \hat{c}_j^\dagger\right\} = 0 \qquad \left\{\hat{c}_i, \hat{c}_j\right\} = 0 \qquad \left\{\hat{c}_i, \hat{c}_j^\dagger\right\} = \delta_{i,j} \tag{2.13}$$

and also define a fermionic *occupation number operator* that is identical to the bosonic one

$$\hat{n}_i \left| \ldots, n_i, \ldots \right\rangle := \hat{c}_i^\dagger \hat{c}_i \left| \ldots, n_i, \ldots \right\rangle = n_i \left| \ldots, n_i, \ldots \right\rangle.$$

Before writing down the expression for a general fermionic basis state we have to discuss one more aspect of the *spin-statistics theorem*. We have already mentioned that fermions obey Pauli's exclusion principle and thus they are particles with half-integer spin. However, two fermions can occupy the same quantum-mechanical "energy level," but in such a case they have different spin eigenvalues σ (with $\sigma = \pm 1$). For this reason it is convenient to define the orbitals i related just to the quantum-mechanical energy level (which mathematically corresponds to the *spatial wave function*) and distinguish two kinds of particles occupying the same orbital, namely with *spin up* ($\sigma = +1$) and *spin down* ($\sigma = -1$).[3] This procedure represents only a formal change and is used within the whole single-particle quantum mechanics by splitting particles wave functions into *spatial* and *spin* parts. Finally we can write a general fermion basis state by:

$$|k\rangle_\sigma = |n_{1\sigma}, \ldots, n_{i\sigma}, \ldots, n_{N\sigma}\rangle = \prod_{i=1}^{N} \prod_{\sigma=-1}^{1} \left(\hat{c}_{i,\sigma}^\dagger\right)^{n_{i,\sigma}} |0\rangle \tag{2.14}$$

where all other variables have the same meaning like in the bosonic case.

2.2.3 Operators in Second Quantization

In the following we want to discuss how to express observables in terms of second quantization. For doing this in a common way it is important to take a precise look on the mathematical connection between first and second quantization. However, so far we have introduced the second quantization just by applying basic thinking and omitting explicit mathematical derivations. We will now proceed in the same way by outlining the rough calculation scheme and summarizing the most important results. It is the aim of this section to provide a general understanding for observables in terms of second quantization so that we can resort to this knowledge in the subsequent chapters.

[3] Later on we will also use "↑" for marking *spin up* and "↓" for marking *spin down* particles.

We now follow the approach in [10, p. 14–20] by first considering *single-particle* operators for many-body systems. The name is somehow confusing since we mean operators which act on a N-particle state, but can be written as a sum of operators, each acting on a single-particle state. We can expand such an operator by

$$\hat{T} = \hat{T}_1 + \hat{T}_2 + \ldots + \hat{T}_N \equiv \sum_{\alpha=1}^{N} \hat{T}_\alpha. \tag{2.15}$$

Subsequently we take a particular $\hat{T}_\alpha$ and express its matrix elements in a single-particle basis [see also 9, p. 108–111] by

$$T_{ij} = \langle i|\hat{T}|j\rangle,$$

where the $|i\rangle$ and $|j\rangle$ are the single-particle basis kets. Thus we are able to rewrite this particular one-particle operator to

$$\hat{T}_\alpha = \sum_{i,j} T_{ij}\, |i\rangle_{(\alpha)}\,{}_{(\alpha)}\langle j|$$

which can finally be used to obtain the expression for the N-particle operator in Eq. (2.15):

$$\hat{T} = \sum_{i,j} T_{ij} \sum_{\alpha=1}^{N} |i\rangle_{(\alpha)}\,{}_{(\alpha)}\langle j|.$$

In the next step one has to apply this operator on a many-body state whereas the case for bosons and fermions again must be treated separately. However, for both particle types the results are the same, and after a few calculation steps it follows that

$$\sum_{\alpha=1}^{N} |i\rangle_{(\alpha)}\,{}_{(\alpha)}\langle j| = \hat{a}_i^\dagger \hat{a}_j$$

where $\hat{a}_i^\dagger$, $\hat{a}_j$ either represent bosonic or fermionic creation and annihilation operators. With this relation we finally obtain the expression for a *single-particle operator* in terms of second quantization by

$$\hat{T} = \sum_{i,j} T_{ij}\, \hat{a}_i^\dagger \hat{a}_j. \tag{2.16}$$

The result above means that we can express any *single-particle operator* by fundamental creation and annihilation operators as well as a constant factor, namely the matrix element from the single-particle basis.

The expression for a *two-particle operator* is derived in the same way. Analogue to Eq. (2.15) such an operator expands to

$$\hat{F} = \frac{1}{2} \sum_{\alpha \neq \beta} F^{(2)}(\hat{\mathbf{r}}_\alpha, \hat{\mathbf{r}}_\beta),$$

where $\hat{\mathbf{r}}_\alpha$ and $\hat{\mathbf{r}}_\beta$ represent the position vectors (operators) for particles α and β respectively. The function $F^{(2)}(\hat{\mathbf{r}}_\alpha, \hat{\mathbf{r}}_\beta)$ mediates the interaction between the particles α and β. Factor $\frac{1}{2}$ is needed for the simple reason that an interaction can only occur once and that the particles are *identical* as discussed before. Therefore $F^{(2)}(\hat{\mathbf{r}}_\alpha, \hat{\mathbf{r}}_\beta)$ is equal to $F^{(2)}(\hat{\mathbf{r}}_\beta, \hat{\mathbf{r}}_\alpha)$, and one can show that $\hat{F}$ can finally be expressed by

$$\hat{F} = \sum_{i,j,k,l} F_{i,j,k,l}\, \hat{a}_i^\dagger \hat{a}_j^\dagger \hat{a}_k \hat{a}_l \tag{2.17}$$

where $F_{i,j,k,l}$ describes a scalar factor. The derivation of this factor would require a more thorough treatment of the whole problem as described very detailed in [6, p. 9–28] and [12, p. 21–27]. For our purposes, however, it is enough to adapt the expression without explicit proof and therefore write

$$F_{i,j,k,l} = \int \mathrm{d}\mathbf{r}_\alpha \int d\mathbf{r}_\beta\, \psi_i^*(\mathbf{r}_\alpha)\psi_j^*(\mathbf{r}_\beta)\, F^{(2)}\,(\mathbf{r}_\alpha, \mathbf{r}_\beta)\psi_k(\mathbf{r}_\alpha)\psi_l(\mathbf{r}_\beta) \tag{2.18}$$

where the $\psi(\mathbf{r}_\alpha)$ and $\psi(\mathbf{r}_\beta)$ (with indices i, j, k, l) represent single-particle basis state functions belonging to particle α and β, respectively.

In this section we have treated *one-* and *two-particle* operators in a very general way, and we showed (without proof) that both kinds in terms of second quantization may be expressed as sums of products of creation and annihilation operators (for the bosonic as well as for the fermionic case). It shall also be mentioned that same formalism can be expanded on operators that act on groups of more than two particles. These, however, are hardly of practical relevance, and as a general rule all observables consist of *one-* and/or *two-particle* terms.

2.3 Lattice Electrons

With the knowledge we have acquired so far we are able to stick to a more detailed treatment of Eq. (2.1). We commence by considering only *electronic terms* and focus on the properties of periodic crystal structures and their consequences for lattice electrons. Subsequently we introduce following simplifications:

(1) We neglect the ions kinetic terms [Term (ii) in Eq. (2.1)] and assign them to rigid lattice positions.

(2) The ions interaction [Term (iv)] as well as their interaction with electrons [Term (v)] are time-independent and form a strictly periodic *lattice potential* $\hat{V}(\hat{\mathbf{r}}_i)$.

(3) We neglect the electrons interactions described by Term (iii).

Simplification (1) reflects the Born-Oppenheimer approximation and follows from the fact that the mass difference of electrons and nuclei is very large (around the factor 2000).

Assuming this we instantly get simplification (2) by which the whole problem reduces to an "electron sea" interacting with a periodic lattice potential, i. e. the electrical potential that keeps the ions on equilibrium distances from each other. On the other hand, both principles apply very closely on systems at low temperatures around 0 K, namely the ground state and first excited states.

However, the approximation of a *non-interacting electron gas* in (3) is not obvious any more and neither justified by experimental knowledge nor any gedanken experiments. It just describes the most simple way for treating a many-body system and actually serves as a counterargument indicating that more complex mathematical considerations of electron-electron interactions are necessary. Since different methods for treating these interactions exist [e. g. Hartree-Fock or DFT (density functional theory)] we will skip all of these *ab initio* techniques and explain this interaction term in detail later on when introducing Hamiltonians used in our latter calculations (see Sec. 2.6).

By taking account of simplifications (1)-(3), the Hamiltonian from Eq. (2.1) transforms to

$$\hat{H} = \hat{H}_{\text{el,kin}} + \hat{H}_{\text{el-ion}} = \sum_{i=1}^{N_{\text{el}}} \left[\frac{\hat{\mathbf{p}}_i^2}{2m} + \hat{V}(\hat{\mathbf{r}}_i) \right] \tag{2.19}$$

while the previously mentioned lattice potential reads as

$$\hat{V}(\hat{\mathbf{r}}_i) = \sum_{k=1}^{N_{\text{ion}}} V_{\text{el-ion}}(\hat{\mathbf{r}}_i - \hat{\mathbf{R}}_k).$$

Since the above Hamiltonian is formed by the sum of one-particle operators, we can treat each particle separately. At the same time the periodicity of the lattice potential (in the real space) can be expressed by

$$V(\mathbf{r}_i) = V(\mathbf{r}_i + \mathbf{R}^{\mathbf{n}}) \qquad \text{with} \qquad \mathbf{R}^{\mathbf{n}} = \sum_{\alpha=1}^{3} n_\alpha \mathbf{a}_\alpha,$$

where the $\mathbf{R}^{\mathbf{n}}$ represent arbitrary ions positions of a *Bravais lattice* with lattice vectors $\mathbf{a}_i$ and integer numbers n_i. With this relation and the Hamiltonian from Eq. (2.19) the static Schrödinger equation is obtained by making use of

Theorem 2.1 (Bloch's theorem) *Let $V(\mathbf{r})$ be a periodic potential with periodicity $\mathbf{R}^{\mathbf{n}}$. Then the solution of the static Schrödinger equation is given by*

$$\psi_{\mathbf{k}}(\mathbf{r}) = \mathrm{e}^{\mathrm{i}\mathbf{k}\mathbf{r}} \cdot u_{\mathbf{k}}(\mathbf{r}),$$

where $u_{\mathbf{k}}(\mathbf{r})$ is a periodic function with periodicity $\mathbf{R}^{\mathbf{n}}$ and $\mathbf{k}$ being a wave vector of the first Brillouin zone (FBZ). *The function $\psi_{\mathbf{k}}(\mathbf{r})$ is called* Bloch function.

Accordingly, *Bloch's theorem* states that the periodicity of the lattice potential carries over to the periodicity of the function $u_{\mathbf{k}}(\mathbf{r})$ and thus implies the periodicity of the electron's wave function $\psi_{\mathbf{k}}(\mathbf{r})$. The number of all Bloch functions within the first Brillouin zone (corresponding to different $\mathbf{k}$) together with its eigenvalues $\epsilon(\mathbf{k})$ (called *Bloch energies*) forms a complete basis set in the *reciprocal lattice*. It is therefore convenient to turn to a "new" basis state representation in the reciprocal lattice by introducing so-called *Bloch states* and numbering all $\mathbf{k}$-vectors in FBZ by introducing index i. We do this by following the formalism of second quantization and adopting previously introduced distinction in spin $\uparrow$ and $\downarrow$ electrons. Starting from the one-particle basis representation, a *Bloch state* $|i\rangle_\sigma$ is defined by

$$|i\rangle_\sigma := |\mathbf{k}_i\sigma\rangle,$$

while σ again denotes the spin eigenvalues (± 1). With use of Eq. (2.16) from Sec. 2.2.3 we are able to express the Hamiltonian in second quantization form:

$$\hat{H} = \sum_{i,j,\sigma} \langle \mathbf{k}_i\sigma|\hat{H}|\mathbf{k}_j\sigma\rangle \; \hat{c}^\dagger_{\mathbf{k}_i,\sigma}\hat{c}_{\mathbf{k}_j,\sigma}, \tag{2.20}$$

while the sums are performed over all $\mathbf{k}_i$-vectors from FBZ. In this notation the fundamental operators from above *create* and *annihilate* so-called *Bloch electrons* with particular spin σ and wave vector $\mathbf{k}_i$. Since Bloch states by definition are eigenstates of above Hamiltonian we finally obtain:

$$\hat{H} = \sum_{i,\sigma} \epsilon(\mathbf{k}_i)\, \hat{c}^\dagger_{\mathbf{k}_i,\sigma}\hat{c}_{\mathbf{k}_i,\sigma} = \sum_{i,\sigma} \epsilon(\mathbf{k}_i)\, \hat{n}_{\mathbf{k}_i,\sigma}. \tag{2.21}$$

This result emphasizes the importance of the reciprocal lattice, since the wave vector $\mathbf{k}_i$ (corresponding to a particular Bloch electron) is a conserved quantity and periodic due to the translation by any reciprocal lattice vector. Often, however, we are more interested in building a basis representation in the *real lattice*. This is achieved by introducing so-called *Wannier functions* $\omega_\sigma(\mathbf{r} - \mathbf{R}_j)$, defined as Fourier transforms of Bloch functions:

$$\omega_\sigma(\mathbf{r} - \mathbf{R}_j) := \frac{1}{\sqrt{N_{\text{el}}}} \sum_i \mathrm{e}^{-\mathrm{i}\mathbf{k}_i\mathbf{R}_j} \cdot \psi_{\mathbf{k}_i,\sigma}(\mathbf{r}), \tag{2.22}$$

with real lattice positions $\mathbf{R}_j$, N_{el} being the total number of electrons and i counting all $\mathbf{k}_i$-vectors from FBZ. Thus, in analogy to a Bloch state, we also define a so-called *Wannier state* by

$$|j\rangle_\sigma = |\mathbf{R}_j\sigma\rangle,$$

where $|j\rangle_\sigma$ represents a spin-σ electron with (real lattice) position vector $\mathbf{X}_j$. In analogy to Eq. (2.20) we can express the same Hamiltonian in the Wannier basis by

$$\hat{H} = \sum_{i,j,\sigma} \langle i\sigma|\hat{H}|j\sigma\rangle \; \hat{c}^\dagger_{i,\sigma}\hat{c}_{j,\sigma} = \sum_{i,j,\sigma} T_{ij}\; \hat{c}^\dagger_{i,\sigma}\hat{c}_{j,\sigma} \tag{2.23}$$

and identify T_{ij} as the so-called "hopping energy" (or "hopping integral"), since the above Hamiltonian describes the creation of an electron with spin σ at lattice site $\mathbf{R}_i$ and at the same time an annihilation at $\mathbf{R}_j$. This, on the other hand, can be interpreted as an "electron hopping from site j to site i." As common in contemporary literature, here we already substituted $\mathbf{R}_i$ by i and $\mathbf{R}_j$ by j, respectively.

Finally, the whole formalism is applied to the basis state representation according to second quantization formalism, which in the present work will be maintained from now on. This means that we identify previously introduced *orbitals* with real lattice positions (called "cluster sites") for spin $\uparrow$ and $\downarrow$ electrons and count the number of electrons occupying a certain cluster site (i. e. Wannier state). As shown, the periodic lattice potential only affects the kinetic term which transformed into a "hopping" (term) from one cluster site to another. In retrospect, therefore it seems reasonable to assume a *non-interacting electron gas* first, since this will lead to a drastic simplification of the whole problem and will help characterizing the kinetic term better.

2.4 Lattice Vibrations

In a more accurate description of solids the ions kinetic term [namely Term (ii) from Eq. (2.1)] must also be taken into account which affects the ions interaction among each other [i. e. Term (iv) gets a time-dependent component]. The "picture" of motionless ions may be useful for some simple models (for instance solids at very low temperatures). However, in real solids lattice vibrations are responsible for a number of different effects. In the following we want to discuss basic methods for treating lattice vibrations and introduce main conclusions arising from these. Thereby we mainly follow the descriptions from [6, p. 65–75] and [13, p. 269–290].

We have already stated that for computational reasons we consider a strict periodic arrangement of lattice ions. In such a structure each ion can perform oscillations, whereas the restoring forces for these vibrations are the *binding forces*. Although binding forces have different physical origins which depend on the particular chemical bond, we conduct a uniform approach and make use of the so-called *harmonic approximation*. This means that solids can be described as systems of N coupled *quantum-mechanical harmonic oscillators* which is crucial for a further mathematical treatment.[4] Therefore we consider only linear terms of the binding forces which is justified by the fact that ions displacements only amount about 5% of their distance to each other. On the other hand, as a consequence, we assume that ions are coupled only to their nearest neighbors. In a more descriptive way, which is popular in solid state theory, one can depict such a model by particles (ions) that are connected by springs with each other.

Mathematically, the treatment of a quantum-mechanical oscillator as well as a system of N coupled quantum-mechanical oscillators yields quantized eigenvalues (energies) and

[4] Besides we assume that ions move as a whole and do not get deformed. This assumption, however, represents another simplification of the realistic case.

due to its analogy to a photon we can define a new quasiparticle by

Definition 2.2 (Phonon) *A* phonon *is defined as an energy quantum $\hbar\omega_i$ of a lattice vibration or lattice wave with the angular frequency ω_i.*

Thus each *phonon* can be assigned to a momentum $\hbar\mathbf{q}_i$ where $\mathbf{q}_i$ represents the wave vector of a lattice vibration. Besides, the angular frequency can be written as a function of $\mathbf{q}_i$ and because of a strict periodic lattice the phonon energies obey

$$\omega(\mathbf{q}_i) = \omega(\mathbf{q}_i + \mathbf{k}), \tag{2.24}$$

where $\mathbf{k}$ represents an arbitrary vector of the reciprocal lattice. Therefore we can restrict the wave vectors $\mathbf{q}_i$ only to FBZ.

Above definition as well as regarding the fact that each phonon has a momentum leads to the conclusion that phonons can be seen as quantum-mechanical particles. Thus they obey the law of conversation of energy and momentum which is important for interactions with other quantum-mechanical particles (see next section). Further mathematical treatment, namely the evaluation of the ionic Hamiltonian for the whole lattice, shows that phonons obey Bose-Einstein statistics, i. e. they are bosons. In terms of second quantization the ionic Hamiltonian transforms to a sum of products of bosonic fundamental operators and one can write the (popular) Hamiltonian for a set of phonons (in Bloch state representation) by

$$\hat{H} = \sum_{\mathbf{q}_i, l} \hbar\omega_l(\mathbf{q}_i) \left(\hat{b}^\dagger_{\mathbf{q}_i, l} \hat{b}_{\mathbf{q}_i, l} + \frac{1}{2} \right), \tag{2.25}$$

where $\hat{b}^\dagger_{\mathbf{q}_i}$ and $\hat{b}_{\mathbf{q}_i}$ represent bosonic creation and annihilation operators for phonons corresponding to lattice sites l with wave vectors $\mathbf{q}_i$. It is also evident that the whole problem transformed to a system of N *uncoupled* harmonic oscillators. Only the allowance of *higher* (*anharmonic*) terms in the binding forces can be interpreted as a coupling amongst phonons which again emphasizes the fact that the result in Eq. (2.25) emerges from a simplified model. More usually anharmonicity (of lattice vibrations) plays a big role and is also responsible for a lot of condensed matter properties.

Finally it shall also be mentioned that phonons have a broad energy range, and for lattices with different atoms (different masses or binding forces) two types of phonons exist, namely *acoustic* and optical *phonons*, which we will not treat in particular. For practical purposes phonons are important to explain typical properties of solids such as specific heat, elasticity, electrical resistivity and so on. More thorough treatment of phonons, such as effects that appear in "real" lattices (with lattice disorders and so on), can be found in solid state literature and we refer e. g. to [13] for further reading.

2.5 Electron-Phonon Interaction

For now we have treated electronic and ionic parts from the *ab intio* Hamiltionian in Eq. (2.1) completely separately, only the influence of a rigid lattice potential was discussed in Sec. 2.3 which lead to the definition of Bloch and Wannier states. In the previous section it was shown that ions generally perform vibrations, so it is obvious that the lattice potential has to be extended by a dynamic term. In other words, electrons and phonons are coupled with each other, which must be considered in a mathematical treatment, and finally leads to new physical properties of solids. In the following a summary of the mathematical derivation is given by making use of the results gathered so far, whereby explicit treatment can be found in [6–8].

At first we include phonons in the ions and electrons interaction term [Term (v) in Eq. (2.1)] at which the interaction potential $V_{\text{el-ion}}$ transform like

$$V_{\text{el-ion}}(\hat{\mathbf{r}}_i - \hat{\mathbf{R}}_k) \quad \longrightarrow \quad V_{\text{el-ion}}(\hat{\mathbf{r}}_i - \hat{\mathbf{R}}_k - \hat{\mathbf{u}}_k),$$

where $\hat{\mathbf{r}}_i$ are the electrons position vectors, $\hat{\mathbf{R}}_k$ the (rigid) ions position vectors and $\hat{\mathbf{u}}_k$ the ions displacements. Further mathematical derivation is conducted similar to Sec. 2.3 and the obtained result in Eq. (2.21) expands to

$$\hat{H} = \sum_{i,\sigma} \epsilon(\mathbf{k}_i)\, \hat{c}^{\dagger}_{\mathbf{k}_i,\sigma} \hat{c}_{\mathbf{k}_i,\sigma} - \sum_{i,j,\sigma} \langle \mathbf{k}_i\sigma | V_{\text{el-ion}}(\hat{\mathbf{r}}_i) | \mathbf{k}_j\sigma \rangle\, \hat{c}^{\dagger}_{\mathbf{k}_j,\sigma} \hat{c}_{\mathbf{k}_i,\sigma}. \tag{2.26}$$

The matrix element $\langle \mathbf{k}_i\sigma | V_{\text{el-ion}}(\hat{\mathbf{r}}_i) | \mathbf{k}_j\sigma \rangle$ can be evaluated by following the discussion from Sec. 2.2.3, and we finally obtain the (most general) Hamiltonian for the electron-phonon interaction (in Bloch state representation):

$$\hat{H} = \sum_{i,\sigma} \epsilon(\mathbf{k}_i)\, \hat{c}^{\dagger}_{\mathbf{k}_i,\sigma} \hat{c}_{\mathbf{k}_i,\sigma} + \sum_{i,j,k,l,\sigma} M_{\mathbf{k}_i,\mathbf{q}_j+\mathbf{K}_k}\, (\hat{b}_{\mathbf{q}_j,l} + \hat{b}^{\dagger}_{-\mathbf{q}_j,l})\, \hat{c}^{\dagger}_{\mathbf{k}_i+\mathbf{q}_j+\mathbf{K}_k,\sigma} \hat{c}_{\mathbf{k}_i,\sigma}, \tag{2.27}$$

where $M_{\mathbf{k}_i,\mathbf{q}_j+\mathbf{K}_k}$ is the matrix element of the electron-phonon interaction, $\mathbf{q}_j$ are the phonons wave vectors (of FBZ), $\mathbf{K}_k$ the reciprocal lattice vectors of FBZ, and all other letters have the same meaning as before. This Hamiltonian, often referred to as *Fröhlich model*, can be further simplified, e. g. by considering uniquely longitudinal or transversal polarized phonons. We can skip this part and proceed by noting the main consequences arising from this result.

The electrons wave vectors $\mathbf{k}_i$ are no conserved quantities any more. The interaction with phonons generally leads to a transformation

$$\mathbf{k}_i \quad \longrightarrow \quad \mathbf{k}_i + \mathbf{q}_j + \mathbf{K}_k,$$

and thus the changes of electrons momentums obey strict selection rules which is due to the fact that phonons wave vectors (and momentums) are quantized. The laws of momentum

and energy conservation are mantained during all these processes, as well. All possible electron-phonon interactions are either elementary or can be composed out of four elementary processes.

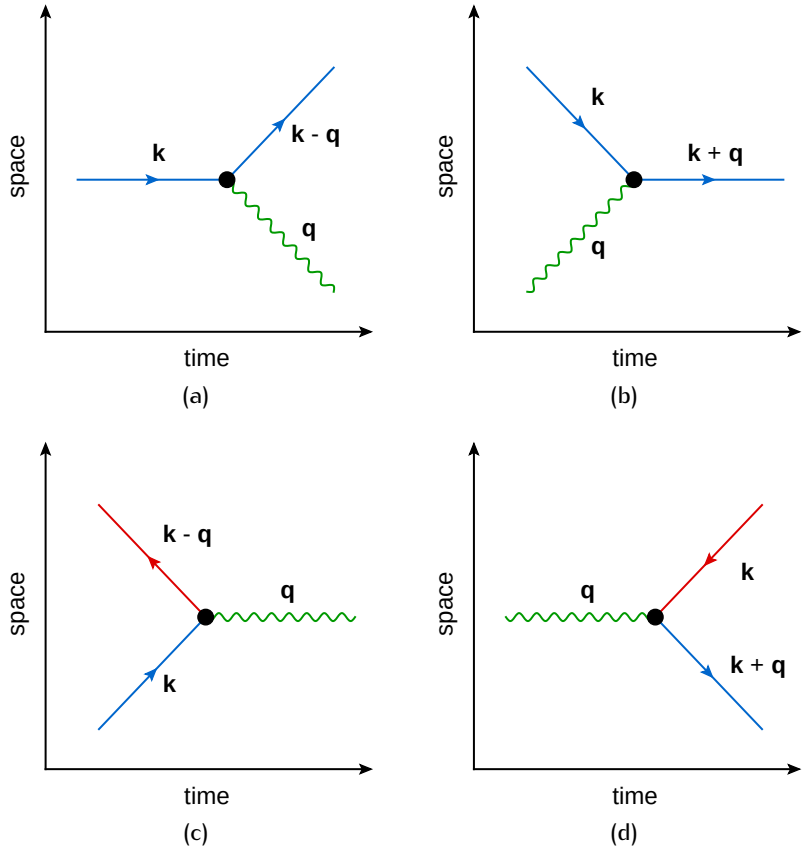

Figure 2.1. Four kinds of elementary electron-phonon interactions: **(a)** describes the phonon *emission* of an electron; **(b)** describes the phonon *absorption* of an electron; **(c)** describes the phonon *creation* due to an electron-hole recombination; and **(d)** describes the phonon *annihilation* due to an electron-hole creation.

In Fig. 2.1 all four kinds are depicted: the phonon *emission* of an electron [Fig. 2.1(a)], the phonon *absorption* of an electron [Fig. 2.1(b)], the phonon *creation* due to an electron-hole recombination [Fig. 2.1(c)] and the phonon *annihilation* due to an electron-hole creation [Fig. 2.1(d)]. For describing such processes it is handy to make use of Feynman diagrams, a powerful tool in particle and solid state physics to describe all kinds of interactions.[5]

[5]Feynman diagrams are two-dimensional diagrams with a time and space axis. Lines represent different kinds of (quasi)particles (and their illustrated paths) which, in case they run together at a certain point (*vertex*), interact with each other. Charged particles are depicted by arrows pointing in the direction of the time axis while their antiparticles are pointing in the opposite direction. Neutral particles as well as quasiparticles are depicted by squiggly lines.

As a result of these interactions, especially when several elementary processes are superimposed, the electrons eigenstates and energies get changed and "new" effects may occur. For instance, an electron propagating through a lattice may induce a lattice polarisation that moves together with the electron and results in an increased effective mass of the electron. Often one can define a new quasiparticle (called *polaron*) to describe such a state. Another important effect is that phonons may also transfer an *effective* electron-electron interaction in the way that an electron emits a phonon which subsequently gets absorbed by another electron and thus changes its state. This phonon-induced electron-electron interaction must be distinguished carefully from the "standard" Coulomb interaction and can be repulsive as well as attractive. Latter case is important for interpreting conventional superconductivity (in the BCS theory) concerning the stability of Cooper pairs. Many more effects may occur, which again is beyond the scope of our discussion.

Finally we have to take a closer look at the basis states for describing a coupled electron-phonon system. We have concluded so far that electrons are fermions and phonons are bosons and for both kinds of particles we have derived basis states representations [see Eqs. (2.11) and (2.14)]. The Hamiltonian corresponding to a coupled electron-phonon system [Eq. (2.27)] generally consists of electron as well as phonon fundamental operators, each acting only on the subspace of the particular particle type. From elementary quantum mechanics [see 9, p. 135-145] it is known that the Hilbert space of such a system is spanned by the tensor product of the Hilbert subspaces of each particle type. Hence the total Hilbert space dimension equals to the product of the subspaces dimensions. By defining $|k\rangle_{\mathrm{el}}$ as basis kets for an electron system and $|k\rangle_{\mathrm{ph}}$ for a phonon system in terms of second quantization we can write a general basis state for describing a coupled electron-phonon system by

$$|k\rangle_{\mathrm{el-ph}} = |k\rangle_{\mathrm{el}} \otimes |k\rangle_{\mathrm{ph}} = |n_1^{\mathrm{el}}, n_2^{\mathrm{el}}, \ldots, N_{\mathrm{s}}\,;\, n_1^{\mathrm{ph}}, n_2^{\mathrm{ph}}, \ldots, N_{\mathrm{s}}\rangle, \tag{2.28}$$

where n_i^{el} are the occupation numbers for electrons, n_i^{ph} for phonons and N_{s} the number of cluster sites.[6] Thus the total Hilbert space dimension $N_{\mathrm{st,el-ph}}$ is given by

$$N_{\mathrm{st,el-ph}} = N_{\mathrm{st,el}} \cdot N_{\mathrm{st,ph}}, \tag{2.29}$$

where $N_{\mathrm{st,el}}$ and $N_{\mathrm{st,ph}}$ are the electrons and phonons Hilbert space sizes, respectively. Therefore index k from Eq. (2.28) runs from 1 to $N_{\mathrm{st,el-ph}}$.[7]

[6] Here we also assume that all ions (cluster sites) perform vibrations. Later in this work we will learn that electrons and phonons sites don't have to be identical.

[7] It shall be noted that above basis state ket applies to *all* systems that consist of two different particle types. Previously we have considered spin ↑ and ↓ electrons separately. Therefore, a basis state ket describing such a system has a similar form to Eq. (2.28).

2.6 Model Hamiltonians

The various treatments of the *ab initio* Hamiltonian that we have conducted so far are very important for understanding and analyzing main physics out of solids. In many cases they can also be used for numerical calculations, but for making them mathematically (and numerically) treatable further approximations must be applied. In return the realm of these models gets restricted to some special materials only, and mostly it is impossible to determine how realistic a certain approximation is. Strongly correlated electron systems e. g. require an explicit treatment of electron-electron interactions that often outweigh other effects. Besides, macroscopic matter consists of more than $N \sim 10^{23}$ atoms which makes an *ab initio* treatment completely impossible. For describing such systems it is therefore necessary to resort to different models that just take account of some significant effects. Another advantage is that simplified models can often be treated analytically which provides a deeper insight into the investigated system than a bare numerical calculation.

In the following we will introduce all model Hamiltonians that are used throughout our whole calculations as well as their main properties. From now on, unless stated otherwise, we will not mark *operators* by hat accents "ˆ" any more to ensure a better clarity.

2.6.1 Single-band Hubbard Model

Originally introduced independently by John Hubbard [14], Martin C. Gutzwiller and Junjiro Kanamori, the (single-band) *Hubbard model* is the simplest model for describing the interplay of kinetic energy, Coulomb interaction and Pauli principle on a lattice. It is mostly defined as follows:

$$H = -t \sum_{<i,j>,\sigma} \left(c^{\dagger}_{i,\sigma} c_{j,\sigma} + \text{h.c.} \right) + U \sum_{i} n_{i\uparrow} n_{i\downarrow}, \tag{2.30}$$

where t is the hopping integral, $< i, j >$ denote nearest neighbor (n.n.) cluster sites, $c^{\dagger}_{i,\sigma}$ and $c_{j,\sigma}$ are creation and annihilation operators for electrons with spin eigenvalue σ on cluster sites i and j, U is the so called *on-site* Coulomb repulsion and $n_{i\uparrow}$, $n_{i\downarrow}$ are occupation number operators for spin $\uparrow$ and $\downarrow$ electrons, respectively. Since we treat the electron hopping between two cluster sites *in both directions*, "h.c." is included meaning the electron hopping in the complementary (opposite) direction.

As evident, the Hubbard model means a drastic simplification of the electron-electron interaction, since Coulomb repulsion is only accounted for electrons being located on the same lattice site (i. e. Wannier state). This means that long-range interactions between electrons are completely neglected. Initially, in this form the Hubbard model was proposed to explain ferromagnetism. Although it also served for the study of many other physical phenomena, its area of application has drastically expanded till today. Amongst many others, it is used to explain antiferromagnetism, ferrimagnetism, the metal-insulator transition and, more recently, high-T_c superconductivity. [15]

2.6.2 Extended Hubbard Model

Often the complete neglect of long-range Coulomb interactions is not conform with properties of real materials. Especially for materials where the *on-site* Coulomb repulsion U is not large, the long-range Coulomb forces are not screened effectively. So it is important to take these effects into account, as well. This can be done by the *extended Hubbard model* where another term, treating the nearest neighbor Coulomb repulsion, is introduced. [16]

Thus the Hamiltonian reads as

$$H = -t \sum_{<i,j>,\sigma} \left(c^{\dagger}_{i,\sigma} c_{j,\sigma} + \text{h.c.} \right) + U \sum_{i} n_{i\uparrow} n_{i\downarrow} + V \sum_{<i,j>} (n_{i\uparrow} + n_{i\downarrow}) \cdot (n_{j\uparrow} + n_{j\downarrow}), \tag{2.31}$$

where V is the nearest neighbor Coulomb repulsion.

Many previous studies [see, e. g. 15] on the one-dimensional and two-dimensional extended Hubbard model showed that the V-term may have important physical effects such as the transition from a spin-density-wave (SDW) phase to a charge-density-wave (CDW) phase.[8] Recently, as discussed in [17], there has been much effort to study the competition between CDW and superconducting states in various materials.

In the following sections, for simplicity reasons, we relate to the on-site Coulomb repulsion U as *Hubbard-U* and the nearest neighbor Coulomb repulsion V as *Hubbard-V*.

2.6.3 Multi-band Hubbard Model with Phonon Interaction

For many materials (e. g. clusters with different kinds of atoms) the Hubbard models from above cannot be used to describe main physical properties. On the one hand they only treat *electronic* quantum states and furthermore only electron fluctuations from one *energy band*. On the other hand they don't take any account of phonons. For the first case many different kinds of so called *multi-band Hubbard models* have been proposed until now, e. g. treating $3d_{x^2-y^2}$ and $2p_\sigma$ orbitals explicitly in order to describe different kinds of chemical bonds. Likewise, for treating phonons many different models exist, of which the *Holstein model* may be worth mentioning. Often, in contemporary scientific articles one can find combinations of one of the Hubbard models from before and the Holstein model, referred to as *Hubbard-Holstein model*.

Due to the high variety of these models (each adapted to its sphere of application), we will only introduce the two models, namely for the *buckling* and *breathing* case, that we use in our later calculations. Besides, here we only present the bare formulas, all further descriptions and explanatory statements etc. are given in Sec. 6.1. As will be discussed at the same place, both Hamiltonians apply for a one-dimensional chain of copper (Cu) and oxygen (O) atoms while the oxygen atoms may perform vibrations.

[8] SDW and CDW describe quantum-mechanical states where electrons arrange themselves in some kind of regular patterns, related to spin or charge distributions within a cluster.

For the *buckling* case the Hamiltonian reads as:

$$H = \sum_i \left[\varepsilon_\mathrm{d} + \sum_l g_\mathrm{a} \left(f_l^\dagger + f_l \right) \right] n_i^\mathrm{d} + \sum_j \varepsilon_\mathrm{p}\, n_j^\mathrm{p} + \sum_i U_\mathrm{d}\, n_{i\uparrow} n_{i\downarrow} + \\ + \sum_{i,l,\sigma} t_\mathrm{dp} \left(d_{i,\sigma}^\dagger p_{l,\sigma} + \mathrm{h.c.} \right) + \sum_l \omega\, f_l^\dagger f_l, \quad (2.32)$$

where i runs over all Cu sites, j over all oxygen sites and l enumerates two oxygen sites being neighbors of one Cu site. Operators $d_{i,\sigma}^\dagger$ and $p_{l,\sigma}$ create holes in $3d_{x^2}$ orbitals on Cu and p_σ orbitals on O sites with occupation number operators $n_i^\mathrm{d} = d_{i\uparrow}^\dagger d_{i\uparrow} + d_{i\downarrow}^\dagger d_{i\downarrow}$ and $n_j^\mathrm{p} = p_{\mathrm{j}\uparrow}^\dagger p_{\mathrm{j}\uparrow} + p_{\mathrm{j}\downarrow}^\dagger p_{\mathrm{j}\downarrow}$. Operators $f_l^\dagger, f_l$ are phonons creation and annihilation operators while g_a represents the coupling constant for the *buckling* case. The parameters ε_d and ε_p are the on-site energies on Cu and O, while t_dp is the n.n. Cu-O hopping integral, U_d is the on-site Coulomb repulsion energy on Cu and ω is the phonon frequency.

For the *breathing* case the Hamiltonian reads as

$$H = \sum_i \left\{ \varepsilon_\mathrm{d} + \sum_l \left[(-1)^{S_l} g_\mathrm{d} \left(e_l^\dagger + e_l \right) \right] \right\} n_i^\mathrm{d} + \sum_j \varepsilon_\mathrm{p}\, n_j^\mathrm{p} + \sum_i U_\mathrm{d}\, n_{i\uparrow} n_{i\downarrow} + \\ + \sum_{i,l,\sigma} \left[t_\mathrm{dp} - (-1)^{S_l} g_\mathrm{pd} \left(e_l^\dagger + e_l \right) \right] \left(d_{i,\sigma}^\dagger p_{l,\sigma} + \mathrm{h.c.} \right) + \sum_l \omega\, e_l^\dagger e_l, \quad (2.33)$$

where all variables have the same meaning, while g_d represents the *diagonal* coupling constant for the *breathing* case and g_pd the coupling constant that modulates the change of the hopping integral. Value S_l is needed according to a convention for the *breathing* case, also discussed in Sec. 6.1.

2.7 Physical Quantities of Interest

When treating many-body systems, we mainly want to examine physical properties that not only characterize a system, but can also be compared with measurable quantities. We already know that a certain measuring result is based on a probability distribution. Consequently, when repeating a measuring process N times under identical conditions, one obtains many different results that are statistically distributed. Only for $N \longrightarrow \infty$ their mean value converges towards a constant value. It is therefore obvious to define the so-called *expectation value* (also called *mean value*) of a observable which corresponds to the previously discussed mean value, i. e. the mean value of the results one obtains if a large number of N measurements is conducted. If H is the observable which is measured in the quantum-mechanical state $|\psi\rangle$, it can be shown that the expectation value is given by

$$\langle H \rangle = \frac{\langle \psi | H | \psi \rangle}{\langle \psi | \psi \rangle}, \quad (2.34)$$

which means that if $|\psi\rangle$ is given we can predict probabilities for all possible results, and if the expectation value is calculated we obtain a direct comparison for experimental mean values. Therefore we are mainly interested in the calculation of expectation values of observables, whereas in the following we will always relate to the quantum-mechanical ground state $|\psi_0\rangle$ given by

$$|\psi_0\rangle = \sum_k c_k \, |k\rangle, \tag{2.35}$$

while $|k\rangle$ are the orthonormal basis state kets [i. e. the configuration basis as introduced in Eqs. (2.14) and (2.28) for electron and electron-phonon systems, respectively] with coefficients c_k.

Subsequently we want to introduce all observables needed for our later calculations and transform them in the way that they can directly be used for numerical calculations (according to terms of second quantization). Such a step is needed for the latter numerical implementation of the formulas and is crucial for any programming steps, as it represents the only way to prove the correct functionality of the algorithms. We start by stating all quantities related to charge distributions and continue with observables derived from spin configurations. In the end we give an overview about energy terms. In the whole discussion we focus on giving an overview of their practical relevance in order to describe main physics for the investigated systems.

(Local) Charge Density

The most trivial quantity to begin with is the (local) charge density, defined as follows [see 6, p. 203]:

$$\langle n_i \rangle := \langle \psi_0 | \, (\hat{n}_{i\uparrow} + \hat{n}_{i\downarrow}) \, | \psi_0 \rangle, \tag{2.36}$$

where $\hat{n}_{i,\sigma}$ are the occupation number operators for spin $\uparrow$ and $\downarrow$ electrons, and index i represents a certain cluster site. We can simplify above equation by expanding ground state $|\psi_0\rangle$ in terms of the basis states $|k\rangle$ as follows:

$$\langle n_i \rangle = \sum_{k,k'} c_k^* c_{k'} \, \langle k | \, (\hat{n}_{i\uparrow} + \hat{n}_{i\downarrow}) \, | k' \rangle = \sum_{k,k'} c_k^* c_{k'} \, \left[n_{i\uparrow}(k') + n_{i\downarrow}(k') \right] \underbrace{\langle k | k' \rangle}_{\delta_{k,k'}},$$

while we make use of the orthonormality amongst basis states $|k\rangle$. Besides we know from Sec. 2.2.2 that the appliance of the occupation number operators $\hat{n}_{i,\sigma}$ yields the occupation numbers $n_{i,\sigma}$. Finally we obtain:

$$\langle n_i \rangle := \sum_k |c_k|^2 \cdot \left[n_{i\uparrow}(k) + n_{i\downarrow}(k) \right]. \tag{2.37}$$

It is evident that above quantity, if calculated for all i, yields charge densities for each cluster site within the system.

Charge Correlation

The previously discussed local charge density provides a clear insight into the charge distribution of a system. This can be changed if some charge fluctuations occur. Therefore, we often want to examine the influence of a certain cluster site's charge density on another one, i. e. to which extent the change of a certain cluster site's charge density affects the charge density of another cluster site. It is known that these "influences" are expressed by so-called correlation functions, and we define the charge correlation function [see, e. g. 18] as follows:

$$\langle n_i\, n_j \rangle := \langle \psi_0 | \, (\hat{n}_{i\uparrow} + \hat{n}_{i\downarrow}) \cdot (\hat{n}_{j\uparrow} + \hat{n}_{j\downarrow}) \, | \psi_0 \rangle. \tag{2.38}$$

Now we make use of the identity operator $\mathbb{1} = \sum_{k''} |k''\rangle \langle k''|$ and proceed like before:

$$\begin{aligned}
\langle n_i\, n_j \rangle &= \sum_{k,k'} c_k^* c_{k'} \, \langle k | \, (\hat{n}_{i\uparrow} + \hat{n}_{i\downarrow}) \cdot \mathbb{1} \cdot (\hat{n}_{j\uparrow} + \hat{n}_{j\downarrow}) \, | k' \rangle = \\
&= \sum_{k,k',k''} c_k^* c_{k'} \, \langle k | \, (\hat{n}_{i\uparrow} + \hat{n}_{i\downarrow}) \, | k'' \rangle \langle k'' | \, (\hat{n}_{j\uparrow} + \hat{n}_{j\downarrow}) \, | k' \rangle = \\
&= \sum_{k,k',k''} c_k^* c_{k'} \, \left[n_{i\uparrow}(k'') + n_{i\downarrow}(k'') \right] \cdot \left[n_{j\uparrow}(k') + n_{j\downarrow}(k') \right] \underbrace{\langle k | k'' \rangle}_{\delta_{k,k''}} \underbrace{\langle k'' | k' \rangle}_{\delta_{k'',k'}},
\end{aligned}$$

by which we obtain the final formula for the charge correlation:

$$\langle n_i\, n_j \rangle = \sum_k |c_k|^2 \cdot \left[n_{i\uparrow}(k) + n_{i\downarrow}(k) \right] \cdot \left[n_{j\uparrow}(k) + n_{j\downarrow}(k) \right]. \tag{2.39}$$

Charge Structure Factor

Another way for investigating the charge distribution of a system is the calculation of the *charge structure factor*. It is defined as the Fourier transform of the charge correlation function and can be used to uniquely characterize charge alterations (such as CDW) on a lattice. In our latter work we use a slightly different form [see, e. g. 19] defined as

$$N(\mathbf{q}) := \frac{1}{N_s} \sum_{i,j} e^{i\mathbf{q}(\mathbf{R}_i - \mathbf{R}_j)} \left[\langle n_i\, n_j \rangle - \langle n_i \rangle \langle n_j \rangle \right] \tag{2.40}$$

which is identical to

$$N(\mathbf{q}) = \frac{1}{N_s} \sum_{i,j} e^{i\mathbf{q}(\mathbf{R}_i - \mathbf{R}_j)} \left\langle \left(n_i - \langle n_i \rangle \right) \cdot \left(n_j - \langle n_j \rangle \right) \right\rangle. \tag{2.41}$$

In both formulas $\mathbf{R}_i$ and $\mathbf{R}_j$ are the real lattice vectors (with N_s cluster sites) while $\mathbf{q}$ is a reciprocal lattice vector, and we can directly use the results from before to calculate $N(\mathbf{q})$. As it is visible from both equations, $N(\mathbf{q})$ gives informations on the charge density's deviation from the mean value. Thus a uniform charge distribution results in $N = 0$ while a CDW is visible by a cusp in the function $N(\mathbf{q})$.

Density Matrix

For many studies, one often also considers the *density matrix (element)* ρ_{ij}, defined by

$$\rho_{ij} := \sum_{\sigma} \langle \psi_0 | \, c^{\dagger}_{i,\sigma} c_{j,\sigma} \, | \psi_0 \rangle. \tag{2.42}$$

It shall be noted that the above formula cannot be simplified further unless one chooses a concrete basis state representation. In our latter calculations we used formulas and principles discussed in Sec. 3.2.1 whereupon the numerical implementation of the density matrix is straight-forward. Besides, the results where checked with known paper's results (as will be shown later).

The physical meaning of the density matrix is described in two parts: The diagonal elements, on the one hand, describe the occupation numbers of single-particle states, i. e. they give the probability of finding an electron on a particular cluster site (which is identical to the charge density from before). The off-diagonal elements, on the other hand, describe coherences between two states (cluster sites). They include the information over phase relations between the different states and describe coherent superpositions of two states. Thus, off-diagonal elements contain direct information about the bond strength of two cluster sites. [20, 21]

Total Spin

We now turn to spin observables and begin with the squared *total spin operator* $\mathbf{S}^2$. Since the study of angular momentum operators in quantum mechanics is very extensive, we adapt known results without explanation and refer to [9, p. 585–619] for further reading.

The total spin operator is defined by

$$\mathbf{S} := \begin{pmatrix} S^x \\ S^y \\ S^z \end{pmatrix} = \begin{pmatrix} \sum_i S_i^x \\ \sum_i S_i^y \\ \sum_i S_i^z \end{pmatrix}, \tag{2.43}$$

where index i runs over all cluster sites. According to quantum mechanics theory it is impossible to determine all three components of $\mathbf{S}$ simultaneously, however $\mathbf{S}^2$ and one arbitrary component (as a general rule: S^z) are compatible. From the eigenvalue equation for $\mathbf{S}^2$ we obtain

$$\langle \mathbf{S}^2 \rangle = \langle \psi_0 | \, \mathbf{S}^2 \, | \psi_0 \rangle = S(S+1), \tag{2.44}$$

where S is the *total spin*. We first evaluate $\mathbf{S}^2$ by

$$\langle \mathbf{S}^2 \rangle = \left\langle \left[\sum_i S_i^x \right]^2 + \left[\sum_i S_i^x \right]^2 + \left[\sum_i S_i^x \right]^2 \right\rangle =$$

$$= \left\langle \left[\sum_i \left(S_i^x\right)^2 + \sum_{i\neq j} S_i^x S_j^x\right] + \left[\sum_i \left(S_i^y\right)^2 + \sum_{i\neq j} S_i^y S_j^y\right] + \left[\sum_i \left(S_i^z\right)^2 + \sum_{i\neq j} S_i^z S_j^z\right] \right\rangle =$$

$$= \left\langle \sum_i \left[\left(S_i^x\right)^2 + \left(S_i^y\right)^2 + \left(S_i^z\right)^2\right] + \sum_{i\neq j} \left[S_i^x S_j^x + S_i^y S_j^y + S_i^z S_j^z\right] \right\rangle =$$

$$= \left\langle \sum_i \left(\mathbf{S}_i\right)^2 + \sum_{i\neq j} \mathbf{S}_i \mathbf{S}_j \right\rangle$$

Since $(\mathbf{S}_i)^2 = \mathbf{S}_i \mathbf{S}_i$ we can combine the two terms from above and allow i and j to run over all cluster sites independently

$$\langle \mathbf{S}^2 \rangle = \left\langle \textstyle\sum_{ij} \mathbf{S}_i \mathbf{S}_j \right\rangle,$$

and finally the expectation value for the squared total spin operator is given by

$$\langle \mathbf{S}^2 \rangle = \sum_{ij} \langle \mathbf{S}_i \mathbf{S}_j \rangle. \tag{2.45}$$

By comparing the sum with our results from before it is evident that the sum is conducted over a correlation function, namely the *spin correlation function* which we will treat explicitly below.

Before doing so, some further notes about the above calculations are in order. We have shown that the total spin of a system can be found by calculating the expectation value of the squared total spin operator and making use of Eq. (2.44). Its value is very important for characterizing magnetic properties for a whole system as well as the effect of an external magnetic field etc.

Spin Correlation

The spin correlation function can be interpreted in analogy to the charge correlation function, i. e. it represents an important value for studying the correlations of different spin configurations amongst each other. As mentioned before, it is defined [see, e. g. 18] by:

$$\langle \mathbf{S}_i \mathbf{S}_j \rangle := \langle\, S_i^x S_j^x + S_i^y S_j^y + S_i^z S_j^z \,\rangle. \tag{2.46}$$

For its explicit evaluation we make use of following relations [6, p. 223]:

$$S_i^x = \frac{1}{2}(S^\uparrow + S^\downarrow) \qquad S_i^y = \frac{1}{2\mathrm{i}}(S^\uparrow - S^\downarrow) \qquad S_i^\sigma = c_{i,\sigma}^\dagger c_{i,-\sigma} \qquad S_i^z = \frac{1}{2}\sum_\sigma z_\sigma \hat{n}_{i,\sigma},$$

where σ denotes the spin eigenvalues for spin $\uparrow$ and $\downarrow$, $z_\uparrow = +1$ and $z_\downarrow = -1$. With these relations the spin correlation function from Eq. (2.46) transforms to

$$\begin{aligned}\langle \mathbf{S}_i \mathbf{S}_j \rangle &= \left\langle \frac{1}{4}\left(S_i^\uparrow + S_i^\downarrow\right)\left(S_j^\uparrow + S_j^\downarrow\right) + \frac{1}{4\mathrm{i}^2}\left(S_i^\uparrow - S_i^\downarrow\right)\left(S_j^\uparrow - S_j^\downarrow\right) + S_i^z S_j^z \right\rangle = \\ &= \left\langle \frac{1}{2}\left(S_i^\uparrow S_j^\downarrow + S_i^\downarrow S_j^\uparrow\right) + S_i^z S_j^z \right\rangle = \left\langle \frac{1}{2}\left(c_{i\uparrow}^\dagger c_{i\downarrow} c_{j\downarrow}^\dagger c_{j\uparrow} + c_{i\downarrow}^\dagger c_{i\uparrow} c_{j\uparrow}^\dagger c_{j\downarrow}\right) + S_i^z S_j^z \right\rangle\end{aligned}$$

and we finally obtain:

$$\langle \mathbf{S}_i \mathbf{S}_j \rangle = \frac{1}{2}\langle \psi_0 | c_{i\uparrow}^\dagger c_{i\downarrow} c_{j\downarrow}^\dagger c_{j\uparrow} | \psi_0 \rangle + \frac{1}{2}\langle \psi_0 | c_{i\downarrow}^\dagger c_{i\uparrow} c_{j\uparrow}^\dagger c_{j\downarrow} | \psi_0 \rangle + \langle \psi_0 | S_i^z S_j^z | \psi_0 \rangle. \tag{2.47}$$

Again, the numerical implementation of the first two terms is straight-forward according to descriptions in Sec. 3.2.1. The z-component of the spin correlation is treated separately because of its simple form. Besides, it is often sufficient to only study the z-component of the spin-correlation function, especially in rotation invariant systems. Following previous relations the z-component spin correlation function is given by

$$\langle S_i^z S_j^z \rangle = \langle \psi_0 | \, \tfrac{1}{2}\left(\hat{n}_{i\uparrow} - \hat{n}_{i\downarrow}\right) \cdot \tfrac{1}{2}\left(\hat{n}_{j\uparrow} - \hat{n}_{j\downarrow}\right) | \psi_0 \rangle, \tag{2.48}$$

which can be directly compared with the definition of the charge correlation function in Eq. (2.38). The calculation is conducted in a similar way and we finally obtain:

$$\langle S_i^z S_j^z \rangle = \frac{1}{4}\sum_k |c_k|^2 \cdot \left[n_{i\uparrow}(k) - n_{i\downarrow}(k)\right] \cdot \left[n_{j\uparrow}(k) - n_{j\downarrow}(k)\right] \tag{2.49}$$

Local Magnetic Moment

Often the diagonal elements of the z-component spin correlation function $(S_i^z)^2$ are studied explicitly and referred to as *squared local magnetic moment*. One may also often find definitions for a *local magnetic moment* m (also referred to as *local magnetization*) [see, e. g. 6, p. 203] like

$$m := \hat{n}_{i\uparrow} - \hat{n}_{i\downarrow}. \tag{2.50}$$

Both quantities can be interpreted in analogy to the local charge density, but as a spin quantity. Namely, if two electrons occupy the same cluster site they have opposite spin and thus the magnetic moment of the cluster site is zero. On the other hand, if there are many cluster sites occupied by single electrons each has a magnetic moment and their arrangement among each other is responsible for the overall magnetic properties of the system (paramagnetic, ferromagnetic etc.).

Spin Structure Factor

For studying particular spin configurations (such as SDW) we introduce the *spin* (or *magnetic*) *structure factor* [see, e. g. 22] in analogy to the charge structure factor from Eq. (2.40). It is defined as the Fourier transform of the spin correlation function

$$S(\mathbf{q}) := \frac{1}{N_s} \sum_{i,j} e^{i\mathbf{q}(\mathbf{R}_i - \mathbf{R}_j)} \langle \mathbf{S}_i \, \mathbf{S}_j \rangle. \tag{2.51}$$

Often, only the z-component of the spin correlation function is used (as we do in Chapter 4):

$$S(\mathbf{q}) := \frac{1}{N_s} \sum_{i,j} e^{i\mathbf{q}(\mathbf{R}_i - \mathbf{R}_j)} \langle S_i^z \, S_j^z \rangle. \tag{2.52}$$

As mentioned above, the spin structure factor serves for describing regularities in spin distribution within the lattice. Besides, it is used to calculate other quantities like magnetic susceptibilities etc.

Energy-Related Quantities

Finally we want to introduce some energy quantities that are associated with the used Hamiltonian. We already know that the ground-state energy is defined as the expectation value of the Hamiltonian:

$$E_0 := \langle \psi_0 | \, H \, | \psi_0 \rangle. \tag{2.53}$$

However, as will be discussed later, the ground-state energies are derived directly from the Lanczos diagonalization, so that above relation is not used directly. In Chapter 6 we also calculate single energy terms from Hamiltonians in Eqs. (2.32) and (2.33), which we want to discuss in the following.

The **electrical potential** is defined as follows:

$$E_{\text{pot}} := \left\langle \psi_0 \right| \sum_j \varepsilon_p \, n_j^p + \sum_i U_d \, n_{i\uparrow} n_{i\downarrow} \left| \psi_0 \right\rangle. \tag{2.54}$$

The **phonon energy** ($e_l^\dagger$, e_l represent *breathing* and *buckling* operators) reads as:

$$E_{\text{ph}} := \left\langle \psi_0 \right| \sum_l \omega \, e_l^\dagger e_l \left| \psi_0 \right\rangle, \tag{2.55}$$

The **kinetic energy** is defined by

$$E_{\text{kin}} = \left\langle \psi_0 \right| \sum_{i,l,\sigma} t_{dp} \, (d_{i,\sigma}^\dagger p_{l,\sigma} + \text{h.c.}) \left| \psi_0 \right\rangle. \tag{2.56}$$

The **electron-phonon interaction** (energy) for the *buckling* case is defined by

$$E_{\text{el-ph}} = \left\langle \psi_0 \right| \sum_{i,l} g_{\text{a}} \left(f_l^\dagger + f_l \right) n_i^{\text{d}} \left| \psi_0 \right\rangle \tag{2.57}$$

and for the *breathing* case by

$$E_{\text{kin,breath}} = \left\langle \psi_0 \right| \sum_{i,l,\sigma} \left[-(-1)^{S_l} g_{\text{pd}} \left(e_l^\dagger + e_l \right) \right] \left(d_{i,\sigma}^\dagger p_{l,\sigma} + \text{h.c.} \right) \left| \psi_0 \right\rangle. \tag{2.58}$$

Another quantity that is important especially for the examination of superconductors according to BCS theory is the **(pair) binding energy** defined in [23]:

$$\epsilon_{\text{b}}(N_{\text{e}}) := 2E(N_{\text{e}} + 1) - E(N_{\text{e}}) - E(N_{\text{e}} + 2). \tag{2.59}$$

Here N_{e} is the number of electrons and E is the energy of the system (in our case the ground-state energy). Often the above formula is treated as a function of holes (not electrons) which is described by the same formula with changed sign. The pair binding energy describes whether the paring of two electrons with opposite spin is energetically favorable or not. According to BCS theory this mechanism is responsible for conventional superconductivity.

Chapter 3

Numerical Methods

3.1 General Overview

After we have got to know the basic mathematical knowledge for treating many-body systems we will now deal with concrete numerical methods. It is our aim to provide a general overview of the contemporary methods used in computer science and give a short summary about the main principles. Thereby we mainly follow descriptions from [24–27].

Generally speaking we have two basic strategies for a numerical treatment of many-body systems. The most obvious approach is the "brute force" numerical formulation and evaluation of the Hamiltonian matrix, i. e. the *exact (numerical) diagonalization* (ED) of the many-body Hamiltonian matrix. This means that we use a numerical representation for quantum-mechanical basis states and formulate the Hamiltonian in this particular basis state representation. Subsequently the Hamiltonian is diagonalized in an iterative way, and we obtain "exact" ground states and ground-state energies. The main advantage of this (ED) method is the high numerical accuracy, which makes it an important tool for calculating complex problems (e. g. Hamiltonians that cannot be formulated by other methods) as well as for cross-checking results. However, due to the enormous Hilbert space sizes (which result in an extremely high memory and computation time demand), they are restricted to cluster sizes with ~ 20 atoms and may also require a lot of care for optimizing the algorithm. The most popular ED method is the Lanczos diagonalization method that is treated later in detail.

A fundamentally different approach is that of quantum Monte Carlo (QMC) methods for treating many-body systems. Although many different QMC methods exist, such as variational Monte Carlo (VMC) and determinantal quantum Monte Carlo (DQMC), all techniques are based on random (number) sampling. The starting point of any QMC simulation is to represent quantum-mechanical physics by a statistical problem. In the next step one formulates expectation values for observables (such as the Hamiltonian etc.) in terms of (mostly $3N$-dimensional) integrals that are evaluated by stochastic means, known as "importance

sampling." The main advantage of QMC is the very efficient (and relatively easy) usage of accessible algorithms so that they can be applied on cluster sizes up to $\sim$ 100 atoms. Besides, a wide range of parameters can be studied with same methods and relatively little (numerical) effort. However, QMC methods have disadvantages as well, as e. g. they can only be applied on a restricted class of models or they suffer from the so-called *sign problem* at low temperatures. Further details about these issues and descriptive overviews of QMC methods are given in [24, 25].

Both approaches, ED and QMC, are faced with further difficulties when applied to real materials. Due to the cluster size restrictions which are enormous compared to realistic (macroscopic) matter, many effects that are present in the *thermodynamic limit* ($\hat{=}$ approximately infinite size lattices) remain unrevealed in ED and QMC treatments. Mean-field theories, on the other hand, are defined in the thermodynamic limit, but rely on some uncontrolled approximations and thus fail to describe effects typical for strongly correlated systems, such as nonlocal fluctuations. Therefore, in the recent past, there has been much effort concentrated on *new* models and theories in order to make the treatment of bigger cluster sizes (towards the thermodynamic limit) accessible. These new "advanced" methods, although they have specific names, are all labelled *quantum cluster methods* and can be seen as a "third" approach treating many-body systems. The basic principle of all these methods is to consider finite clusters embedded in an infinite lattice. Once the finite clusters are evaluated by specific *solvers* (e. g. ED or QMC) they are "added" to the infinite lattice in the way that their overall field contributes to the surrounding lattice as a whole. By doing this the full effects of strong correlations are retained, although the interaction of little clusters with the environment is treated on a mean-field basis. Without going into further details, some popular methods are named in the sequel: variational cluster approximation (VCA), (variational) cluster perturbation theory [(V)CPT], dynamical cluster approximation (DCA), etc. Further description can be found in [26, 27].

In the following we will give an explicit description for the usage of an ED method, namely the *Lanczos diagonalization method*. We begin by introducing numerical basis states and matrix representations which are used throughout our latter calculations. Here it is important to state that these representations can be chosen rather arbitrarily according to the theory from Chapter 2, but they must be consequently maintained during the whole calculation process. Following that we describe the most important principles of the Lanczos diagonalization method, and in the end some final remarks about the implementation in FORTRAN 90/95 are given.

3.2 Numeric Basis Representation

It is now important to have a detailed look on the numeric creation of basis states. In the following we will only treat the methods used in this work which proved to be very useful. Before going into detail, we first have to reflect about some general principles.

Basically (as will be shown in Chapters 5 and 6) we investigate composite particle sys-

tems, i. e. systems with different kinds of particles. In our present work these are compound electron systems of spin ↑ and ↓ or interacting systems of electrons and phonons. From Sec. 2.5 we already know that this kind of systems is described by combined basis states and the total basis state number corresponds to the product of single-basis state numbers. From the numerical point of view it is therefore very useful to treat the creation of basis states for each subsystem separately since it keeps the total computer memory very small. For this reason we can treat the case for bosons and fermions again separately whereas we only have two different kinds of particles, namely *phonons* as representatives of bosons and *electrons* (belonging to fermions).

Before beginning with any numerical calculation it is also important to give thoughts to the total basis states numbers. Since a small change of particular parameters (e. g. number of cluster sites or electrons) may rapidly slow down the whole calculation process, it is useful to determine the theoretical size of the Hilbert space analytically. Depending on the model Hamiltonian in use this can always be done *a priori* and provides a good insight into the complexity of all calculations.

In Tab. 3.1 we listed some examples for Hilbert space dimensions to depict the great dependency on *slight* changes of some parameters.

Table 3.1. Number of total basis states dependent on various parameters:[a]
N_s ..... number of cluster sites
$N_\uparrow$,$N_\downarrow$ ..... numbers of spin ↑, ↓ electrons
N_{ph} ..... number of maximum phonons in system .

N_s	$N_\uparrow = N_\downarrow$	N_{ph}	Tolal basis state number
4	2	5	4,536
		15	139,536
		30	1,699,536
6	3	5	184,800
		15	21,705,600
		30	779,116,800
8	3	5	4,036,032
		15	1,537,624,704
		30	153,361,350,912

[a] Values calculated according to formulas presented in Secs. 3.2.1 and 3.2.2.

For simplicity reasons we will introduce the numerical basis state representation for electrons first and then proceed with the phonons part.

3.2.1 Electron Basis

As already mentioned several times before we consider electrons with spin ↑ and ↓ separately. In this notation each lattice site of an arbitrary cluster may be occupied by one electron (with given spin) or none. To illustrate this fact we choose a random four-site cluster like depicted in Fig. 3.1 and construct the appropriate kets in terms of second quantization.

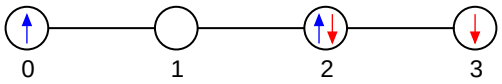

Figure 3.1. Four-site cluster with a particular electron distribution. Blue arrows mark electrons with spin ↑ and red arrows electrons with spin ↓. The cluster sites are numbered from 0 to 3.

We can write the kets describing this particular electron distribution for spin ↑ and ↓ by

$$|\psi\rangle_\uparrow = |0,1,0,1\rangle_\uparrow$$
$$|\psi\rangle_\downarrow = |1,1,0,0\rangle_\downarrow$$

where we begin the counting from *right* to *left* (therefore in both kets site 0 is represented by the rightmost position). Since the only possible values within these kets are sequences of zeros and ones, we can identify these as sequences of (computer) bits which are used to represent integer numbers in the so-called *binary numeral system*. Thus we are able to map the states to individual integer numbers:

$$|\psi\rangle_\uparrow = |0,1,0,1\rangle_\uparrow \longrightarrow |\overbrace{0101}^{\text{binary code}}\rangle_\uparrow \longrightarrow |5\rangle_\uparrow$$
$$|\psi\rangle_\downarrow = |1,1,0,0\rangle_\downarrow \longrightarrow |\underbrace{1100}_{\text{binary code}}\rangle_\downarrow \longrightarrow |12\rangle_\downarrow .$$

By convention in computing the rightmost position is called *least significant bit* (LSB) and marks the beginning of any bit sequence. Therefore the numbering in the above kets is chosen from right to left. The integer numbers I that can be represented in this way read as

$$I = 0, 1, 2, \ldots, 2^N - 1$$

where N corresponds to the available digits of the binary code and therefore is equivalent to the number of cluster sites N_s. However, not all integers in this range represent realistic quantum-mechanical states. Namely, we have only a particular amount of bits with value 1 (in both kets) which are determined by the quantity of spin ↑ and ↓ electrons. Therefore the computer algorithm for creating basis states is realized by counting integers from 0 to

$2^N - 1$ and checking if the corresponding amount of bits with value 1 is equal to the number of electrons. This implementation can be realized with the so-called *modulo* function (also popular in *modular arithmetic*) which is very efficient. In this way we obtain all possible pattern combinations of zeros and ones which finally serve as basis states for electrons.

The number of basis states can be calculated by applying basic knowledge from *combinatorics*. Seen from this angle we treat a *set* of N cluster sites (*elements*) that can be divided into two *groups* (*subsets*), namely cluster sites with value 0 and value 1. The number of basis states is equal to the number of all possible arrangements (*permutations*) of zeros and ones within. It follows from this simple derivation that this number is given by the *binomial coefficient* [see 28, p. 31-34]. If $N_{\mathrm{st}}^{\uparrow}$ represents the number of basis states for spin $\uparrow$, then we can write

$$N_{\mathrm{st}}^{\uparrow} = \binom{N_{\mathrm{s}}}{N_{\uparrow}}$$

where N_{s} is the number of cluster sites and $N_{\uparrow}$ the number of spin $\uparrow$ electrons. By analogy we obtain the same expression for spin $\downarrow$ basis states and thus we are able to write the total number of electron basis states $N_{\mathrm{st,el}}$ by

$$N_{\mathrm{st,el}} = N_{\mathrm{st}}^{\uparrow} \cdot N_{\mathrm{st}}^{\downarrow} = \binom{N_{\mathrm{s}}}{N_{\uparrow}} \cdot \binom{N_{\mathrm{s}}}{N_{\downarrow}} \tag{3.1}$$

where $N_{\downarrow}$ represents the number of spin $\downarrow$ electrons and $N_{\mathrm{st}}^{\downarrow}$ their number of basis states.

Finally we have to focus on the appliance of creation and annihilation operators in this particular basis notation. For this purpose we take a more detailed look at the *binary numeral system*. Integers in this numeral system are expressed by

$$I = \sum_{i=0}^{N_{\mathrm{s}}} n_i \cdot 2^i \qquad \text{with} \qquad n_i \in \{0, 1\} \tag{3.2}$$

and N_{s} again marks the number of cluster sites and available digits, respectively. From Sec. 2.2.2 it is already known that the action of a creation or annihilation operator means a change of the occupation number n_i and consequently a change of the coefficient n_i in Eq. (3.2). It is now evident that this represents an increase or a decrease of integer I by the i-th power of 2. Hence we can express *numeric* creation and annihilation operators by

$$c_i^{\dagger} |I\rangle = |I + 2^i\rangle$$
$$c_i \, |I\rangle = |I - 2^i\rangle,$$

but, additionally, we have to consider the following two conditions when performing an explicit numerical implementation:

(1) Following Pauli's exclusion principle, the creation operator $c_i^\dagger$ can only be applied if cluster site i is unoccupied. The annihilation operator c_i, on the other hand, can only be applied on an occupied cluster site since the appliance on an empty one yields zero.

(2) We have to take into account the antisymmetry of fermionic wave functions, which means that a sign change occurs if two electrons change their order.

In a numerical implementation, condition (1) is realized by making use of *modulo* function and checking if a particular cluster site is occupied or not. After doing this the creation or annihilation process can be performed.

Condition (2), however, is crucial if any products of creation and annihilation operators are regarded (e. g. "electron hopping"). In such a case the electrons can change their order amongst each other which means a sign change of the fermionic wave function. This fact requires some additional programming since one has to compare the resulting quantum-mechanical state with the initial one, but the implementation itself is straight-forward and follows from our previous discussion.

3.2.2 Phonon Basis

Compared with the electrons case the numerical creation of phonon basis states is not so obvious. We already know that phonons or, more generally speaking, bosons obey Bose-Einstein statistics which means that their theoretical Hilbert space is infinite. Further on this implies that any system may have an arbitrary amount of phonons (up to infinity) and thus any cluster site may be occupied by an arbitrary number of phonons (up to infinity). This fact necessitates some *a priori* simplifications in order to make the phonons numerically treatable.

In the underlying work we adapt a truncation method for the phononic Hilbert space discussed in [29]. The basic idea behind this method is to suppose a *maximum* number of phonons N_{ph} in the whole system with all possible distributions (and permutations) on all cluster sites. In therms of a general basis state (see Sec. 2.2.2)

$$|k\rangle_{\mathrm{ph}} = \prod_{i=1}^{N} \frac{\left(b_i^\dagger\right)^{n_i^k}}{\sqrt{n_i!}} |0\rangle_{\mathrm{ph}}$$

we can define the above mentioned truncation method by:

$$\sum_{i=1}^{N} n_i^k \leq N_{\mathrm{ph}}. \tag{3.3}$$

Subsequently we are able to obtain the total number of phononic basis states (following this truncation method):

$$N_{\mathrm{st,ph}} = \binom{N_{\mathrm{s}} + N_{\mathrm{ph}}}{N_{\mathrm{s}}} \tag{3.4}$$

where N_s again represents the number of available cluster sites. Here we adapted Eq. (3.4) from [29] (see, however, Appendix A.1 for an explicit derivation done by the author).

This means that the given system can have any amount of phonons reaching from 0 to N_{ph}. In order to create a full set of basis states we have to consider all possible phonon distributions within. As a consequence we use vectors (integer arrays) to represent phononic basis states where each dimension corresponds to a cluster site containing phonons. Thus an arbitrary phononic basis ket reads as

$$|k\rangle_{ph} = |n_1, n_2, \ldots, n_{N_s}\rangle_{ph} \longrightarrow (n_1, n_2, \ldots, n_{N_s})_{k,ph}$$

and we must create a $N_{st,ph} \times N_s$ matrix in order to describe a full basis. The author tested several methods for creating such basis sets that can be summarized by the following:

(1) In the case one assumes less then ten phonons in a given many-body system it is possible to map the basis states to integer numbers following *decimal numeral system*. For ten and more phonons, however, this representation is not unique.

(2) There are several alternative ways of forming all possible combinations of phonon numbers and choosing just those states where the total phonon number is *less* than or *equal* to N_{ph}. For bigger cluster sites (more than 6 sites) these algorithms become very slow.

(3) The most efficient method, also used in the present work, proved to be a *recursive algorithm* written by the author in FORTRAN 90/95 (see Appendix A.2 for a detailed description). The biggest advantage of this method is that the number of iteration steps is equal to the total basis state number [as stated in Eq. (3.4)].

Concerning creation and annihilation operators in the phonon basis, they read exactly as shown in Sec. 2.2.2, but according to the truncation method in Eq. (3.3) we have to introduce two restrictions for the bosonic creation operator:

$$b_i^\dagger |\ldots, n_i = N_{ph}, \ldots\rangle := 0$$
$$b_i^\dagger |\ldots, n_i < N_{ph}, \ldots\rangle := 0 \qquad \text{if} \qquad \sum_{i=1}^{N_s} n_i = N_{ph}.$$

3.3 Numeric Matrix Representation

In the above basis state representations (for electrons and phonons) the Hamiltonian matrices from Sec. 2.6 are sparce matrices with very big dimensions where only a fractional amount of matrix elements is non-zero. It is therefore obvious to use a different matrix representation where we only store non-zero matrix elements. This is achieved by the *compact storage* principle in the way that we store *diagonal* matrix elements and *off-diagonal* matrix elements separately.

The diagonal matrix elements, on the one hand, are saved in a vector whose dimension is equal to the Hilbert space dimension. It shall be noted that diagonal elements describe potential terms, since they leave the quantum-mechanical states unchanged.

Off-diagonal matrix elements, on the other hand, correspond to fundamental operators and thus they change quantum-mechanical states. In the compact storage we only store the values of the off-diagonal matrix elements in connection with their column and row numbers. With this drastic simplification we save an enormous amount of computer memory. However, the memory can be reduced much more if we apply basic thinking from before. Namely, we have learned that we treat different kinds of particles (spin $\uparrow$, $\downarrow$ electrons and phonons), and thus each particle type is represented in its own basis. Since a particular fundamental operator ($\hat{=}$ off-diagonal element) acts only on the Hilbert subspace corresponding to a particular particle we can build matrices for each particle type separately and use the compact storage for all of them.

Although these principles are derived from trivial considerations, their numerical implementation is not so trivial and may cost a lot of time. Especially for programming a "simple" matrix-vector multiplication one must be very careful. However, they are absolutely necessary when treating big Hilbert space dimensions because otherwise the computer memory can be exceeded very easily which means a drastic slowdown or even a breakdown of the calculation process.

3.4 Lanczos Method

The Lanczos algorithm, originally introduced by Cornelius Lanczos [30] is an iterative method for finding eigenvectors and eigenvalues of a square matrix as well as an approximative method for solving linear equation systems. Together with the power method, CG method and others it is part of the so called *Krylov subspace methods* and it is very useful for big and sparse matrices. In common literature exist quite different approaches for the evolution of the Lanczos algorithm, and also Lanczos's initial algorithm has been drastically developed and improved in the last decades. In this section we will describe the basic ideas together with certain disadvantages that arise in numerical applications. The exact mathematical derivations and proofs will be omitted, but, if necessary, we will give exact reference for further reading. The following lines are mainly adapted from [31], but for consistency purpose we will use a slightly different notation and form.

We start with the standard eigenvalue problem

$$H\mathbf{x}_i = \varepsilon_i \mathbf{x}_i, \tag{3.5}$$

where H denotes the Hamiltonian matrix with its eigenvectors $\mathbf{x}_i$ and eigenvalues (energies) ε_i. Further on it is known that the Hamiltonian matrix is a real symmetric matrix and for simplicity reasons, here we will treat the *symmetric* Lanczos method which can only be applied on symmetric matrices. However, it is easy to show that the same formalism can be expanded also for non-symmetric matrices. For the beginning we introduce the

transformation matrices B and B^* that satisfy the biorthogonality property

$$BB^* = \mathbb{1}. \tag{3.6}$$

Now we can transform Eq. (3.5) by multiplying with B^* and using the above relation

$$B^* \cdot H \cdot \overbrace{(BB^*)}^{\mathbb{1}} \cdot \mathbf{x}_i = \varepsilon_i \cdot B^* \cdot \mathbf{x}_i.$$

With the definitions

$$T := B^*HB \qquad \text{and} \qquad \tilde{\mathbf{x}}_i := B^*\mathbf{x}_i \tag{3.7}$$

we develop a transformed eigenvalue problem, but with the same eigenvalues ε_i from Eq. (3.5):

$$T\tilde{\mathbf{x}}_i = \varepsilon_i\tilde{\mathbf{x}}_i \tag{3.8}$$

Furthermore we need the definition of the *Krylov subspace*.

Definition 3.1 *Take a matrix $H \in \mathbb{R}^{n\times n}$ and a vector $\mathbf{x} \in \mathbb{R}^n$. The subspace defined by*

$$\mathcal{K}_k(H, \mathbf{x}) = \text{span}\{\mathbf{x}, H\mathbf{x}, \ldots, H^{k-1}\mathbf{x}\}$$

is the k-order Krylov subspace *of A in respect to $\mathbf{x}$.*

The main idea behind the Lanczos algorithm is to transform the eigenvalue problem from Eq. (3.5) to Eq. (3.8) and solve the latter one which can be done with much higher efficiency. The actual *Lanczos iteration* describes a way of building an orthonormal basis of the Krylov subspace which is crucial for forming the eigenvalue problem in Eq. (3.8). It can be proved that the columns of the matrices B and B^* are represented by Krylov subspace basis vectors $\mathbf{b}_i$ and $\mathbf{b}_i^*$, respectively. Furthermore it follows that matrix T is tridiagonal, so alltogether we can write:

$$B = (\mathbf{b}_0, \mathbf{b}_1, \ldots, \mathbf{b}_{k-1}) \qquad , \qquad B^* = (\mathbf{b}_0^*, \mathbf{b}_1^*, \ldots, \mathbf{b}_{k-1}^*) \tag{3.9}$$

and

$$T = B^*HB = \begin{pmatrix} \alpha_1 & \beta_1 & & 0 \\ \beta_1 & \alpha_2 & \ddots & \\ & \ddots & \ddots & \beta_{n-1} \\ 0 & & \beta_{n-1} & \alpha_n \end{pmatrix}. \tag{3.10}$$

After generating and diagonalizing the tridiagonal matrix T (e. g. by QR or bisection method), which is done very efficiently, we use the results to find the eigenvectors of the initial matrix H.

In order to understand these principles more detailed we will derive the actual algorithm. For this purpose we multiply Eq. (3.10) with B and perform a columnwise calculation

$$\underbrace{B \cdot B^*}_{\mathbb{1}} HB = B \cdot T$$

which gives us:

$$\begin{aligned} H\mathbf{b}_0 &= \alpha_0 \mathbf{b}_0 + \beta_0 \mathbf{b}_1 \\ H\mathbf{b}_1 &= \beta_0 \mathbf{b}_0 + \alpha_1 \mathbf{b}_1 + \beta_1 \mathbf{b}_2 \\ &\vdots \qquad\qquad \vdots \\ H\mathbf{b}_n &= \beta_{n-1} \mathbf{b}_{n-1} + \alpha_n \mathbf{b}_n + \beta_n \mathbf{b}_{n+1}. \end{aligned}$$

Now we are able to formulate Lanczos's three-step recursion formula

$$\beta_i \mathbf{b}_{i+1} = (H - \alpha_i \mathbb{1})\mathbf{b}_i - \beta_{i-1}\mathbf{b}_{i-1} \tag{3.11}$$

with $\mathbf{b}_i$ called the *Lanczos vectors*. For this recursion formula we note the following

Theorem 3.1 *Let $H \in \mathbb{R}^{n\times n}$ be hermitian and $\mathbf{b}_0$ an arbitrary vector with $|\mathbf{b}_0| = 1$. If we define*

$$\beta_0 = 0 \qquad\qquad \alpha_i = \mathbf{b}_i^* H \mathbf{b}_i \qquad\qquad \beta_i = |\mathbf{b}_{i+1}|,$$

then the vectors $\mathbf{b}_i$ in Eq. (3.11) form a basis of $\mathcal{K}_k(H, \mathbf{b})$, only if all $\beta_i \neq 0$ for $i = 1, \ldots, n-1$.

The explicit mathematical proof for this theorem as well as proofs for all statements written before can be found in [32, p. 259-268].

So far we have treated the Lanczos algorithm strictly analytically. However, the process of building the matrix T [as shown in Eq. (3.11)] is iterative, which means that the actual dimension n of the matrix T in Eq. (3.10) depends on the number of iteration steps (n). After every *Lanczos step* we get a new matrix $T_n \in \mathbb{R}^{n\times n}$ whose eigenvalues (with increasing n) become better approximations for the eigenvalues of the initial matrix H. Before describing the computational implementation (Sec. 3.4.2) in detail, we first have to discuss some side effects that occur with the Lanczos method.

3.4.1 Calculation in Finite Precision

Whenever approaching numerical calculations we have to consider the finite preciseness of every computer. This fact makes us aware of some new aspects when treating the Lanczos algorithm numerically.

Terminating process

In practical use we terminate the process of calculating the Lanczos vectors when a certain convergence is reached. The easiest way for doing this is to observe the convergence of the β_i-values after every Lanczos step. For the case that after a certain amount of Lanczos steps $\beta_i \equiv 0$, an invariant Krylov subspace is reached and the whole eigenvalue problem can be solved uniquely. However, this method is not practical in finite preciseness calculations because we have no knowledge about the exact preciseness of the calculated eigenvalues which is actually more relevant. Another problem is that the case $\beta_i \equiv 0$ can hardly be reached (due to rounding errors which occur in every numerical calculation). So far better methods exist like e. g. making use of the *Schur decomposition*. Further descriptions on this issue can be found in [33, p. 473–478].

In our calculations we use a simple but effective method: As will be discussed in the following, we are mainly interested in calculating the ground-state energy ε_0 (i. e. the smallest eigenvalue) of the Hamiltonian matrix H. We therefore observe the convergence of this value directly.

Rounding errors

The rounding errors of the Lanczos vectors lead to a loss of orthogonality amongst each other. In such a case so-called *ghost eigenvalues* may occur when diagonalizing the tridiagonal matrix T. We already know that after every Lanczos step each eigenvalue of the matrix T becomes a better approximation for every eigenvalue of the original matrix H. However, if many Lanczos steps are performed, multiple eigenvalues of the tridiagonal matrix may approximate the same eigenvalue of matrix H, which is the reason why they are called *ghosts*. This effect is very annoying if one wants to determine *all* eigenvalues of H with a negligible rounding error but makes no difference if one is just interested in the smallest and highest eigenvalue. The reason for this is the fact that after a huge number of Lanczos steps all ghosts either approximate the smallest or the biggest eigenvalue of H. For treating this kind of problems many solutions have been proposed in the past, whereas the *implicitly restarted Lanczos method* [34] may be worth mentioning.

As a general rule, for the smallest eigenvalues very good convergence is achieved already after a few Lanczos steps, even before any ghosts occur. Therefore, the loss of orthogonality represents no real restriction, and we obtain very good results if we concentrate on the ground-state and the first-excited-state energies only.

3.4.2 Computational Implementation

We now want to take a closer look at the computational implementation of the Lanczos method and the way in which we conduct the complete diagonalization of matrix H. We can describe the whole implementation in four steps:

(1) At first we perform the Lanczos interation several times, but with a somewhat changed

algorithm. This is because of the fact, that the three-step recursion formula from Eq. (3.11) can be implemented in a numerical calculation just by storing two vectors which is very important for reducing the memory (see next section). Therefore, in our work we use the *exact arithmetic implementation* proposed in [33, p. 480] with a slightly different realization.

(2) After doing this the tridiagonal matrix is diagonalized using algorithms from the *Linear Algebra PACKage* (LAPACK), and the convergence of the ground-state energy is checked.

(3) If needed (1) and (2) are repeated as long as the ground-state energy reaches an accuracy of 10^{-14}.

(4) Once the ground-state energy is calculated we use a combined CG method with *inverse iteration* to obtain the ground-state eigenvector. This kind of combined method very well applies for largest and smallest eigenvalues corresponding to big sparse symmetric matrices. The explicit realization would go too far to be discussed here, so we refer to the original work presented in [35]. The ground-state eigenvector, unless otherwise stated, is calculated with an accuracy of 10^{-9}.

3.5 Remarks about Fortran

In this section we want to summarize some important aspects of numerical calculations that we encountered during our calculations. Subsequently we give an overview in chronological order, the task we have to do when programming a new program/subroutine.

Before starting any coding it proved to be useful to build up a framework and give thoughts to the overall number and properties of required variables. Apart from the fact that it can be helpful for other persons who study the same code, it becomes absolutely necessary when conducting very extensive and complex calculations. One important issue in this matter is the discussion about memory requirements. We explain this by an example: In Chapter 6 e. g. we conduct calculations with Hilbert space dimensions up to more than 30 millions. In the Lanczos iteration we have to save altogether four Lanczos vectors with this size (two from the iteration step, one temporary and one static initial vector). On the other hand, the diagonal term of the Hamiltonian matrix has the same size and we end up with five vectors with the same memory requirements (for simplicity reasons we neglect all other variables). Since we use "double precision" ($\hat{=}$ 8 bytes memory for one number) we can estimate the total memory demand as follows:

$$\text{MEMORY} \approx 30,000,000 \times 5 \times 8\,\text{bytes} = 1,2 \cdot 10^9\,\text{bytes} \approx 1\,\text{GB}.$$

This means, we need around 1 GB available working memory just for the above variables and one has to be very careful to keep the number of declared variables as small as possible.

Another point is the "connection" with subroutines. One may get a *stack overflow*[9] if too many variables are handed over to a subroutine and vice versa. This affects mostly recursive subroutines, which is the reason why many textbooks suggest a strict iterative[10] programming. We also encountered memory problems when using *modules* which will be avoided if all variables are distributed smartly within multiple *modules*. So it is suggested to make a clever use of *static* and *dynamic* variable declaration which can be done efficiently with the use of *parameters*. We also strongly suggest to use "implicit none" in every program unit. Although the effort seems high, it is very helpful for eventual failure searches.

Probably the most important point in FORTRAN 90/95 is the fact that elements are saved columnwise into multidimensional arrays (like matrices). This is very important when writing routines that involve matrix multiplications etc. By taking care of this fact one can optimize the algorithms up to 80% and more.

When exporting data to external files it is suggested to export (unformated) *binary* files because this is the fastest way. In our work we used binary files for the communication between FORTRAN 90/95 and MATLAB to create data plots. Our method is well described in Appendix A.3.

Concluding, one also has to be very careful when using different compilers. On the one hand, the numerical results may vary in the last few digits (due to their internal architectures). On the other hand, some compilers demand a more "strict language" than others. When treating very complex algorithms one may also make use of MPI (message passing interface) for multi-core programming and/or turn to newer (object-oriented) versions of Fortran (such as Fortran 2003). However, for our calculations this was not necessary, and even the longest set of calculations took less than 24h (distributed on four nodes).

[9] Stack memory is the temporary memory used for the communication between program units.

[10] Theory states that any recursive program can be realized iteratively, often however, with an enormous increase of complexity.

Chapter 4

Introductory 1D Problems

At first the one-band Hubbard model [Eq. (2.30) from Sec. 2.6.1] was studied on 1D six- and eight-site clusters with periodic boundary conditions. Although not of particular physical interest, these initial calculations proved very useful for the latter work. On the one hand they helped to make familiar with the numerical methods and to develop an efficient "work routine." On the other hand they revealed some problems with the used algorithm which had to be considered from then on. Here we only present the results for the eight-site cluster and summarize the most important facts.

We calculated spin and charge correlation functions as well as spin and charge structure factors for Hubbard-U varying from 0 to 16 in units of the hopping integral t. The eight-site cluster was examined at half-filling (i. e. where the number of electrons is equal to the number of cluster sites) with equal number of spin $\uparrow$ and $\downarrow$ electrons, and all subsequent discussions relate to the quantum-mechanical ground state of the system.

The spin correlation functions $< S_i^z \, S_j^z >$ and charge correlation functions $< n_i n_j >$ in dependency on different Hubbard-U values are plotted in Figs. 4.1 and 4.2, respectively, and depict correlations between cluster site 0 and all other cluster sites. Similarly, the spin structure factor $S(q)$ and charge structure factor $N(q)$ are shown in Figs. 4.3 and 4.4. Finally, both quantities are compared for $q = \pi$ in Fig. 4.5.

It was observed that an increase of the Hubbard on-site energy U leads to a staggered spin correlation function with alternating sign (as can be seen in Fig. 4.1) which converges very fast for $U > 6$. Physically, this fact corresponds to a strong antiferromagnetic state with long-range order and can be compared directly with results from [22].

Similar convergent behavior is also visible from the charge correlation function depicted in Fig. 4.2 leading to a uniform distribution of electrons within the eight-site cluster when U is increased. Both, spin and charge correlation functions, show a periodic behavior due to periodic boundary conditions. However, the strict periodicity is not maintained for $U = 0$, which can be explained by the fact that for $U = 0$ various electron distributions exist which all correspond to the ground state. In such a case the ground-state wave function is heavily

dependent on the initial vector in the Lanczos diagonalization, which could also be proved by our calculations.

The spin and charge structure factors in Figs. 4.3 and 4.4 confirm our discussion so far, since the peak for $q = \pi$ in Fig. 4.3 means an oscillating spin correlation (antiferromagnetic) related to the real lattice. On the other hand, the function's behavior in Fig. 4.4 represents a decrease of all charge fluctuations and thus corresponds to a uniform electron distribution within the cluster.

Finally, in Fig. 4.5, both are plotted in dependency on U for $q = \pi$, where it is visible that for increasing U both converge towards fixed values.

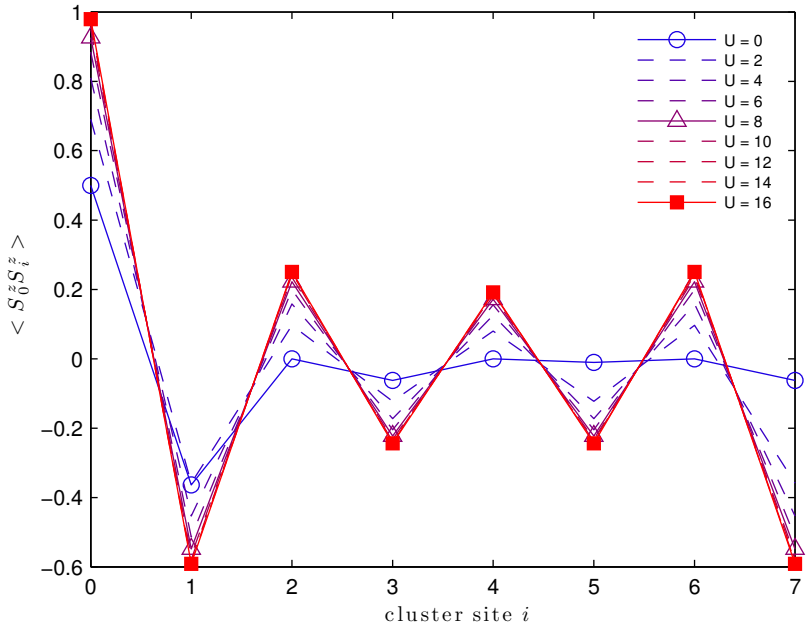

Figure 4.1. Spin correlation functions between cluster site 0 and i for different Hubbard-U (in units of t) on a one-dimensional eight-site cluster.

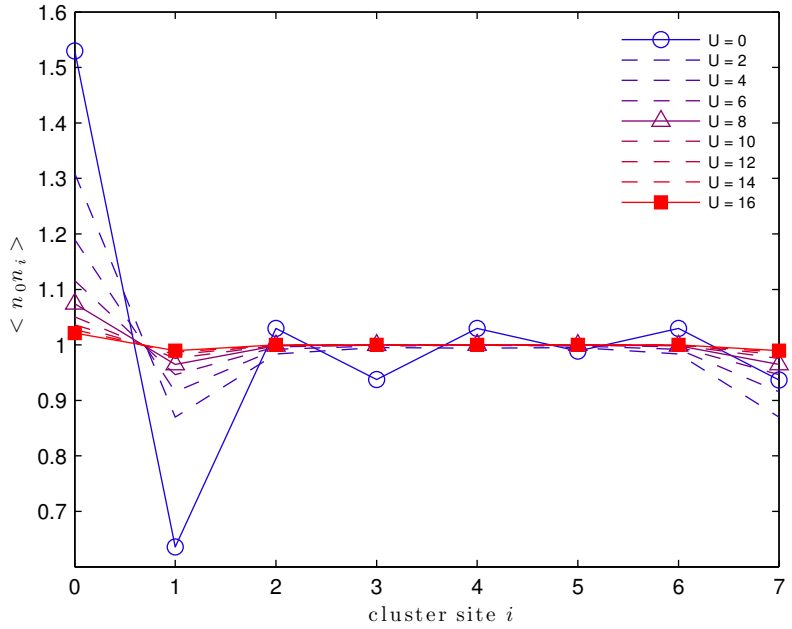

Figure 4.2. Charge correlation functions between cluster site 0 and i for different Hubbard-U (in units of t) on a one-dimensional eight-site cluster.

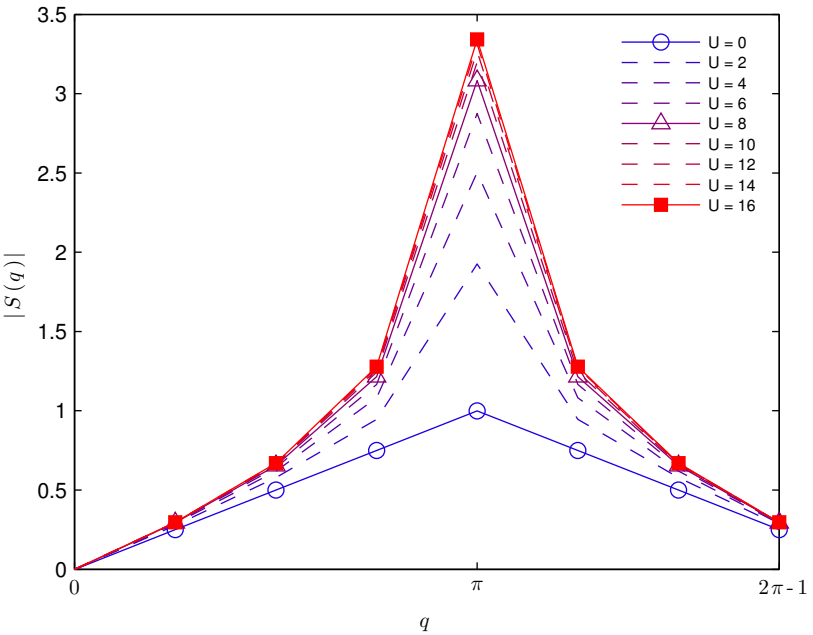

Figure 4.3. Spin structure factor for a one-dimensional eight-site cluster in dependency on different reciprocal lattice vectors $\mathbf{q}$ (more precisely q_x) and Hubbard-U (in units of t). For computational reasons, the absolute value of the spin structure factor is plotted.

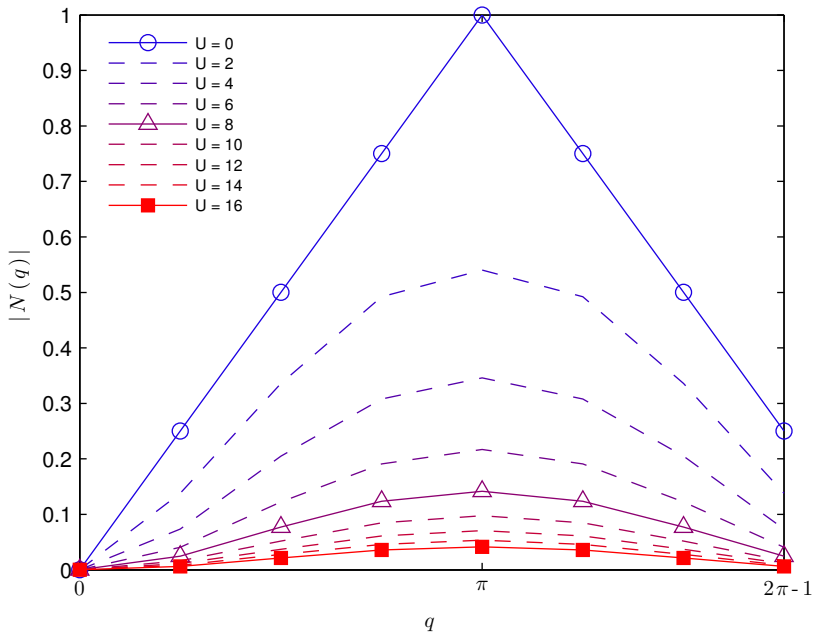

Figure 4.4. Charge structure factor for a one-dimensional eight-site cluster in dependency on different reciprocal lattice vectors **q** (more precisely q_x) and Hubbard-U (in units of t). For computational reasons, the absolute value of the charge structure factor is plotted.

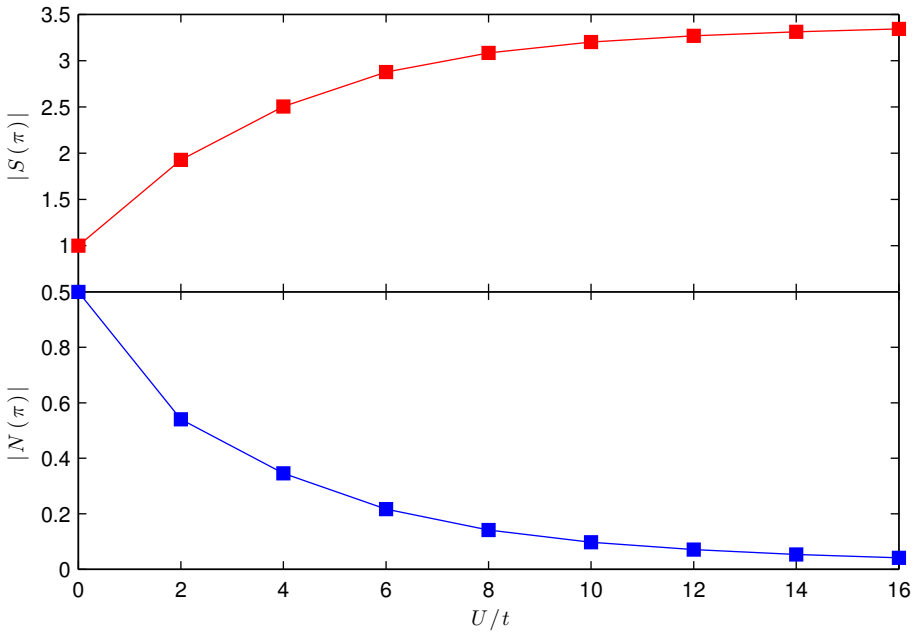

Figure 4.5. Spin and charge structure factors for $q = \pi$ in dependency on different Hubbard-U (in units of t).

Chapter 5

Magnetic Properties of Individual Carbon Clusters

5.1 Introduction

The interest in carbon nanostructures nowadays expands over most science areas and is still growing. Due to the fact that Carbon forms many different crystal structures with different coordination numbers ranging from two to four (with different bond angles) and thus forming materials with different physical properties, many questions are still unanswered. One, for example, is the discussion about three-dimensional carbon clusters with $N \sim 10$ atoms concerning the formation of stable and metastable states. [1]

Recently, experimental reports on magnetic carbon opened up a whole new sphere of interest, questioning the existence of "new" magnetic materials made of light elements (such as carbon). On the other hand, many new theoretical studies were started as an attempt to give theoretical explanations for these phenomenons. In this direction, the authors of [2] investigated all sp^2 carbon species with $N = 10 - 14$ using many-body schemes. By performing a single-band Hubbard model approach in connection with Lanczos diagonalization method for obtaining ground-state energies and wave functions, they found that these clusters could exhibit spin switching when the electron-electron interaction is increased, i. e. a transition from singlet to triplet states.

With reference to [2] it was the aim of the present work to give these results a more detailed review and conduct further investigations on the properties of some of these carbon clusters.

Therefore we investigated all sp^2 carbon clusters with 10 atoms and one π-electron per atom with an extended Hubbard model approach in connection with Lanczos diagonalization method and conducted further calculations treating the quantum-mechanical stability of our results.

5.2 Structures and Properties

For carbon clusters with ten atoms being connected by sp^2 hybridized bonds (corresponding to three coordinate atoms) nine different isomers exist, as discussed in [2]. In the following we adopt the same formalism and nomenclature as in [2] and refer to Fig. 5.1 for explicit cluster structures.

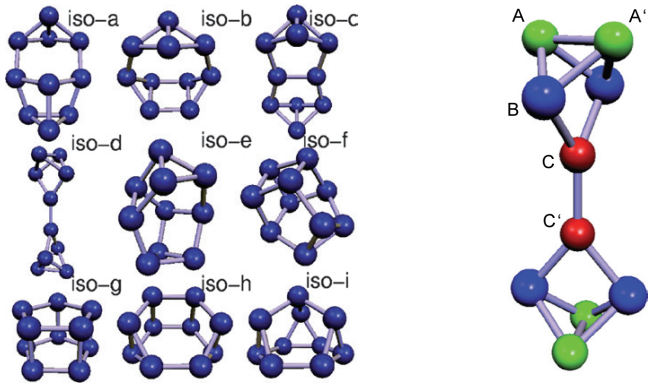

Figure 5.1. Crystal structures of investigated carbon isomers: **(a)** shows all structure types with ten atoms; and **(b)** describes the isomer "iso-d" in detail. Both graphics are adopted as they stand from [2].

In order to prove the functionality of the used algorithms, we first checked the results from [2], particularly those for isomer "iso-d." In Fig. 5.2 the results for the local magnetic moment[11] $\mathbf{S}_i^2$, the on-site charge density n_i, the bond-order density matrix element ρ_{ij} and the spin correlation function $< \mathbf{S}_i \, \mathbf{S}_j >$ are plotted which can be directly compared with Fig. 2 from [2]. The cluster site variables i and j are substituted by A, B, C etc. corresponding to Fig. 5.1(b).

We found that all four quantities are exactly the same, except region $1.0 < U/t < 1.5$ in Fig. 5.2(a) and 5.2(b), where another discontinuity in the curve of site B (at $U/t \sim 1.2$) is missing. This fact, however, has no practical relevance and we can neglect it in our further discussion.

In Fig. 5.3 the total spin is plotted in dependency of the Hubbard-U, where it is visible that "iso-d" exhibits a triplet state in a particular U-region. Without going into further details, one can summarize that all quantities exhibit an abrupt change for the U-region, where the total spin S switches from 0 to 1.

[11] It shall be noted that, previously, the local magnetic moment was defined by the z-component of the spin operator: $< (S_i^z)^2 >$. For consistency reasons, however, we follow the somewhat different definition from [2].

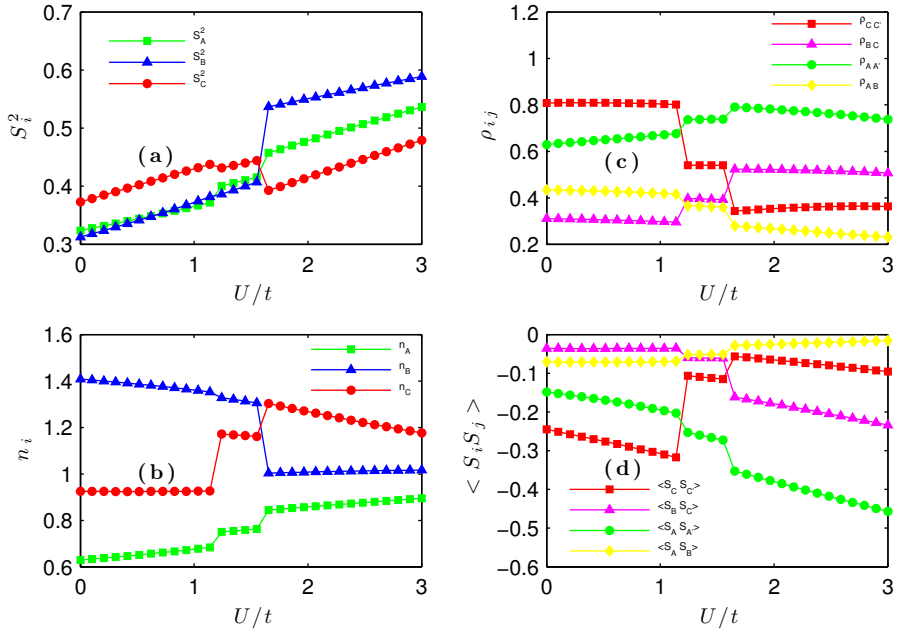

Figure 5.2. Ground-state properties of isomer "iso-d" and one π-electron per atom as a function of the Hubbard-U (in units of the hopping integral t): **(a)** shows the local magnetic moment S_i^2; **(b)** on-site charge density n_i; **(c)** bond-order density matrix element ρ_{ij}; and **(d)** the spin correlation function $< \mathsf{S}_i \, \mathsf{S}_j >$. The bond names correspond to the nomenclature in Fig. 5.1(b).

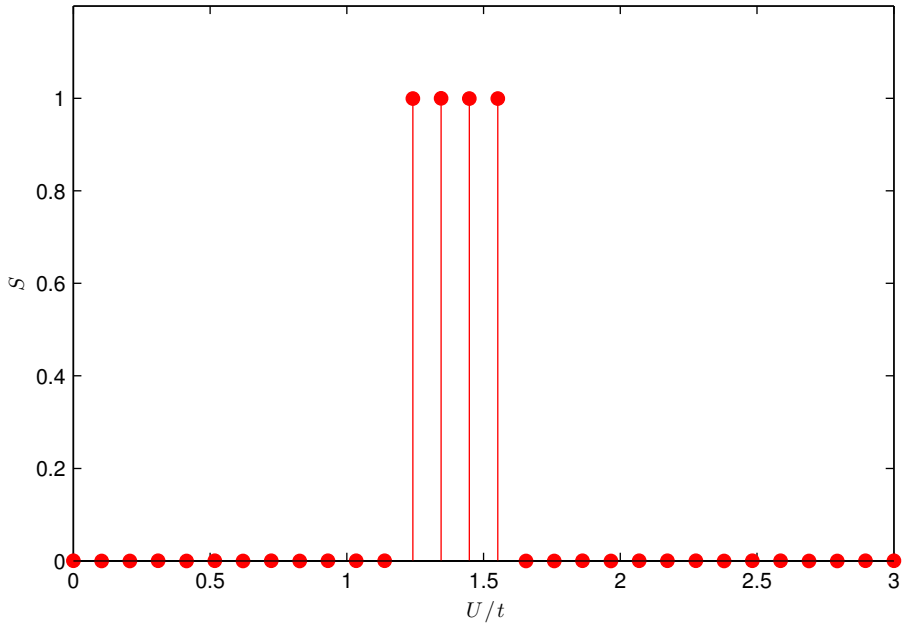

Figure 5.3. Total spin of isomer "iso-d" as a function of the Hubbard-U (in units of the hopping integral t). As visible, for particular U the cluster exhibits a triplet state.

5.3 Extended Hubbard Model Approach

5.3.1 Ground-State Properties of "iso-d"

For consistency reasons, the extended Hubbard model is first studied on isomer "iso-d" with one π-electron per atom. All quantities from Figs. 5.2 and 5.3 that are related to this crystal type are calculated for different values of the nearest neighbor (n.n.) Coulomb interaction V (in the following named "Hubbard-V").

While performing the first calculations we observed that different choices of the Lanczos initial vector may cause different energies and eigenstates. Therefore, the author conducted a whole series of tests related to all kinds of different starting vectors. These tests proved that without any doubt all initial vectors chosen *randomly* produce the same energies and eigenstates. The only difference that may occur relates to initial vectors that describe *uniformly* distributed basis states (i. e. where all basis states have the same coefficient). In most of the cases *uniform* initial vectors yield excited states and therefore seldom describe the same states that are obtained with *random* ones. On the other hand, in the Lanczos algorithm without *reorthogonalization* the eigenvalues related to excited states become equal to the ones related to the ground state if a significant number of Lanczos steps is performed. The strategy now is to calculate four eigenvalues with the Lanczos method, namely the two lowest eigenvalues related to an *arbitrary* initial vector and an *uniform* one. With this method, when comparing the results, one can make sure that the obtained "ground state" indeed corresponds to the lowest eigenvalue (i. e. ground-state energy), and one can also determine the first excited state with very high certainty. Subsequently this method is applied to all problems.

The local magnetic moment $\mathbf{S}_i^2$ (Fig. 5.4), the on-site charge density n_i (Fig. 5.5), the bond-order density matrix element ρ_{ij} (Fig. 5.6), the spin correlation function $< \mathbf{S}_i \, \mathbf{S}_j >$ (Fig. 5.7) and the total spin S (Fig. 5.8) are plotted for different Hubbard-U and Hubbard-V values. Like before, the cluster site variables i and j are replaced by A, B, C etc. according to the nomenclature in Fig. 5.1(b).

The most obvious effect for $V \neq 0$ is the destruction of the triplet ground state (as visible in Fig. 5.8. Specifically, the "critical" region ($1.0 < U/t < 1.5$) with two discontinuities for all quantities mentioned above disappears, and one can observe an overall decrease of the local magnetic moment (Fig. 5.4) towards constant values. The same effect is described in [2], however with increasing U-values, and can be interpreted as charge correlations dominating over spin correlations. This fact is also visible in Fig. 5.5, where an increase of Hubbard-V causes a different charge distribution within the carbon cluster, as well as in Fig. 5.7 where an increase of V "destroys" all spin correlations.

Concerning the density-matrix elements in Fig. 5.6, the drastic decrease of $\rho_{CC'}$ (green line with "square"-symbols) completely disappears with increasing V-values. In [2] it is argued that a decrease of this quantity means an increase of the bond length that connects the two cluster parts (C and C') of isomer "iso-d," and thus is responsible for the triplet ground state. Therefore we can state that for $V \neq 0$ the bond length decreases, which

represents a stronger binding of the involved atoms. This fact, on the other hand, has to do with the "stability" of the triplet ground state, which, as we show, is not very stable for "iso-d" (see following section).

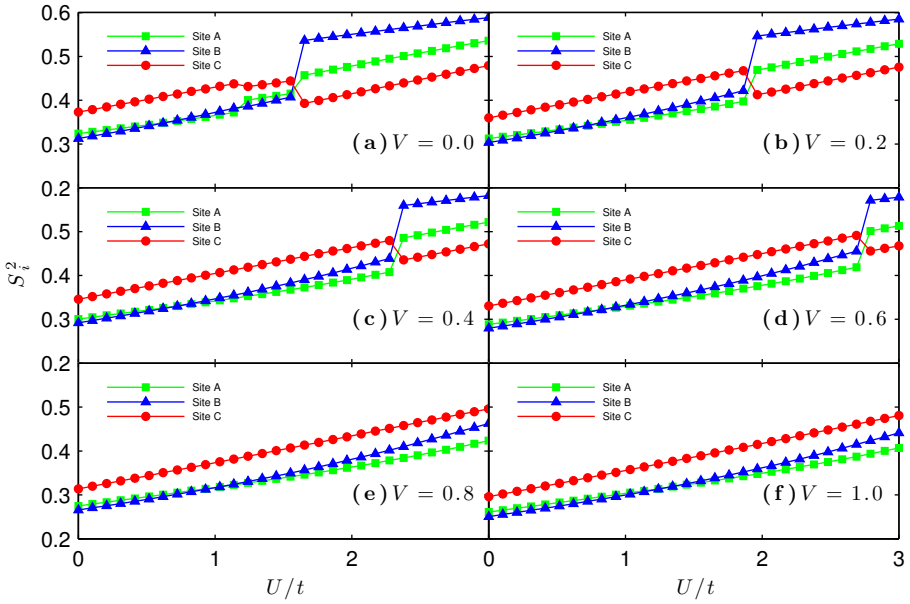

Figure 5.4. Local magnetic moment $\mathbf{S}_i^2$ on cluster sites A, B and C in dependency on various Hubbard-V and Hubbard-U values for isomer "iso-d."

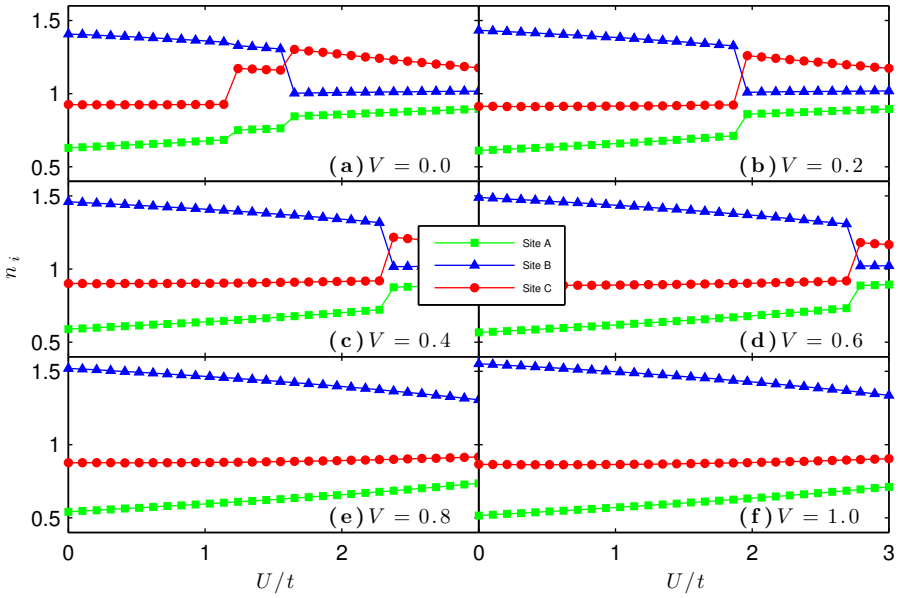

Figure 5.5. On-site charge density n_i on cluster sites A, B and C in dependency on various Hubbard-V and Hubbard-U values for isomer "iso-d."

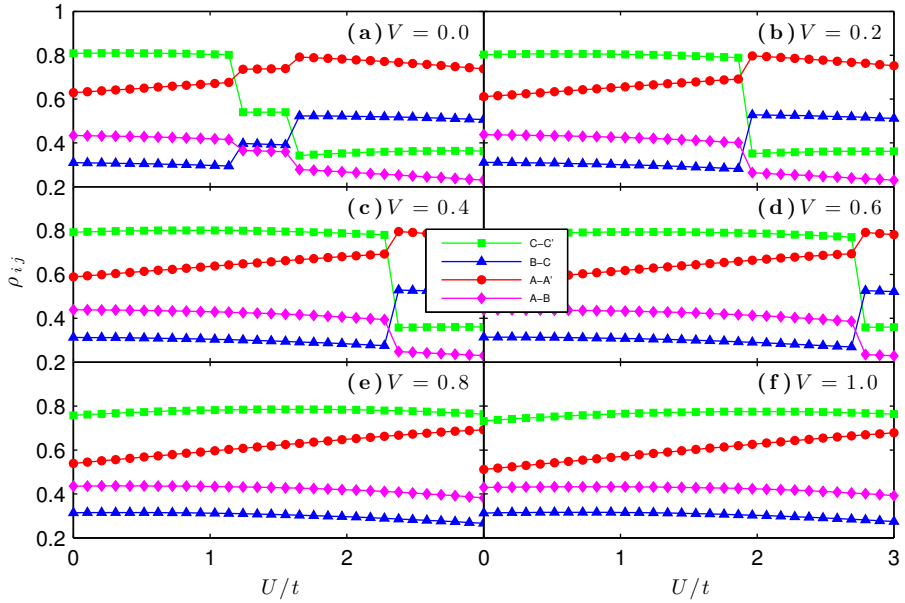

Figure 5.6. Bond-order density matrix element ρ_{ij} (with $i, j \hat{=}$ A, A', B, C and C') in dependency on various Hubbard-V and Hubbard-U values for isomer "iso-d."

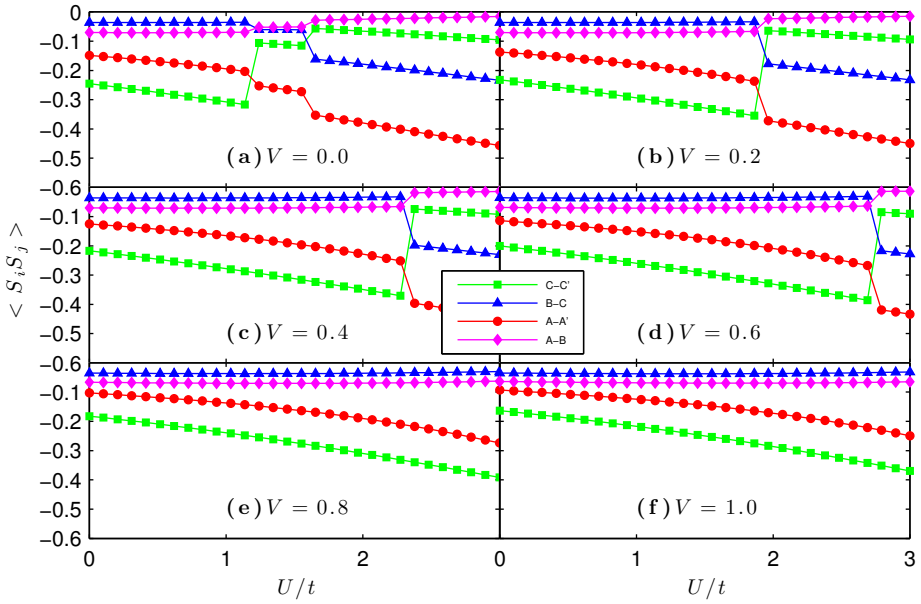

Figure 5.7. Spin correlation function $< \mathbf{S}_i \, \mathbf{S}_j >$ (with $i, j \hat{=}$ A, A', B, C and C') in dependency on various Hubbard-V and Hubbard-U values for isomer "iso-d."

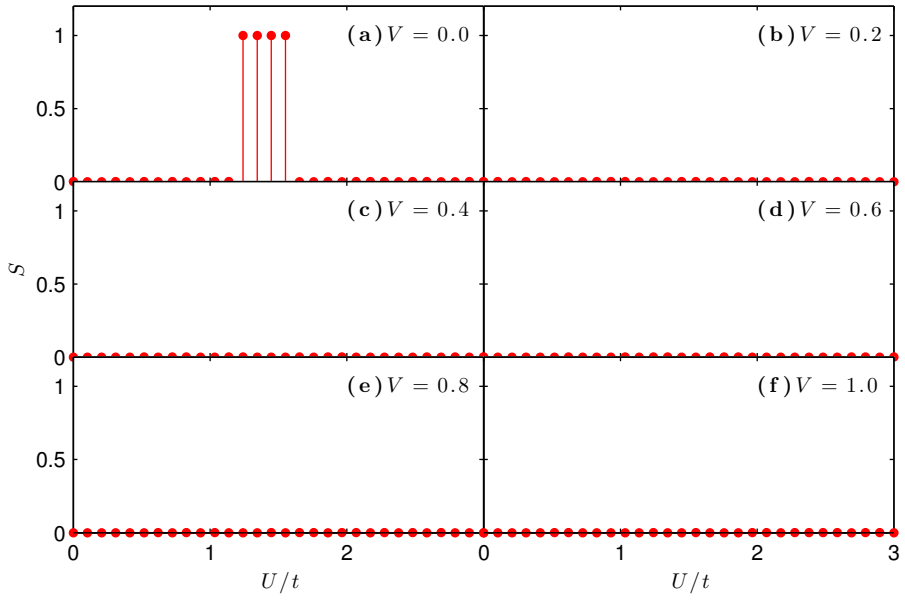

Figure 5.8. Total spin S for different Hubbard-V in dependency on various Hubbard-V and Hubbard-U values for isomer "iso-d."

5.3.2 Total Spin Calculations

Since we are interested in the forming of the triplet ground state and its quantum-mechanical stability, the scope of the following discussion is mainly focused on the total spin value S. Besides, with the strategy from before, the ground state and the first excited state were calculated for all sp^2 carbon species with one π-electron per atom and for different U- and V-values. It was observed that the first excited state in all cases is not a triplet state any more, and most triplet ground states become singlet states for $V \neq 0$. For some species, however, the triplet ground state is maintained also for increasing V-values. Therefore, the most interesting subject of our discussion is the energy difference $\Delta E := E_0 - E_1$ between the (triplet) ground-state energy E_0 and the (singlet) first-excited-state energy E_1 in dependency on U and V. This means that for e. g. a big value ΔE one must apply a higher energy to "destroy" the triplet state by displacing the system to an excited state. A small value of ΔE, on the other hand, means that only a small energy amount is required for "destroying" the triplet state. This is why ΔE offers a direct insight in the stability of the (triplet) ground state.

The first interesting result is that isomer "iso-a" exhibits a triplet ground state when $V = 0.6$ with a rather high stability (as can be seen in Fig. 5.9), although no such ground states for smaller V-values can be seen.

For "iso-d," as previously discussed in great detail, an increase of V "destroys" the triplet ground state (see Fig. 5.10). On the other hand, this can also be explained by the energy difference plot. Since the energy difference in the same figure is rather small, one can already assume that this ground state is not very stable. It should also be mentioned that the peaks in Figs. 5.9 and 5.10 where $\Delta E \equiv 0$, depict ghost eigenvalues as discussed before. Although they represent failures in the calculation, the author left them unchanged to illustrate the problems discussed before. However, they can be eliminated easily, as it was done in all succeeding plots.

For "iso-e" (see Fig. 5.11) the triplet ground state is maintained for small V-values, however the energy difference ΔE rapidly becomes smaller and thus the ground state is not very stable.

For "iso-f" the behaviors are the same as for "iso-d," therefore it was not considered necessary to plot its results explicitly.

For "iso-g" (Fig. 5.12) we observed probably the most interesting properties. With increasing V-values the triplet ground states expand over wider U-regions, and also the energy difference ΔE becomes bigger if V is increased. Both facts may indicate a very stable triplet ground state for this structure type.

Finally, for "iso-h" (Fig. 5.13) and "iso-i" (Fig. 5.14) the triplet ground state is also maintained for increasing V-values and there is only a slight decrease of the energy difference ΔE, which may also imply a rather high stability.

For isomer "iso-b" and "iso-c" no triplet ground state was found.

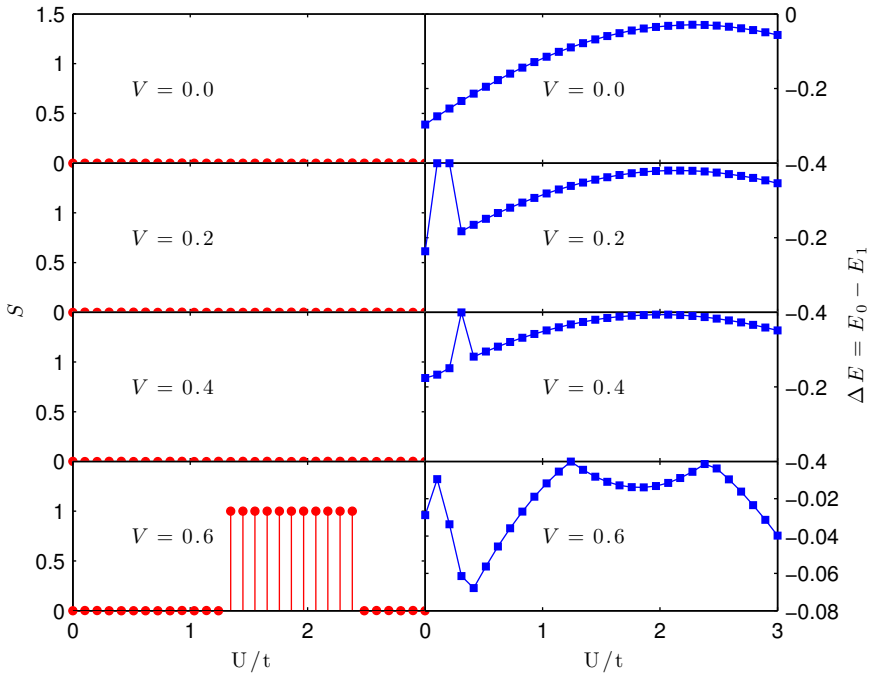

Figure 5.9. Total spin S and energy difference ΔE between the ground-state (E_0) and the first-excited-state (E_1) energies for isomer "iso-a." The peaks, where $\Delta E \equiv 0$, depict problems with ghost eigenvalues and intentionally are left unchanged for illustrating reasons.

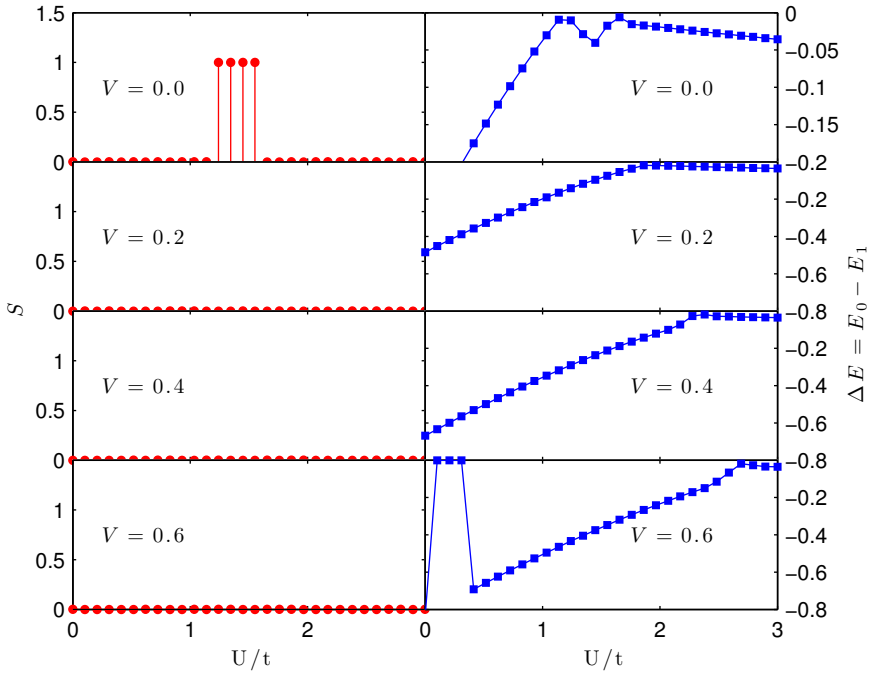

Figure 5.10. Total spin S and energy difference ΔE between the ground-state (E_0) and the first-excited-state (E_1) energies for isomer "iso-d." The peaks, where $\Delta E \equiv 0$, depict problems with ghost eigenvalues and intentionally are left unchanged for illustrating reasons.

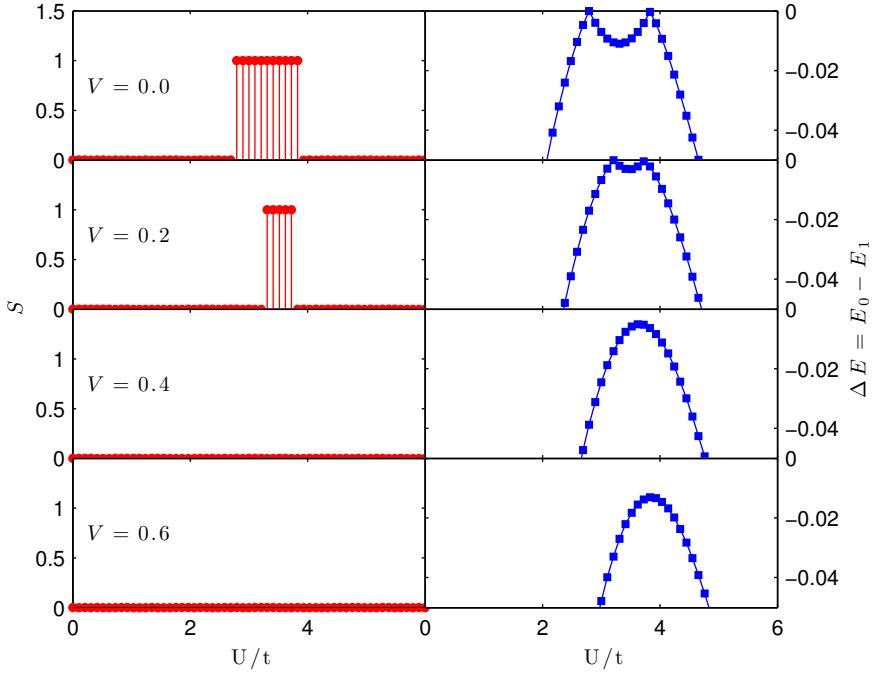

Figure 5.11. Total spin S and energy difference ΔE between the ground-state (E_0) and the first-excited-state (E_1) energies for isomer "iso-e."

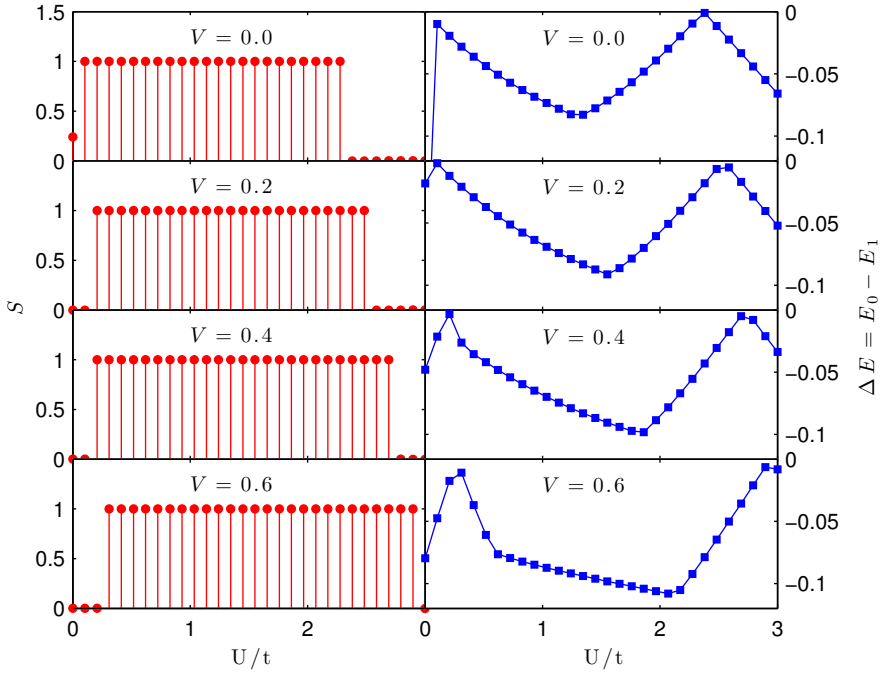

Figure 5.12. Total spin S and energy difference ΔE between the ground-state (E_0) and the first-excited-state (E_1) energies for isomer "iso-g."

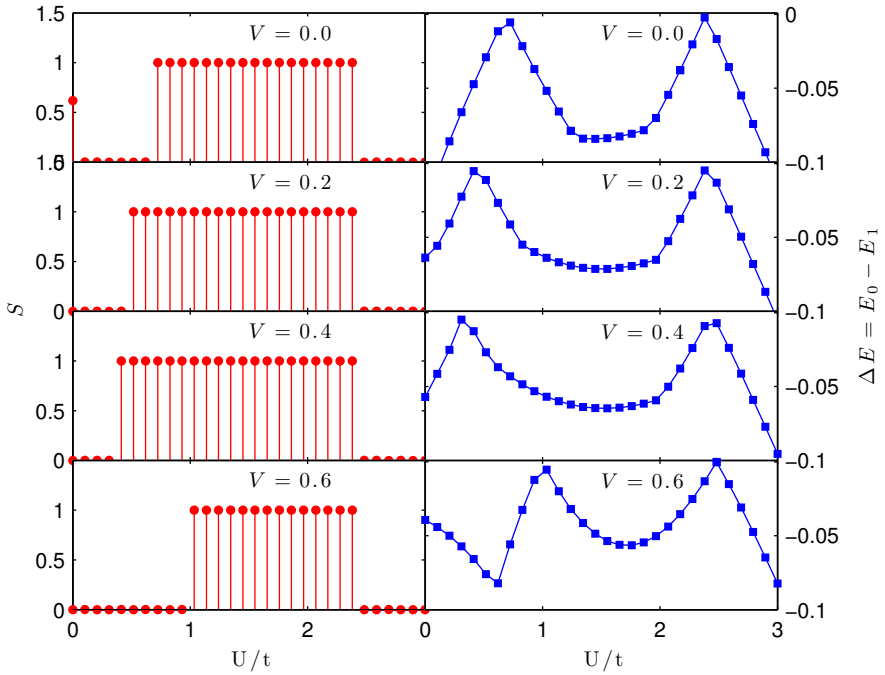

Figure 5.13. Total spin S and energy difference ΔE between the ground-state (E_0) and the first-excited-state (E_1) energies for isomer "iso-h."

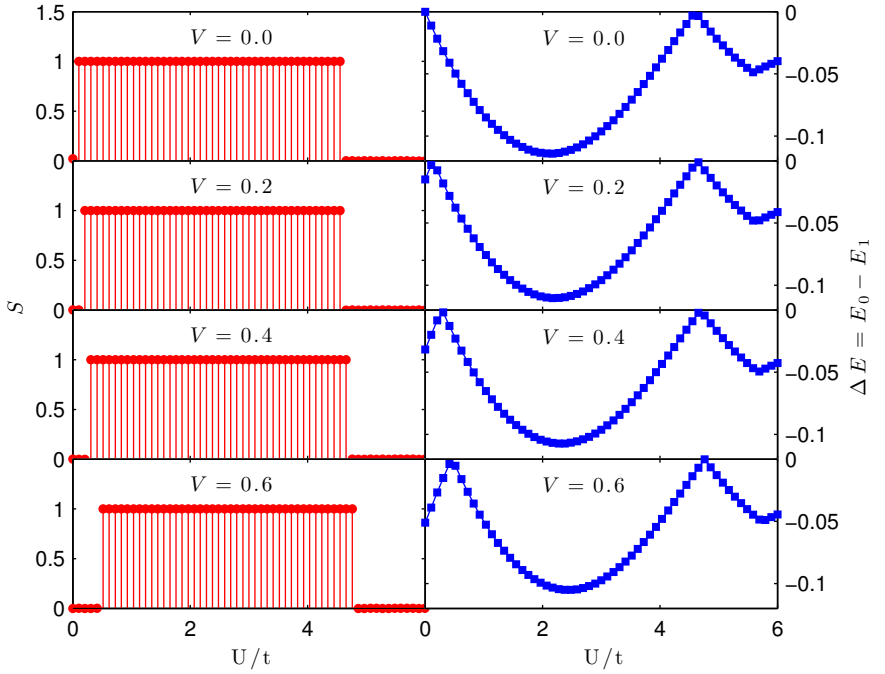

Figure 5.14. Total spin S and energy difference ΔE between the ground-state (E_0) and the first-excited-state (E_1) energies for isomer "iso-i."

5.4 Conclusions

Since we still have no real experimental comparison for previously discussed carbon clusters, we are unable to predict and characterize their existence and real electrical and magnetic properties, respectively. As a preliminary attempt to do so on a theoretical base, we plotted the ground-state energies of these carbon clusters in dependency on different U-values, as shown in Fig. 5.15.

When comparing these ground-state energy curves, one can observe immediately that the isomers "iso-g" and "iso-h," for which the triplet ground state is maintained for increasing V-values, are situated in a rather high position in the subjacent diagram. This fact does not only mean a higher ground-state energy compared to other species, but also reduces the probability that these crystal structures may be synthesized in reality, since other configurations are energetically more favorable. The latter argument, however, is only valid if other contributions to the energy (such as the lattice) can be neglected or if the electrons' contribution to the energy represents the most dominating part.

The same argumentation applies for isomer "iso-i" which has the lowest ground-state energy of all these species for $U > 1.2$. Here we can conclude that the electrons' contributions are responsible for forming a (rather stable) triplet ground state. Following previous discussion, the synthesizing of this material may be the most probable if the electrons' contribution to the energy is most dominating or if other energy contributions are negligible.

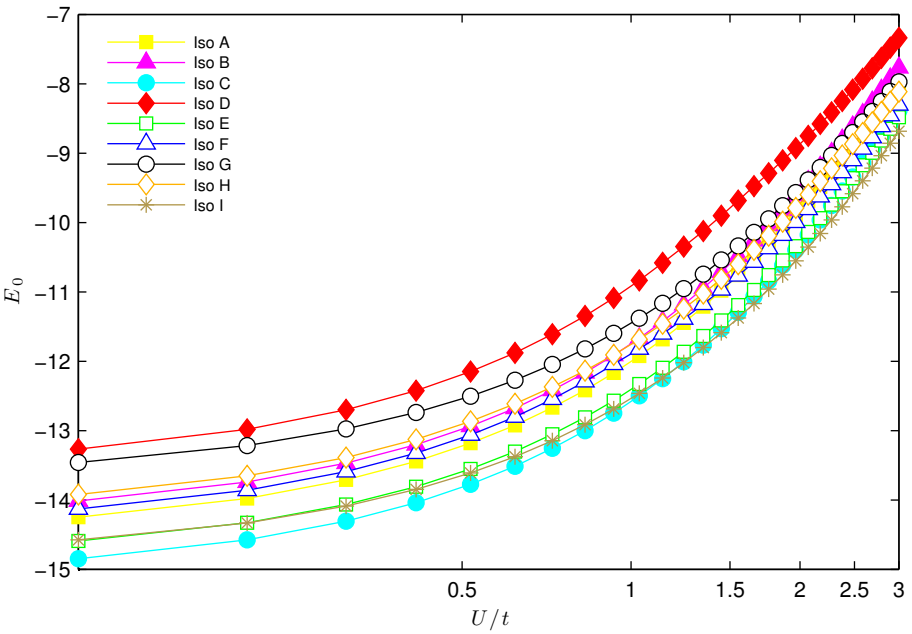

Figure 5.15. Ground-state energies of all sp^2 carbon species in dependency on different U-values. For a better distinction of curves belonging to different carbon species, the abscissa was chosen logarithmic.

Chapter 6

Electron-Phonon Interaction in a 1D CuO-Chain

6.1 Introduction

After decades of intense research and the publishing of an enormous number of scientific articles the explicit mechanism responsible for superconductivity in high-T_c cuprates is still unknown. Although, initially, the interest in electron-phonon interaction (EPI) was rather high, but then it was concluded that its contribution may be too weak to explain superconductivity alone. Still, the phonon contribution to superconductivity in competition with strong electron correlations and anisotropy is still uncertain. However, there is now general agreement that phonons are important for many (other) properties, and a large number of distinctive features of high-T_c cuprates has been examined by now. Recently, the angular resolved photoemission spectroscopy (ARPES) has been a very important tool accompanying these discussions. ARPES represents a powerful method to gain experimental comparisons of results. Indeed, the evidence for strong EPI as well as for many other effects that are not discussed here were provided by ARPES. [3–5]

For a computational many-body treatment of cuprates, the simplest approximation suggests considering a single CuO_2 plane. The reason for this approximation is the fact that the main physics of cuprates takes place in CuO_2 planes and that the planes among each other show relatively weak interplanar coupling. [3]

Further on, we follow the discussion from [4] and introduce another approximation by considering a one-dimensional CuO-chain with a periodic boundary condition (see Fig. 6.1). This simplification is justified by the fact that we limit ourselves to oxygen vibrations[12] only and thus primarily consider charge dynamics between copper and oxygen. Furthermore we can conduct calculations with smaller finite-size effects than with a two-dimensional model. Due to the important effects of the Coulomb interaction in cuprates [see 5] we study a multiband Hubbard model which enables a more detailed description of charge dynamics

[12] The reason for this "limitation" is that the oxygen ions are much lighter than the copper ions.

and interband effects. Such a model is well described in [3] for a two-dimensional CuO_2 plane. We adapt this model to the one-dimensional case and we can further neglect the hopping between two oxygen sites, which is regarded in the original paper. This is because in the 2D case the oxygen orbitals have a small but essential overlap, whereas in the 1D case they are far away from each other as visible from the graphic below.

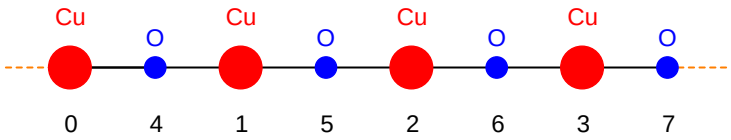

Figure 6.1. One-dimensional CuO-chain with eight atoms and numbering convention of cluster sites. The big (red) atoms denote four copper atoms (Cu) and the little (blue) atoms denote four oxygen atoms (O). Due to the periodic boundary condition cluster site 0 and 7 are connected with each other and electronic hopping is enabled.

For the CuO-chain in Fig. 6.1 we investigated two important phonon modes [see 3, 5]: on the one hand the axial (*buckling*) oxygen phonons describing a motion of oxygen atoms perpendicular to the CuO-chain; and on the other hand the in-plane (*breathing*) oxygen modes describing oxygens bond stretching and thereby changing bond lengths. Both phonon modes (depicted in Fig. 6.2) were treated separately to investigate their different effects. The corresponding Hamiltonians are presented in Sec. 2.6.3, whereas for the *breathing* case we adopt the following convention: in the case that the bond length between a copper atom and an oxygen atom increases, the parameter S_l in Eq. (2.33) is set to zero, but if the bond length decreases it is set to one. With this convention we follow the one of contemporary papers, although mathematically it represents no difference since both cases are studied equally.

For both cases we investigated different electron fillings: half-filling, one-hole and two-hole doping. This is mainly because in [5] it is suggested that different phonon modes show strong interaction with doped holes which we want to examine more detailed.

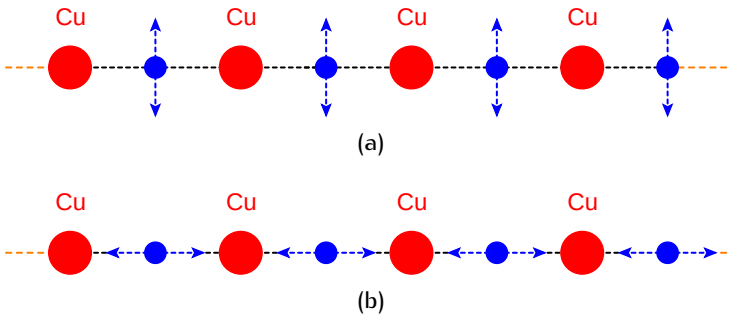

Figure 6.2. Two important phonon modes in a one-dimensional CuO-Chain: **(a)** blue arrows denote the axial (*buckling*) oxygen phonon modes; **(b)** blue arrows denote the in-plane (*breathing*) oxygen phonon modes.

6.2 Exact Numerical Solutions

Like before, we had to prove the functionality of the used algorithm related to the Hamiltonians from Eqs. (2.32) and (2.33) first. Since no articles exist treating the same problem that is being discussed in the following, we had no opportunity for a *direct* comparison. Therefore, the *indirect* proof was conducted in three steps:

(1) After implementing the routine for diagonalizing above Hamiltonian, we slightly changed the routine to make it comparable with accessible "exact" solutions from [36].

(2) After doing this successfully, the changes were set back, and we chose a simplified problem (i. e. where only a few of the constants and parameters were changed) that can be treated in a "semi-analytical" way.

(3) Finally, the constants and parameters again were set back, i. e. adapted to the problem of interest.

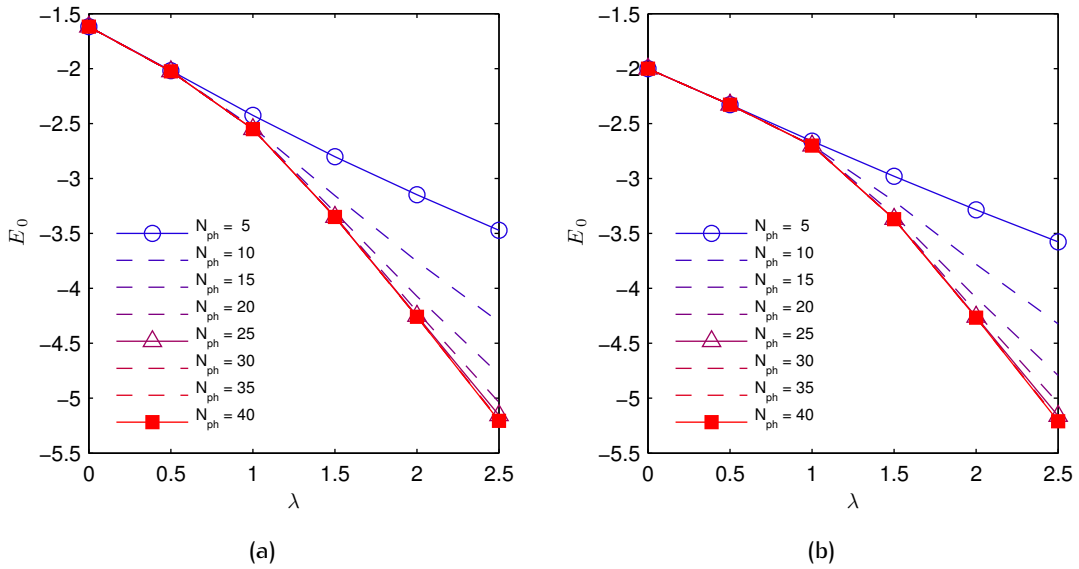

Figure 6.3. Ground-state energies of a four-site cluster corresponding to the Hamiltonian in Eq. (6.1) for different phonon numbers and boundary conditions: **(a)** describes the ground-state energy for *open* boundary condition in dependence on the canonical coupling constant λ; and **(b)** describes the ground-state energy for *periodic* boundary condition in dependence on the canonical coupling constant λ. Both energies are in units of the hopping integral t.

For carrying out (1) we used results from [36], where a model of two, four and six vibrating molecules coupled with one electron was solved using numerical diagonalization. Based

on this work, we concentrated on a four-site cluster with a maximum of 40 phonons treated with the Fröhlich Hamiltonian

$$H = -t \sum_{<i,j>} c_i^\dagger c_j + g\omega \sum_i c_i^\dagger c_i (d_i + d_i^\dagger) + \omega \sum_i d_i^\dagger d_i, \tag{6.1}$$

where t is the nearest-neighbor hopping integral, c_i, d_i are electron and phonon operators, g is a dimensionless interaction constant related to the canonical coupling constant $\lambda = g^2\omega/zt$ and z is a coordination lattice number with $z = 2$ for a one-dimensional chain. Here, the whole formalism as well as the Hamiltonian from Eq. (6.1) are adopted from [36].

Our results in Fig. 6.3 can be compared directly with Fig. 2 from [36] and show an exact agreement. It is also visible that convergence is reached for 25 to 30 phonons. However, it should be noted that in this simple case the phonons couple to one electron only. Therefore, for our succeeding calculations, we are still unable to predict the required number of phonons for reaching convergence since we treat more complex cases with coupling to more than four electrons at the same time.

For step (2) we used the CuO-chain from before, but reduced the problem to four atoms altogether, one electron and one or two phonons. For such a case the Hubbard matrix was calculated "by hand" (analytically) and diagonalized numerically with MATLAB (therefore this method is named "semi-analytical"). Subsequently the "reduced" CuO-chain was also implemented in the Lanczos diagonalization which meant only a slight change of parameters and constants. For both cases, the buckling as well as the breathing Hamiltonian, various parameters (Hubbard-U, electron-phonon coupling constant etc.) were tested and also showed exact agreement with the results obtained with MATLAB . For the sake of completeness all results are listed in tabular form in Appendix A.4.

After doing this, in step (3), the CuO-chain again was expanded to eight atoms and all parameters were set to their physical values.

6.3 Buckling Phonons

We first investigated the effects of buckling phonons with increasing electron-phonon interaction. We used the Hamiltonian from Eq. (2.32) and calculated for four different cases: 5, 10, 15 and 20 phonons. We used a "standard set" of parameters proposed in various previous works which are all listed in Tab. 6.1. For computational reasons we defined

$$\varepsilon := \varepsilon_p - \varepsilon_d \qquad \text{and} \qquad \varepsilon \longrightarrow \varepsilon_p$$

as the difference between oxygen and copper on-site energies which is the reason why the copper on-site energy ε_d is set to zero.

In the following the CuO-chain is treated separately with three different electron-hole fillings: half-filling (2 $\uparrow$, 2 $\downarrow$ electrons), one-hole doping (3 $\uparrow$, 2 $\downarrow$ electrons) and two-holes doping (3 $\uparrow$, 3 $\downarrow$ electrons). For these sets we calculated ground-state energies as well as all energy terms individually (such as kinetic energy etc.), charge densities, local magnetic momenta and spin correlations (z-components). All results are presented separately for each electron-hole filling.

Table 6.1. Parameters for buckling Hamiltonian in Eq. (2.32) .

ε_d	0.0
ε_p	3.0
U_d	6.0
ω	0.2
g_a	$0.0 - 1.0$

6.3.1 Half-filling

The following plots contain data for the *half-filling* case in dependence on the electron-phonon coupling constant g_a. The **ground-state energies** are plotted in Fig. 6.4 whereas different contributions to the energy (**energy terms**) are depicted in Fig. 6.5. The **charge densities** for copper and oxygen sites are plotted in Fig. 6.6 and the **local magnetic momenta** in Fig. 6.7. The **spin correlations** for nearest neighbor (n.n.) and next nearest neighbor copper sites are depicted in Fig. 6.8.

It is clear that with increasing phonon influence (bigger overall phonon number and electron-phonon coupling) the ground-state energies are lowered (Fig. 6.4), however even with 20 phonons no convergence for the ground-state energies is reached.

The increase of phonon influence also leads to an increase of the kinetic energy (as shown in Fig. 6.5) which is evident only at stronger coupling ($g_a > 0.4$). As expected, with increasing phonon numbers and coupling the electron-phonon interaction and phonon energy are also increased while the electrical potential is slightly decreased.

With increased phonon influence we observe a charge transfer from oxygen to copper atoms, and very good convergence for charge densities seems to be reached for 20 phonons (as visible in Fig. 6.6). As a result the local magnetic momenta on copper sites are increased whereas they are decreased (almost suppressed) on oxygen sites (visible in Fig. 6.7).

We also observe a weak antiferromagnetic solution with long-range order which becomes stronger with increased phonon influence (visible in Fig. 6.8).

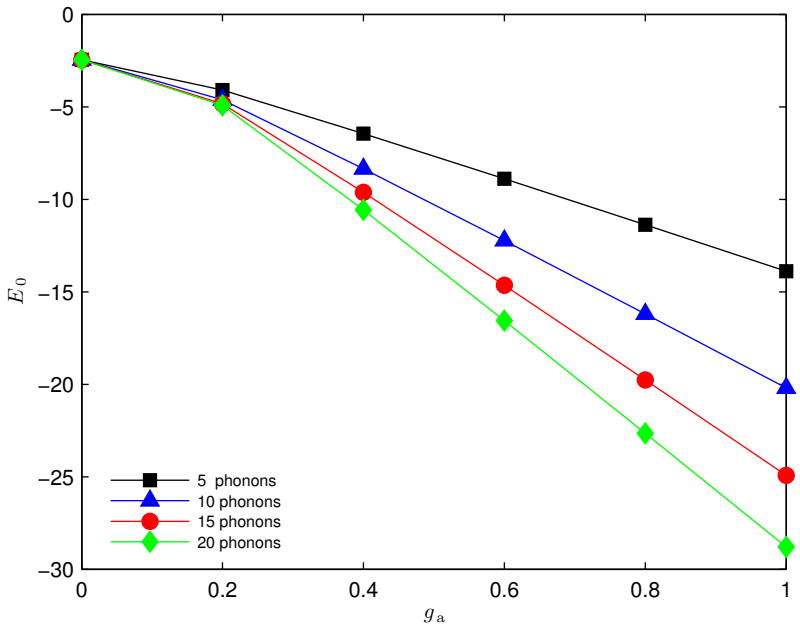

Figure 6.4. Ground-state energies for different *buckling* phonon numbers at half-filling (2 spin ↑ and 2 spin ↓ electrons).

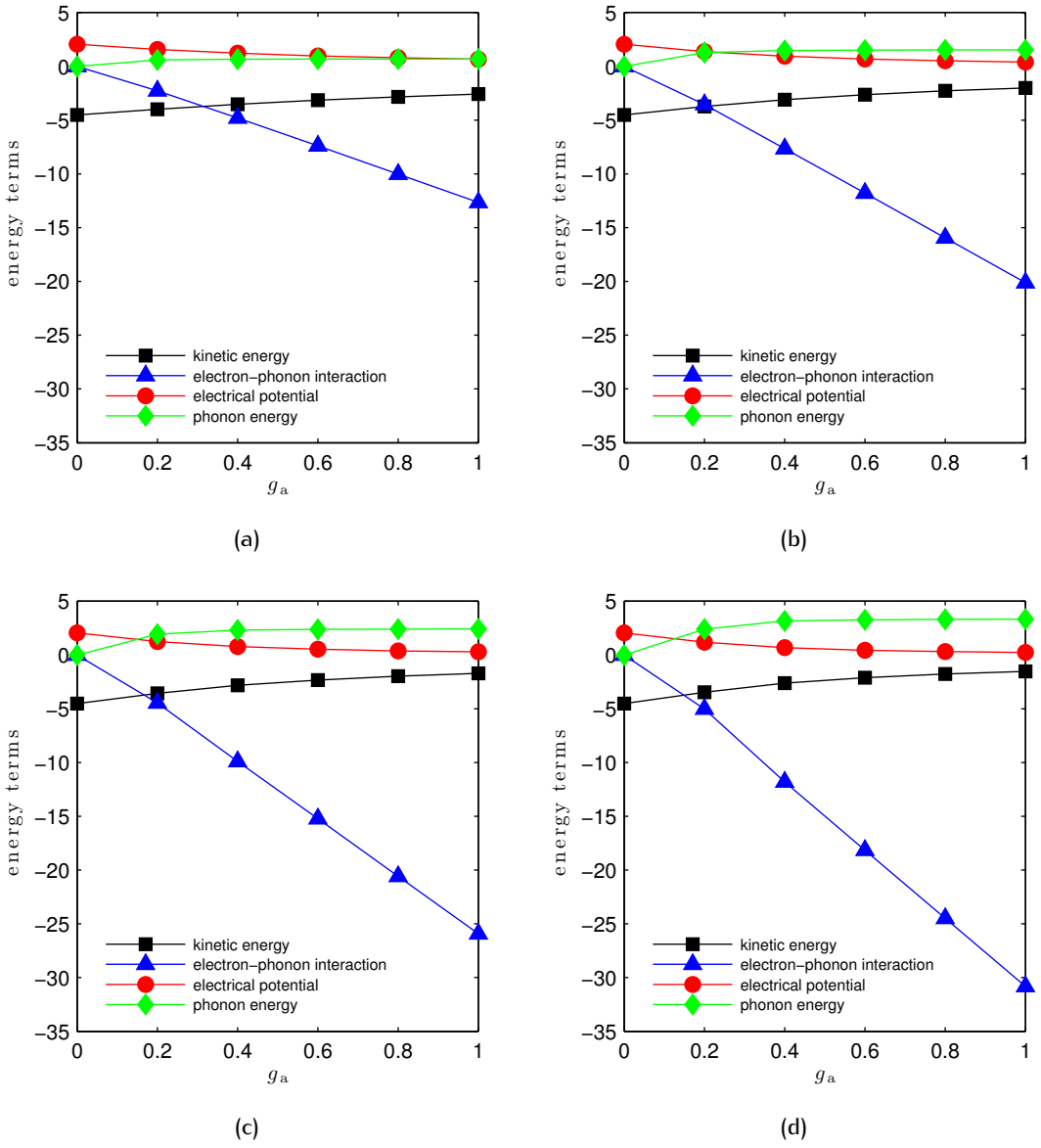

Figure 6.5. Energy terms for different *buckling* phonon numbers at half-filling (2 spin ↑ and 2 spin ↓ electrons): **(a)** 5 phonons; **(b)** 10 phonons; **(c)** 15 phonons; **(d)** 20 phonons.

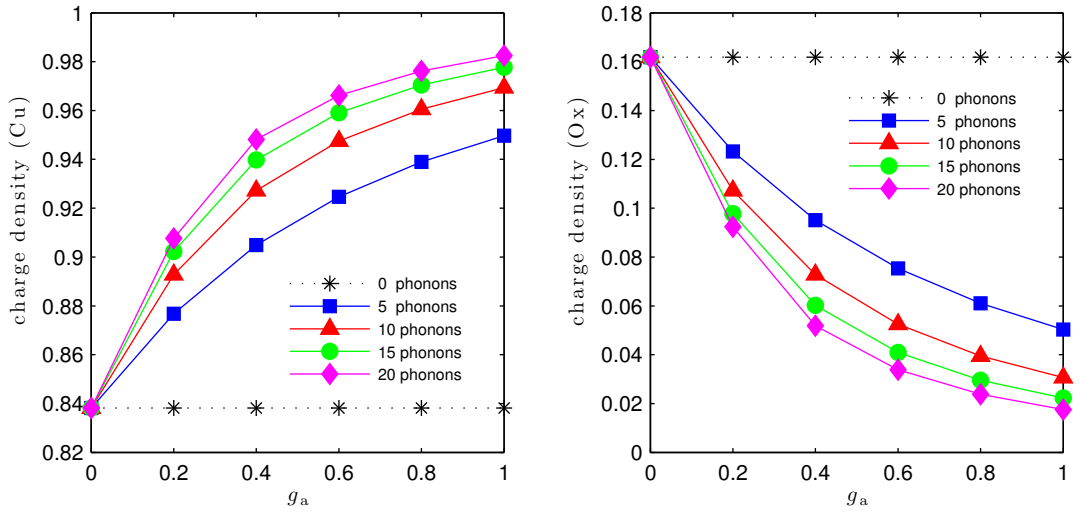

Figure 6.6. Charge densities for different *buckling* phonon numbers at half-filling (2 spin ↑ and 2 spin ↓ electrons): **(a)** describes the charge density at the copper site (Cu); and **(b)** describes the charge density at the oxygen site (Ox).

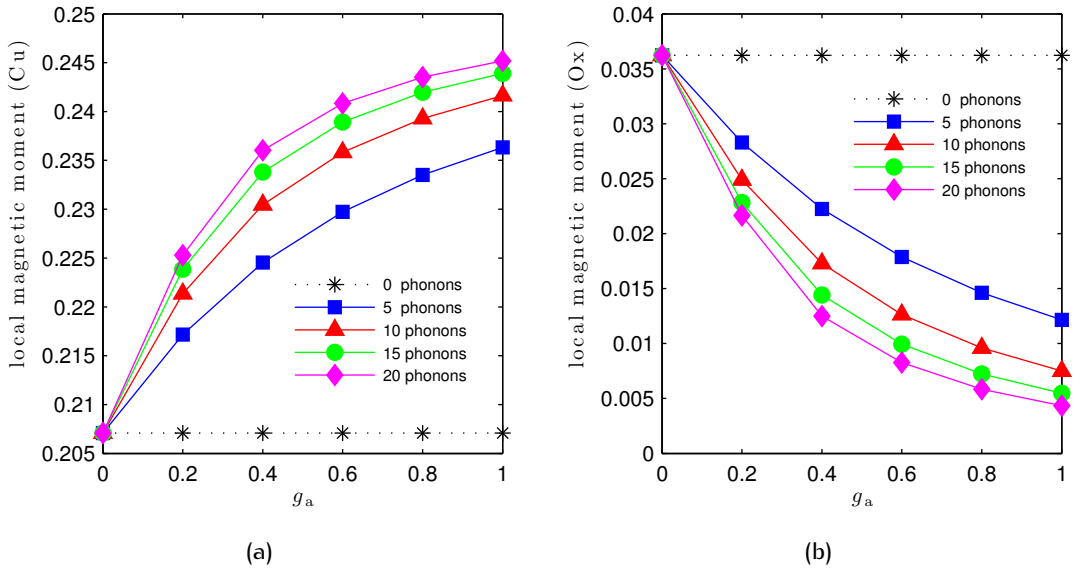

Figure 6.7. Local magnetic momenta for different *buckling* phonon numbers at half-filling (2 spin ↑ and 2 spin ↓ electrons): **(a)** describes the local magnetic moment at the copper site (Cu); and **(b)** describes the local magnetic moment at the oxygen site (Ox).

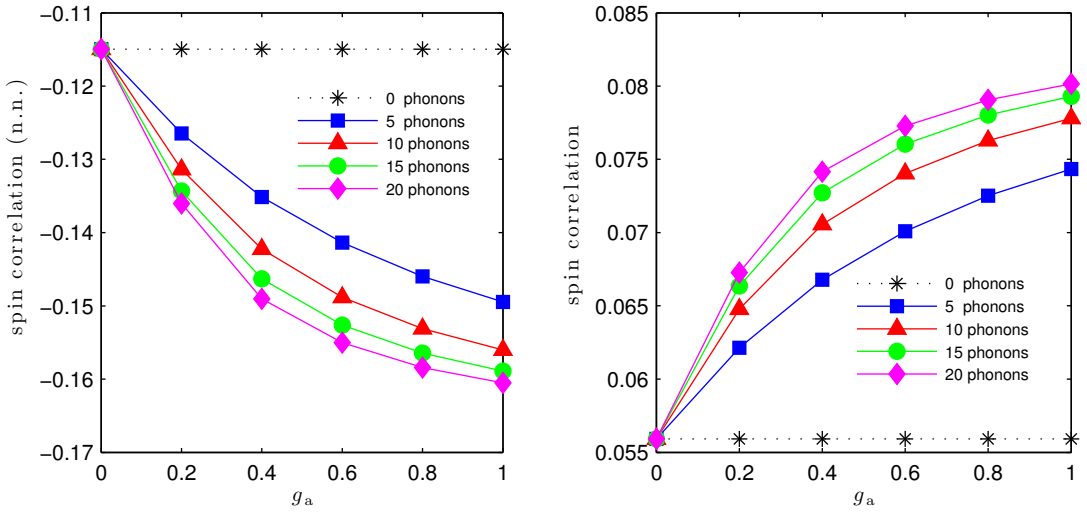

Figure 6.8. Spin correlations for different *buckling* phonon numbers at half-filling (2 spin ↑ and 2 spin ↓ electrons): **(a)** describes the nearest neighbor (n.n.) spin correlation between two copper sites; and **(b)** describes the spin correlation between second next copper site neighbors.

6.3.2 One-hole Doping

The following plots contain data for the *one-hole doping* case in dependence on the electron-phonon coupling constant g_a. The **ground-state energies** are plotted in Fig. 6.9 whereas the different contributions to the energy (**energy terms**) are depicted in Fig. 6.10. The **charge densities** for copper and oxygen sites are plotted in Fig. 6.11 and the **local magnetic momenta** in Fig. 6.12. The spin correlations are not plotted in the following since no significant results were obtained. This is due to the unequal number of spin ↑ and ↓ electrons in the system.

The ground-state energies in Fig. 6.9 show the same behavior as in the half-filling case and are lowered with increasing phonon influence.

Like before the kinetic energy (as shown in Fig. 6.10) is increased with a bigger number of phonons and is linear with stronger coupling. The electron-phonon interaction and phonon energy show the same behavior as before and are also increased. However, the electrical potential is slightly decreased at weak coupling, but increased at stronger coupling. Apart from the half-filling case its energy is bigger than the phonon energy.

Again, we observe a charge transfer from oxygen to copper atoms (as visible in Fig. 6.11). Apart from before, the local magnetic moment of a copper atom is increased at weak coupling and decreased at strong coupling (with increasing number of phonons), whereas on an oxygen site it is decreased for all coupling regimes (visible in Fig. 6.12).

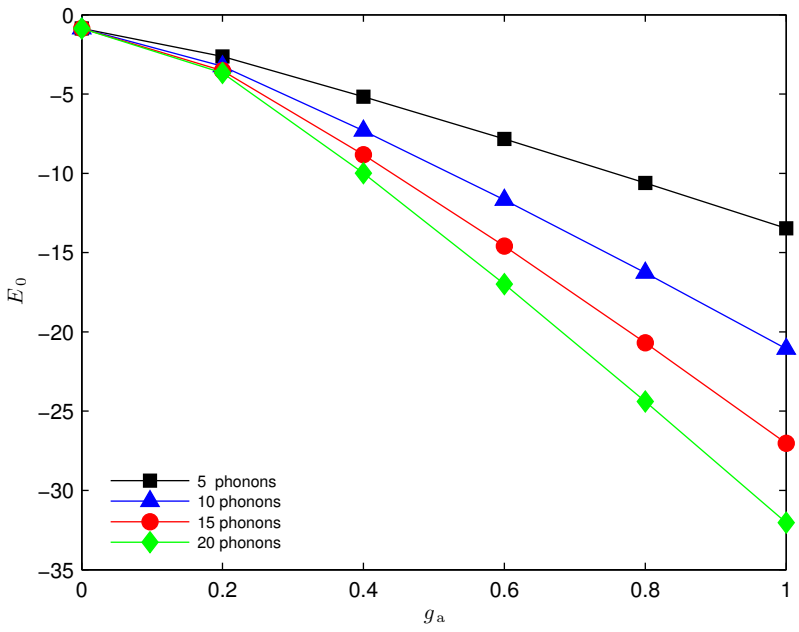

Figure 6.9. Ground-state energies for different *buckling* phonon numbers at one-hole doping (3 spin ↑ and 2 spin ↓ electrons).

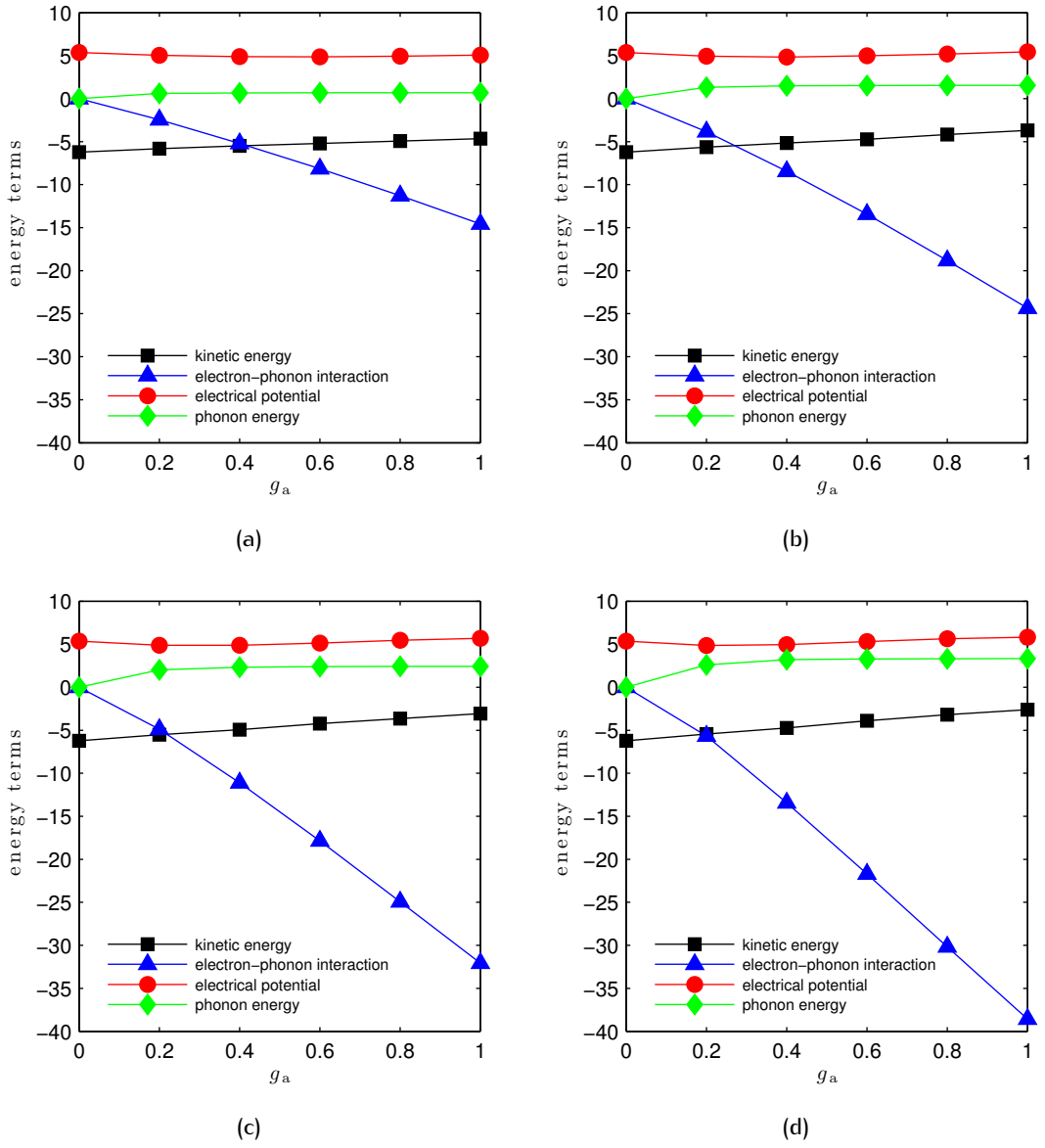

Figure 6.10. Energy terms for different *buckling* phonon numbers at one-hole doping (3 spin ↑ and 2 spin ↓ electrons): (a) 5 phonons; (b) 10 phonons; (c) 15 phonons; (d) 20 phonons.

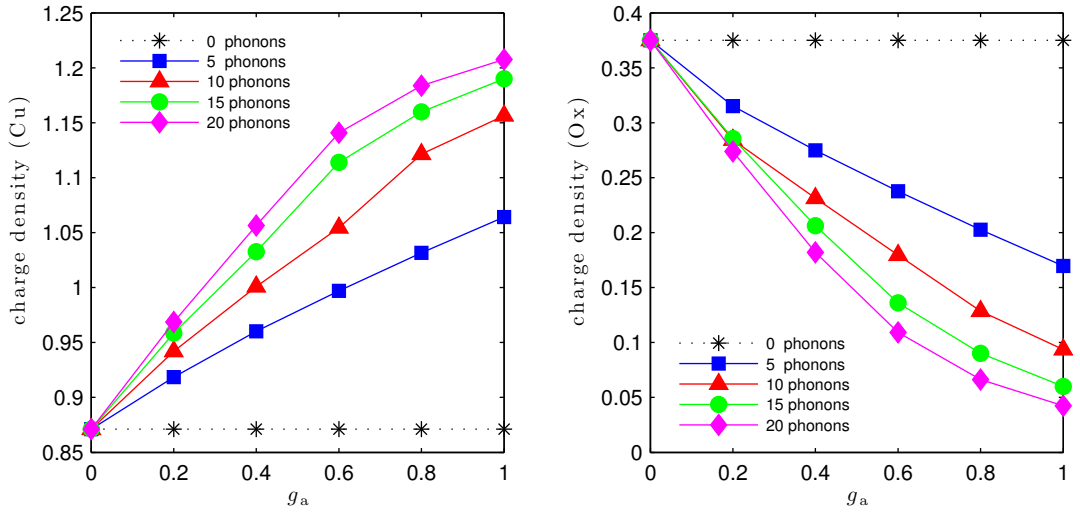

(a) (b)

Figure 6.11. Charge densities for different *buckling* phonon numbers at one-hole doping (3 spin ↑ and 2 spin ↓ electrons): **(a)** describes the charge density at the copper site (Cu); and **(b)** describes the charge density at the oxygen site (Ox).

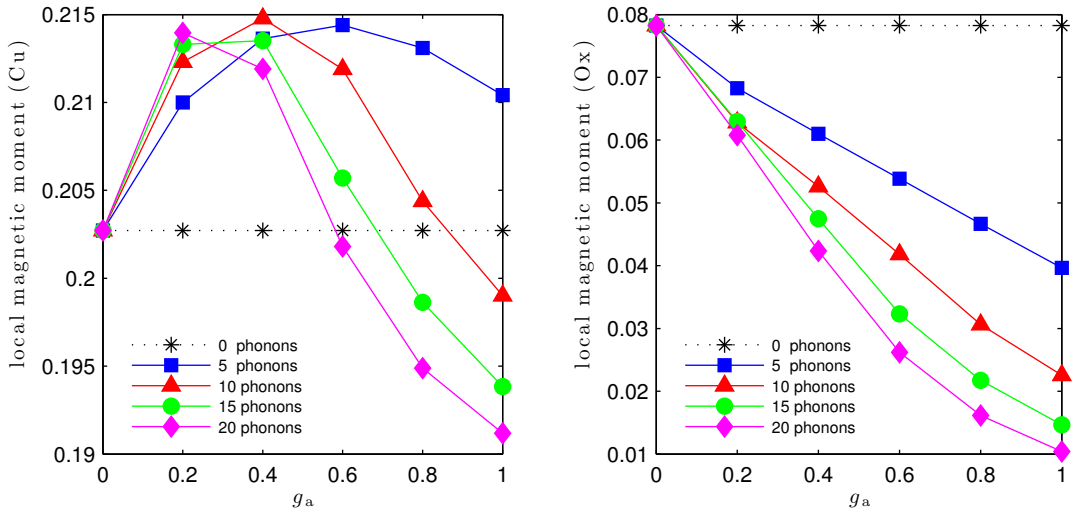

(a) (b)

Figure 6.12. Local magnetic momenta for different *buckling* phonon numbers at one-hole doping (3 spin ↑ and 2 spin ↓ electrons): **(a)** describes the local magnetic moment at the copper site (Cu); and **(b)** describes the local magnetic moment at the oxygen site (Ox).

6.3.3 Two-holes Doping

The following plots contain data for the *two-holes doping* case in dependence on the electron-phonon coupling constant g_a. The **ground-state energies** are plotted in Fig. 6.13 whereas the different contributions to the energy (**energy terms**) are depicted in Fig. 6.14. The **charge densities** for copper and oxygen sites are plotted in Fig. 6.15 and the **local magnetic momenta** in Fig. 6.16. The **spin correlations** for nearest neighbor (n.n.) and next nearest neighbor copper sites are depicted in Fig. 6.17.

The ground-state energies in Fig. 6.13 show the same behavior as in the previous cases and are lowered with increasing phonon influence.

The energy terms in Fig. 6.14 show the same behavior like in the on-hole doping case. With increasing phonon influence the kinetic energy is increased. The electron-phonon interaction and phonon energy are decreased and increased, respectively. The electrical potential is slightly decreased at weak coupling, but increased at stronger coupling.

Again, we observe a charge transfer from oxygen to copper atoms (as visible in Fig. 6.15). The local magnetic moment of a copper atom is increased at weak coupling, however not as much as in the one-hole case, and decreased at strong coupling whereas on oxygen sites it is decreased for all coupling regimes (visible in Fig. 6.16).

We observe the formation of a weak paramagnetic state (visible in Fig. 6.17) identifiable by a decrease of long-range spin correlations with stronger coupling.

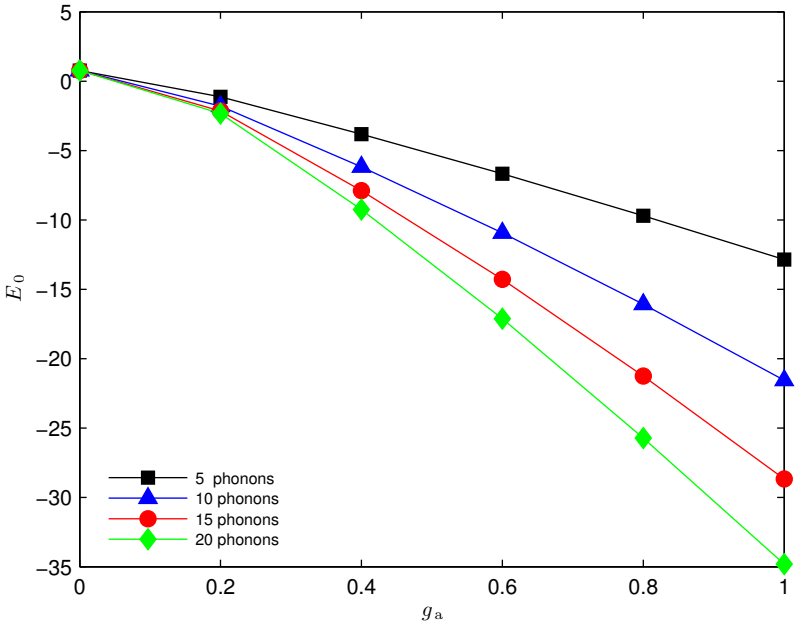

Figure 6.13. Ground-state energies for different *buckling* phonon numbers at two-holes doping (3 spin ↑ and 3 spin ↓ electrons).

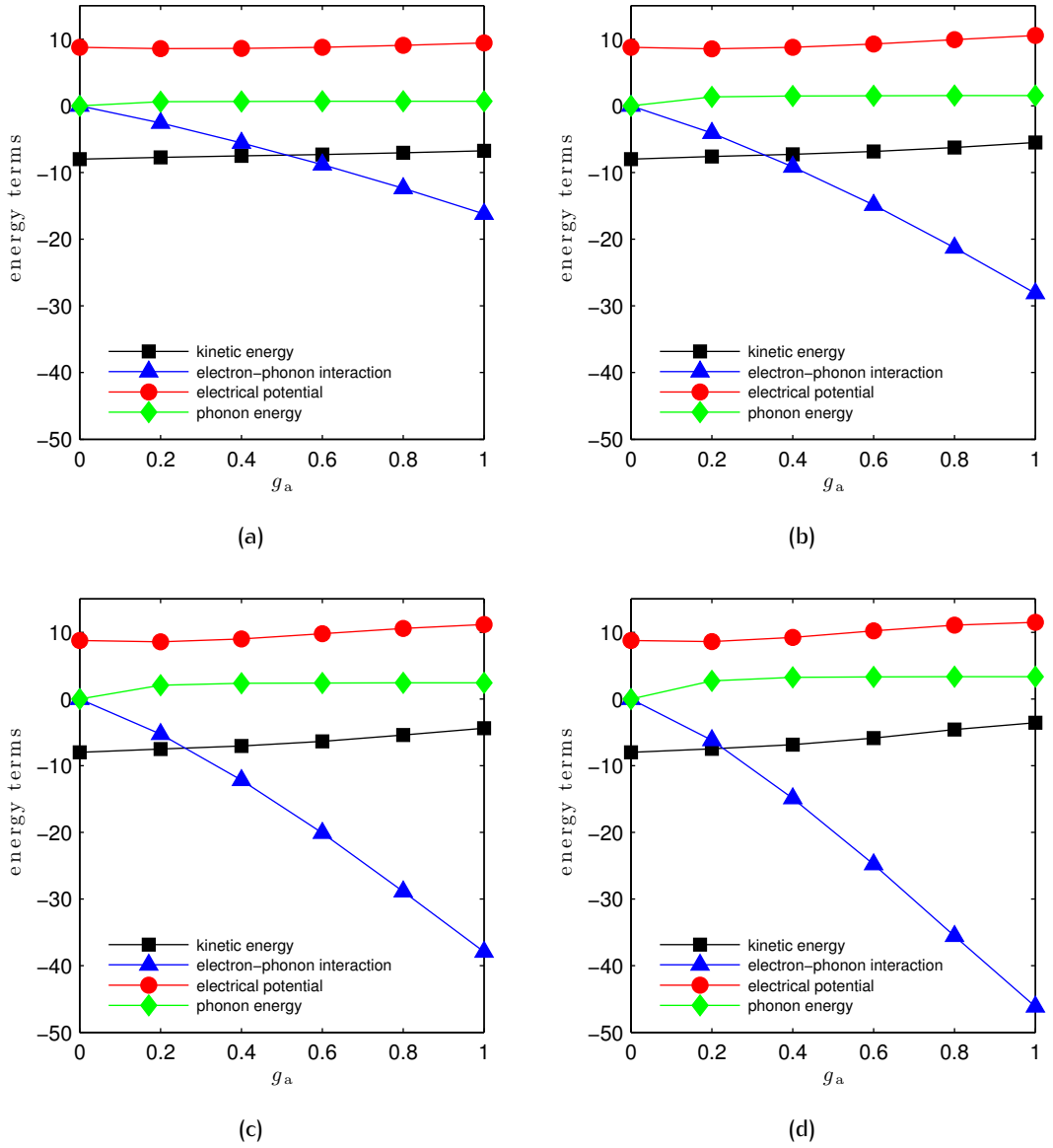

Figure 6.14. Energy terms for different *buckling* phonon numbers at two-holes doping (3 spin ↑ and 3 spin ↓ electrons): (a) 5 phonons; (b) 10 phonons; (c) 15 phonons; (d) 20 phonons.

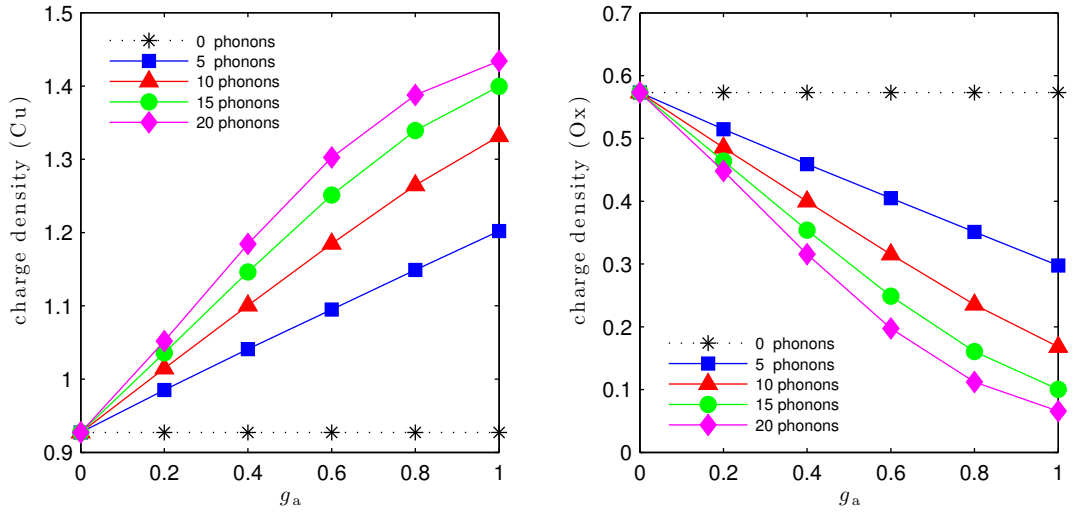

Figure 6.15. Charge densities for different *buckling* phonon numbers at two-holes doping (3 spin ↑ and 3 spin ↓ electrons): (a) describes the charge density at the copper site (Cu); and (b) describes the charge density at the oxygen site (Ox).

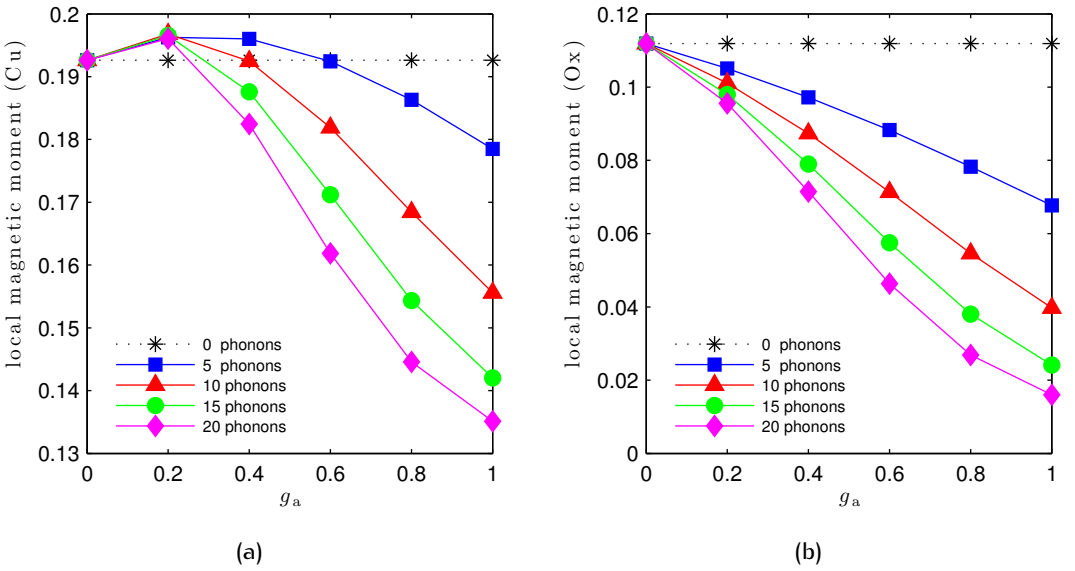

Figure 6.16. Local magnetic momenta for different *buckling* phonon numbers at two-holes doping (3 spin ↑ and 3 spin ↓ electrons): (a) describes the local magnetic moment at the copper site (Cu); and (b) describes the local magnetic moment at the oxygen site (Ox).

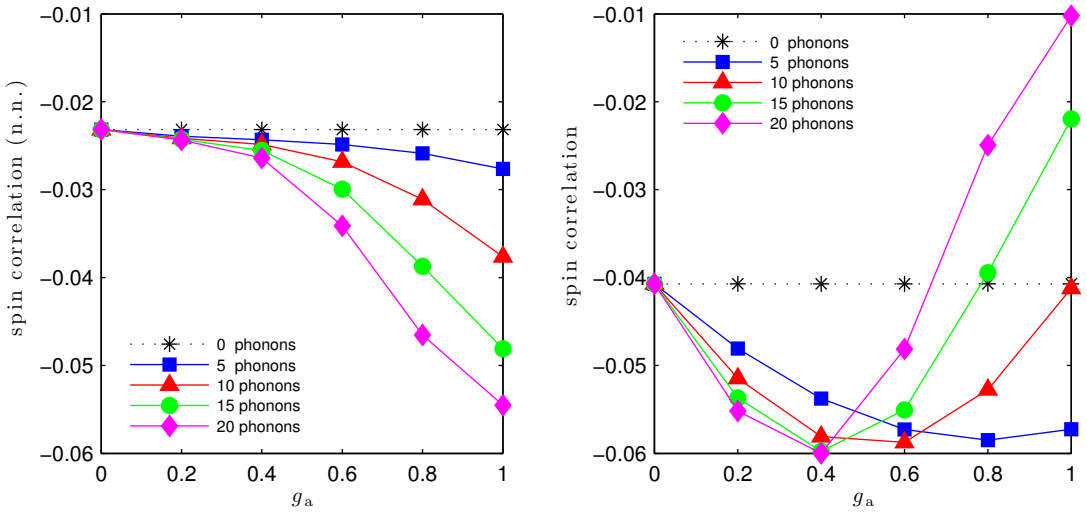

Figure 6.17. Spin correlations for different *buckling* phonon numbers at two-holes doping (3 spin ↑ and 3 spin ↓ electrons): **(a)** describes the nearest neighbor (n.n.) spin correlation between two copper sites; and **(b)** describes the spin correlation between second next copper site neighbors.

6.4 Breathing Phonons

The effects of breathing phonons with increasing electron-phonon interaction were investigated, whereby we only concentrated on the kinetic term. Therefore we set $g_d = 0$ in the used Hamiltonian from Eq. (2.33). Like we did with buckling phonons four different cases were treated: 5, 10, 15 and 20 phonons. The same set of parameters was used, as visible in Tab. 6.1. Like before for computational reasons we defined

$$\varepsilon := \varepsilon_p - \varepsilon_d \qquad \text{and} \qquad \varepsilon \longrightarrow \varepsilon_p$$

as the difference between oxygen and copper on-site energies, which is the reason why the copper on-site energy ε_d is set to zero.

Like for the buckling case we calculated ground-state energies as well as all energy terms individually (such as kinetic energy etc.), local magnetic momenta and spin correlations (z-components). All results are presented separately for each electron-hole filling.

It shall be noted that the convergence in the inverse iteration for obtaining the ground-state vector was very bad, why the accuracy had to be reduced (in some cases up to 10^{-3}) to obtain results within a reasonable time period.

Table 6.2. Parameters for breathing Hamiltonian in Eq. (2.33) .

ε_d	0.0
ε_p	3.0
U_d	6.0
ω	0.2
g_d	0.0
g_{dp}	0.0 – 1.0

6.4.1 Half-filling

The following plots contain data for the *half-filling* case in dependence on the electron-phonon coupling constant g_{dp}. The **ground-state energies** are plotted in Fig. 6.18 whereas different contributions to the energy (**energy terms**) are depicted in Fig. 6.19. The **charge densities** for copper and oxygen sites are plotted in Fig. 6.20 and the **local magnetic momenta** in Fig. 6.21. The **spin correlations** for nearest neighbor (n.n.) and next nearest neighbor copper sites are depicted in Fig. 6.22.

It is visible that with increasing phonon influence the ground-state energies are lowered like in the buckling case (as shown in Fig. 6.18). However, at weak coupling ($g_{\mathrm{dp}} < 0.4$) the influence of phonons is not visible.

The kinetic energy, the electrical potential and the phonon energy increase with stronger coupling and a bigger number of phonons while the electron-phonon interaction drastically decreases (see Fig. 6.19). However no change occurs for very weak coupling ($g_{\mathrm{dp}} < 0.2$).

With increased phonon influence we observe, opposite to the buckling case, a charge transfer from copper to oxygen (as visible in Fig. 6.20). The result is a nearly uniform electron distribution within the whole cluster. Further, the local magnetic momenta on copper sites are decreased whereas they are increased on oxygen sites (visible in Fig. 6.21). We also observe a strong inconsistency for 20 phonons which cannot be interpreted.

With increased phonon influence (visible in Fig. 6.22) the antiferromagnetic state is strongly softened towards a paramagnetic state.

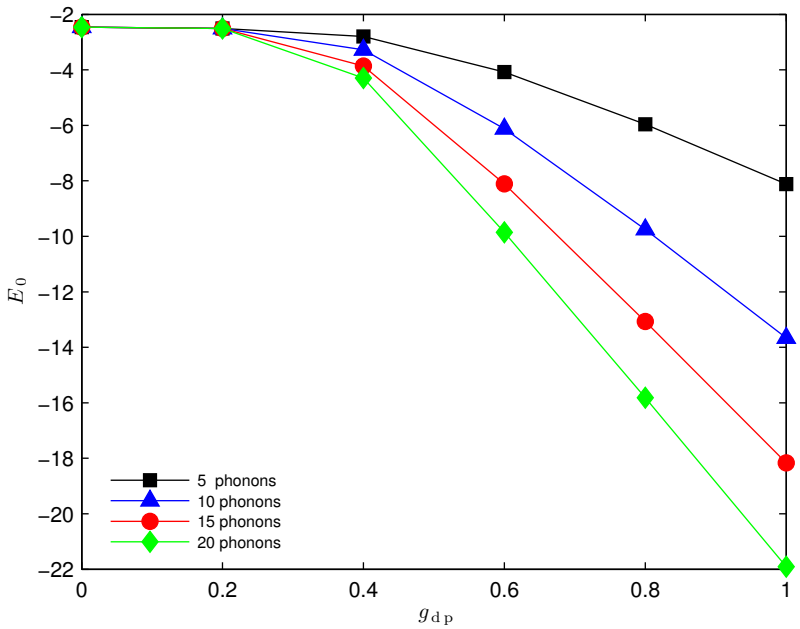

Figure 6.18. Ground-state energies for different *breathing* phonon numbers at half-filling (2 spin ↑ and 2 spin ↓ electrons).

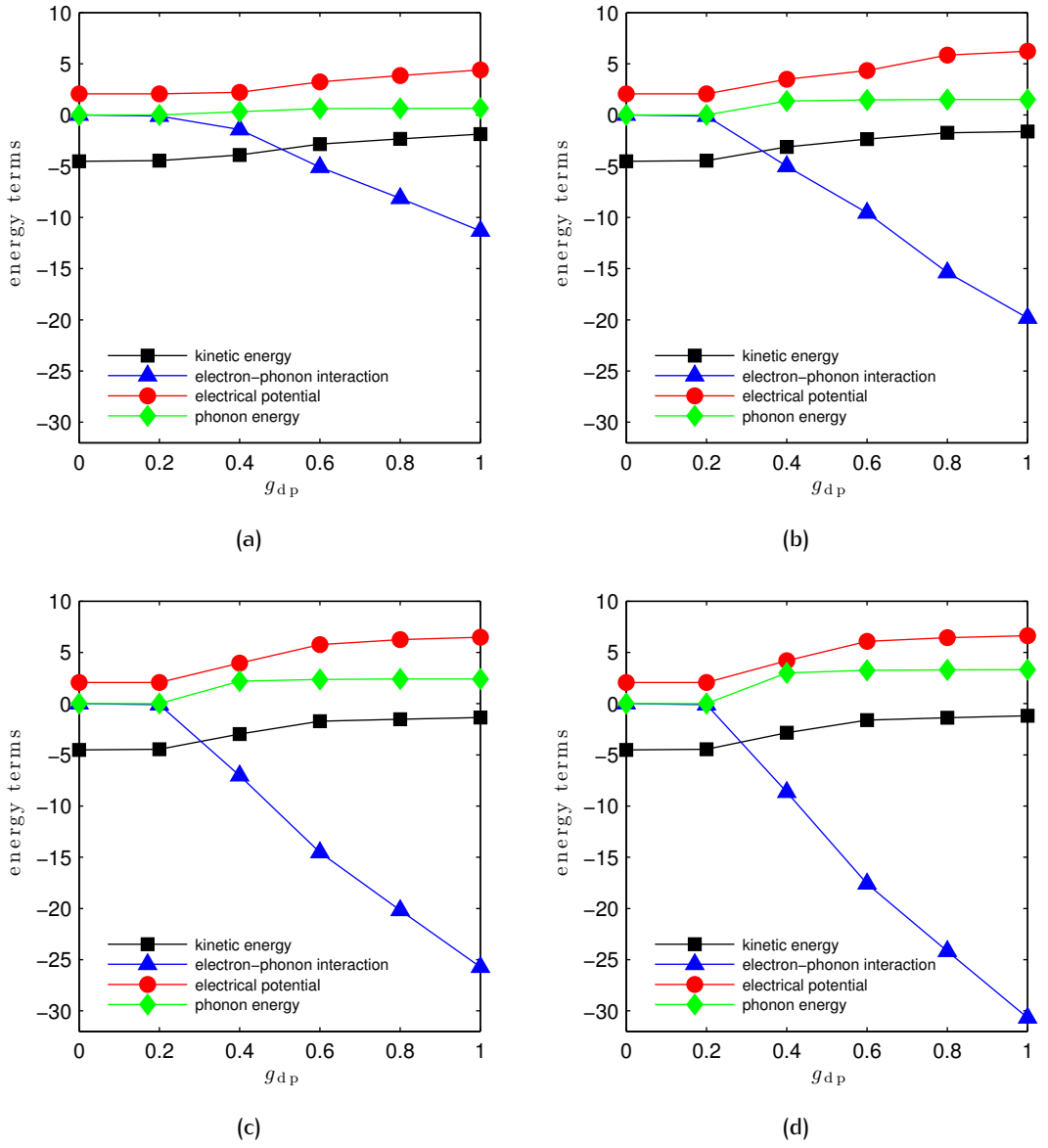

Figure 6.19. Energy terms for different *breathing* phonon numbers at half-filling (2 spin ↑ and 2 spin ↓ electrons): **(a)** 5 phonons; **(b)** 10 phonons; **(c)** 15 phonons; **(d)** 20 phonons.

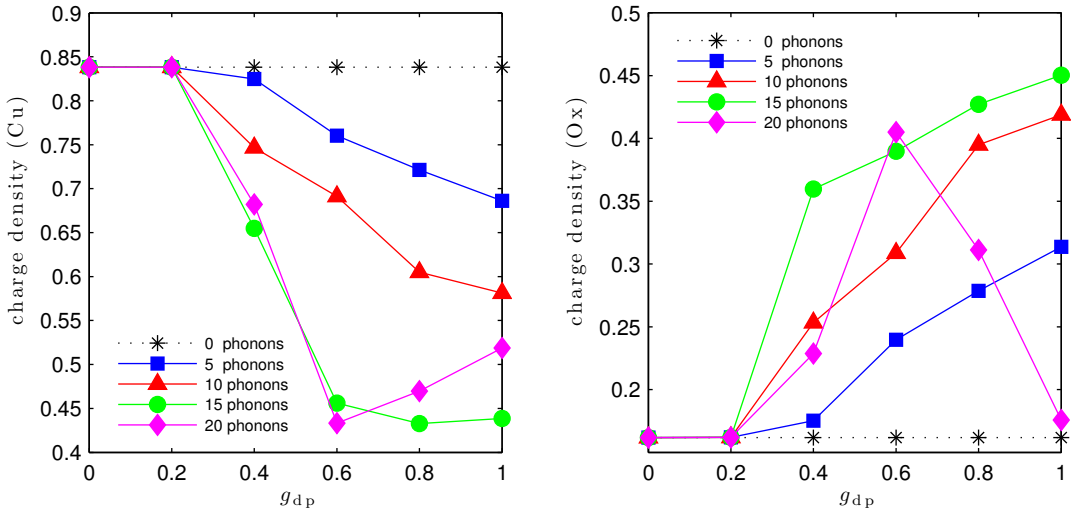

Figure 6.20. Charge densities for different *breathing* phonon numbers at half-filling (2 spin ↑ and 2 spin ↓ electrons): **(a)** describes the charge density at the copper site (Cu); and **(b)** describes the charge density at the oxygen site (Ox).

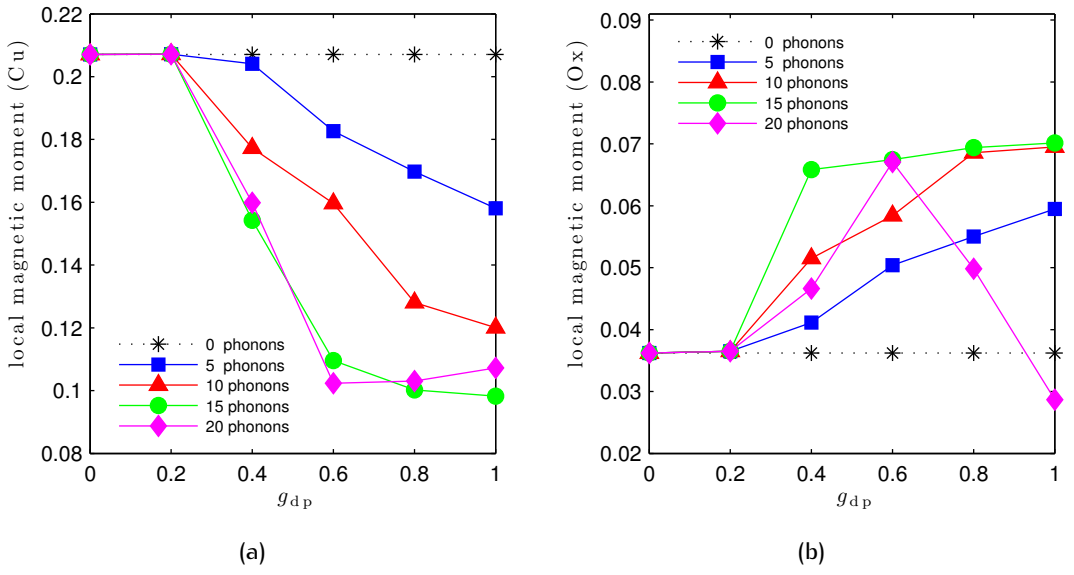

Figure 6.21. Local magnetic momenta for different *breathing* phonon numbers at half-filling (2 spin ↑ and 2 spin ↓ electrons): **(a)** describes the local magnetic moment at the copper site (Cu); and **(b)** describes the local magnetic moment at the oxygen site (Ox).

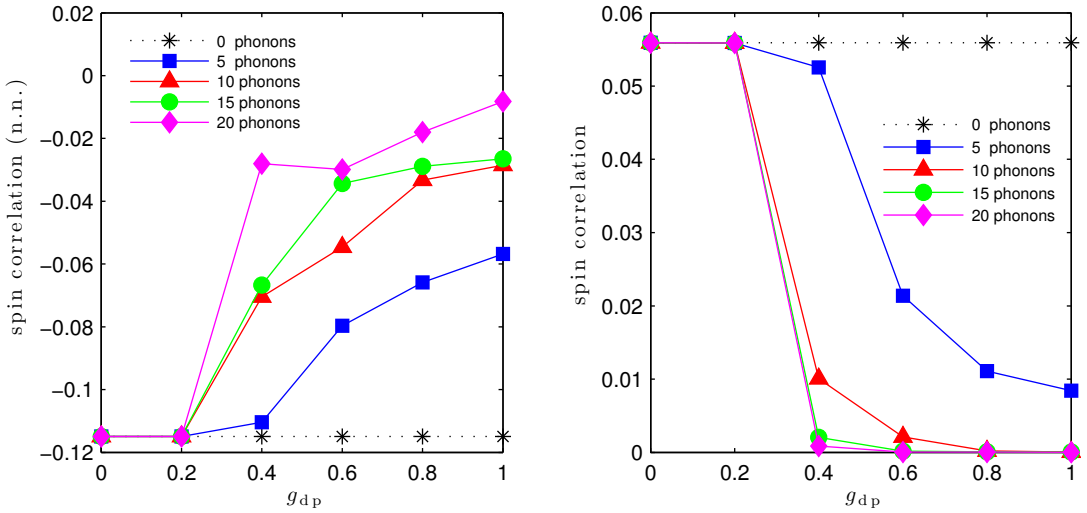

Figure 6.22. Spin correlations for different *breathing* phonon numbers at half-filling (2 spin ↑ and 2 spin ↓ electrons): **(a)** describes the nearest neighbor (n.n.) spin correlation between two copper sites; and **(b)** describes the spin correlation between second next copper site neighbors.

6.4.2 One-hole doping

The following plots contain data for the *one-hole doping* case in dependence on the electron-phonon coupling constant g_a. The **ground-state energies** are plotted in Fig. 6.23 whereas the different contributions to the energy (**energy terms**) are depicted in Fig. 6.24. The **charge densities** for copper and oxygen sites are plotted in Fig. 6.25 and the **local magnetic momenta** in Fig. 6.26. The **spin correlations** for nearest neighbor (n.n.) and next nearest neighbor copper sites are depicted in Fig. 6.27.

The ground-state energies in Fig. 6.23 show the same behavior as in the half-filling case and are lowered with increasing phonon influence.

Like before the kinetic energy, the electrical potential and the phonon energy are increased with a bigger number of phonons and also occur at weaker coupling (as shown in Fig. 6.24). The electron-phonon interaction is reduced with increasing phonon energy.

Again, we observe a charge transfer from copper to oxygen atoms (as visible in Fig. 6.25) and the local magnetic moment of a copper atom is decreased (with increasing number of phonons) whereas on an oxygen sites it is slightly increased (visible in Fig. 6.26). Again, we observe some inconsistencies that we cannot explain.

Like before, antiferromagnetc spin correlations are strongly softened towards a paramagnetic state (visible in Fig. 6.8).

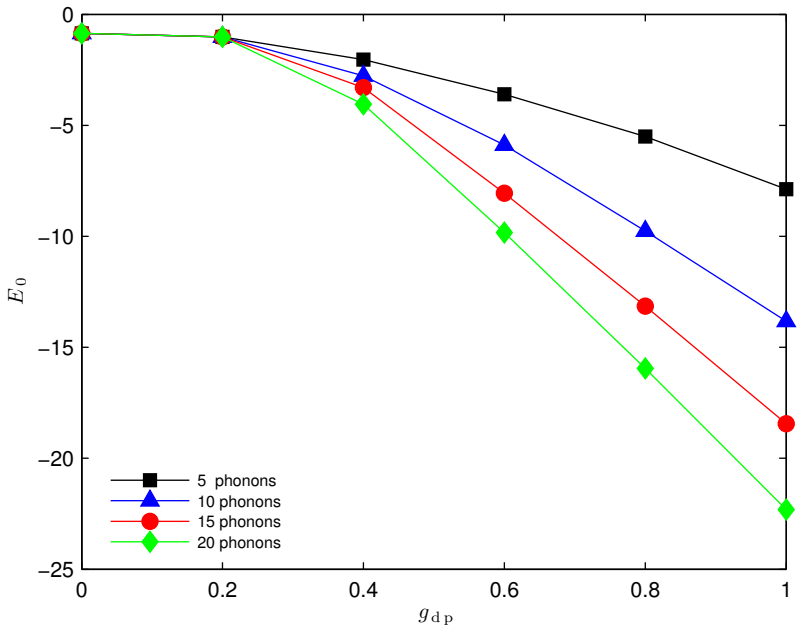

Figure 6.23. Ground-state energies for different *breathing* phonon numbers at one-hole doping (3 spin ↑ and 2 spin ↓ electrons).

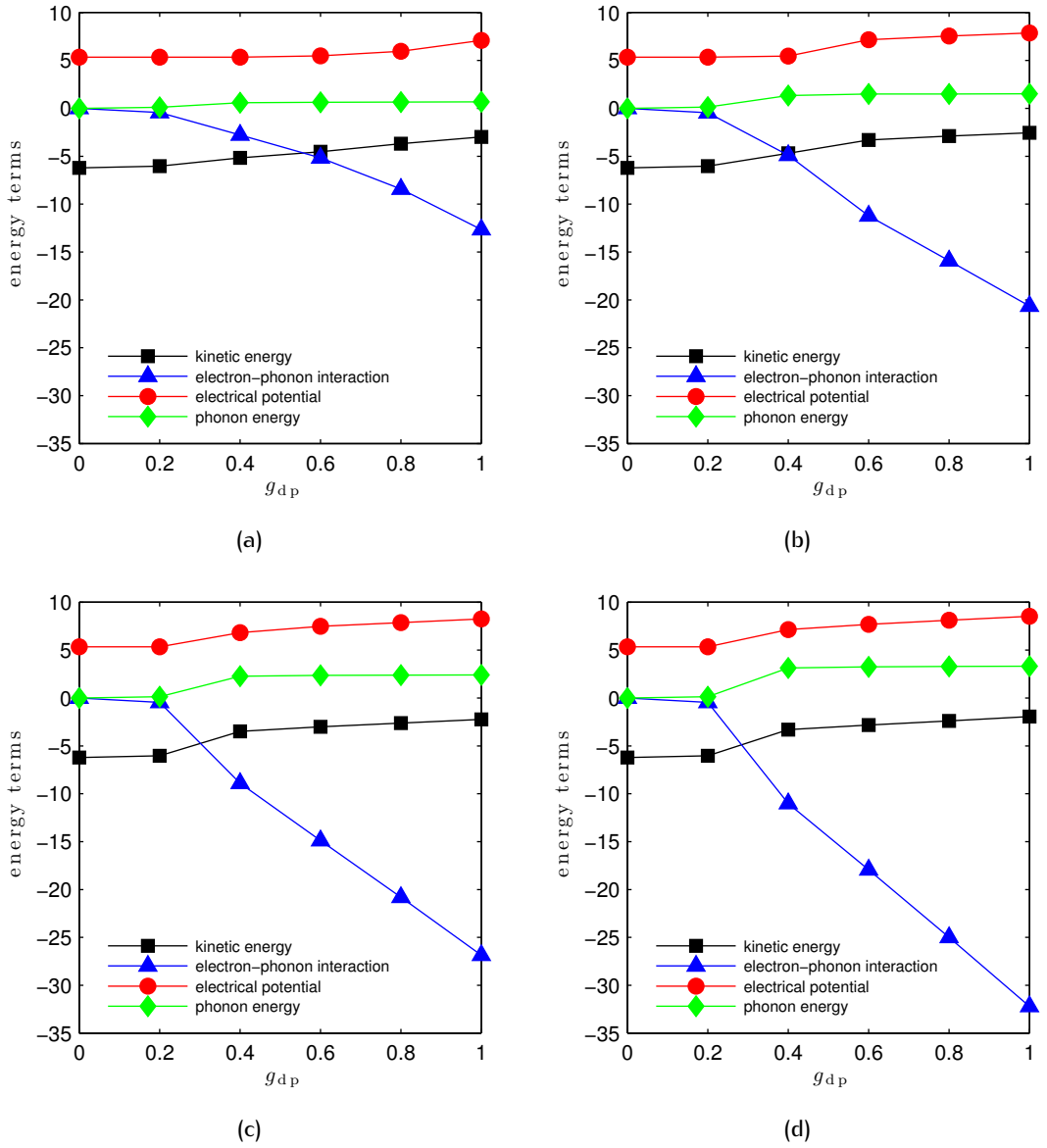

Figure 6.24. Energy terms for different *breathing* phonon numbers at one-hole doping (3 spin ↑ and 2 spin ↓ electrons): **(a)** 5 phonons; **(b)** 10 phonons; **(c)** 15 phonons; **(d)** 20 phonons.

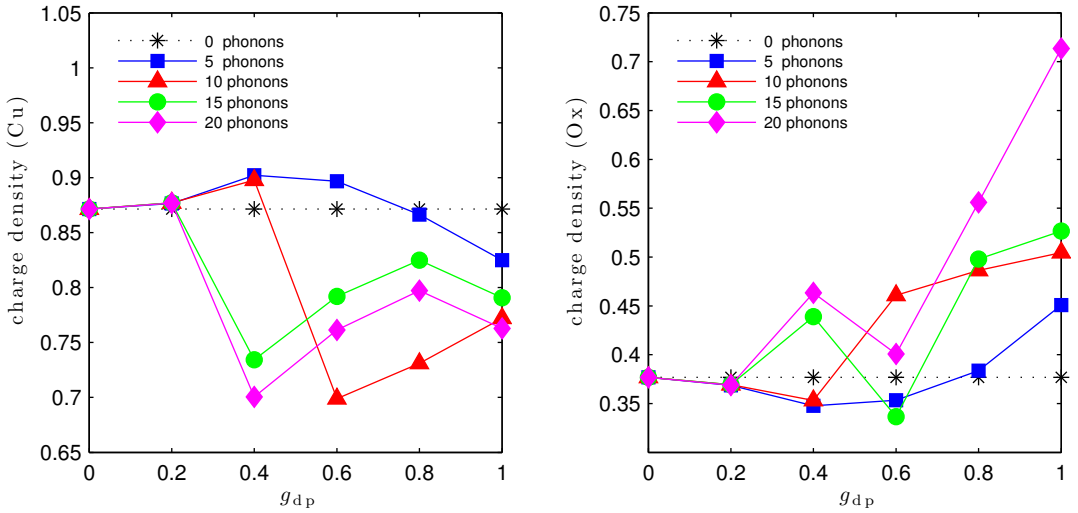

Figure 6.25. Charge densities for different *breathing* phonon numbers at one-hole doping (3 spin ↑ and 2 spin ↓ electrons): (a) describes the charge density at the copper site (Cu); and (b) describes the charge density at the oxygen site (Ox).

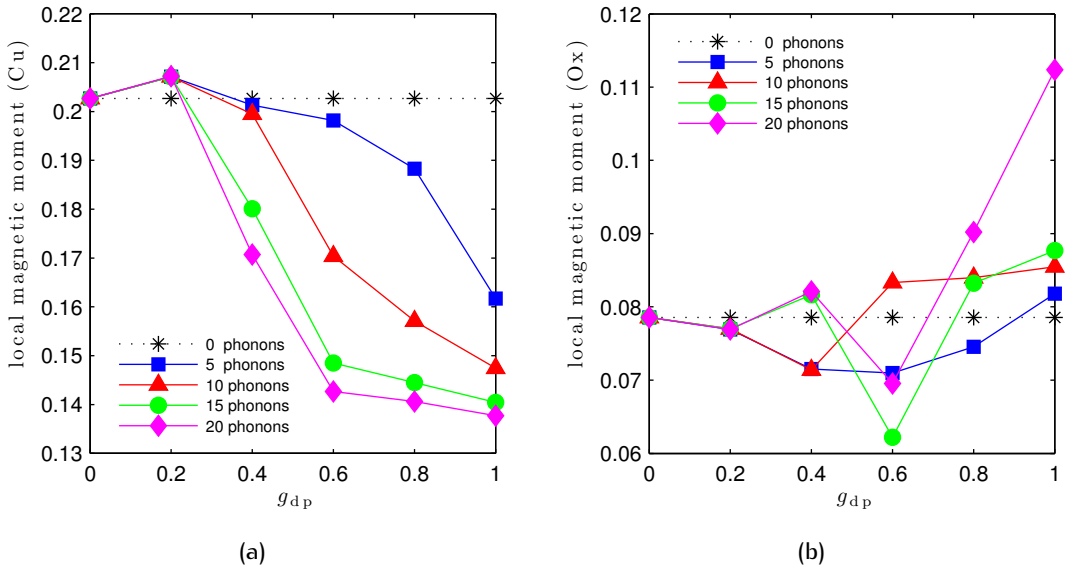

Figure 6.26. Local magnetic momenta for different *breathing* phonon numbers at one-hole doping (3 spin ↑ and 2 spin ↓ electrons): (a) describes the local magnetic moment at the copper site (Cu); and (b) describes the local magnetic moment at the oxygen site (Ox).

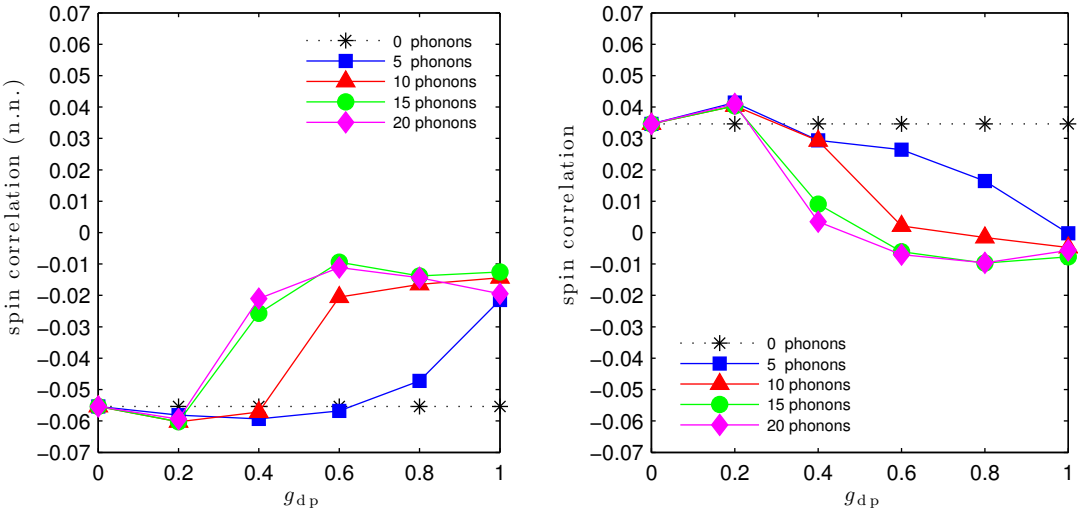

Figure 6.27. Spin correlations for different *breathing* phonon numbers at half-filling (3 spin ↑ and 2 spin ↓ electrons): **(a)** describes the nearest neighbor (n.n.) spin correlation between two copper sites; and **(b)** describes the spin correlation between second next copper site neighbors.

6.4.3 Two-holes doping

The following plots contain data for the *two-holes doping* case in dependence on the electron-phonon coupling constant g_{a}. The **ground-state energies** are plotted in Fig. 6.28 whereas the different contributions to the energy (**energy terms**) are depicted in Fig. 6.29. The **charge densities** for copper and oxygen sites are plotted in Fig. 6.30 and the **local magnetic momenta** in Fig. 6.31. The **spin correlations** for nearest neighbor (n.n.) and next nearest neighbor copper sites are depicted in Fig. 6.32.

The ground-state energies in Fig. 6.28 show the same behavior as in the previous cases and are lowered with increasing phonon influence.

Like before the kinetic energy, the electrical potential and the phonon energy are increased with a bigger number of phonons and also occurs at weaker coupling (as shown in Fig. 6.29). The electron-phonon interaction is reduced with increasing phonon energy.

For all other quantities [Fig. (6.30)-(6.32)] we observe strong inconsistency that we cannot explain in any way.

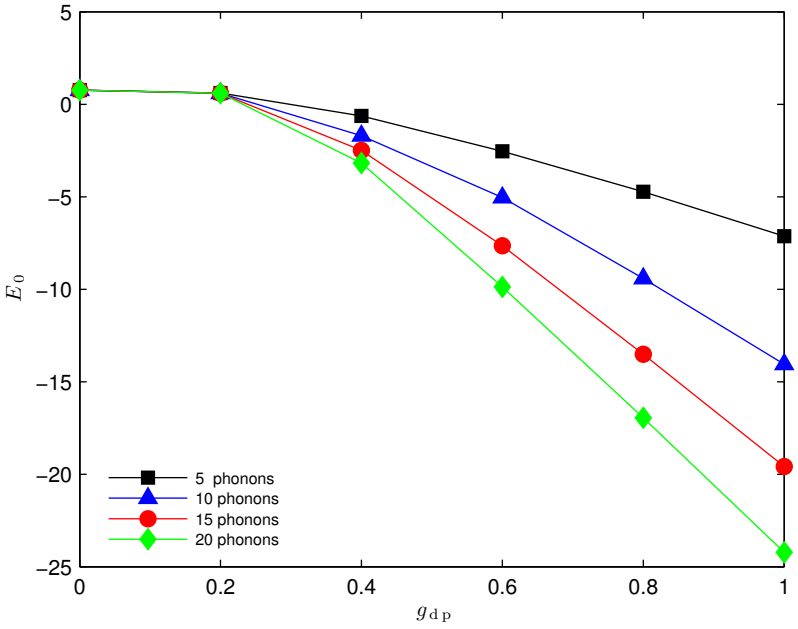

Figure 6.28. Ground-state energies for different *breathing* phonon numbers at two-holes doping (3 spin ↑ and 3 spin ↓ electrons).

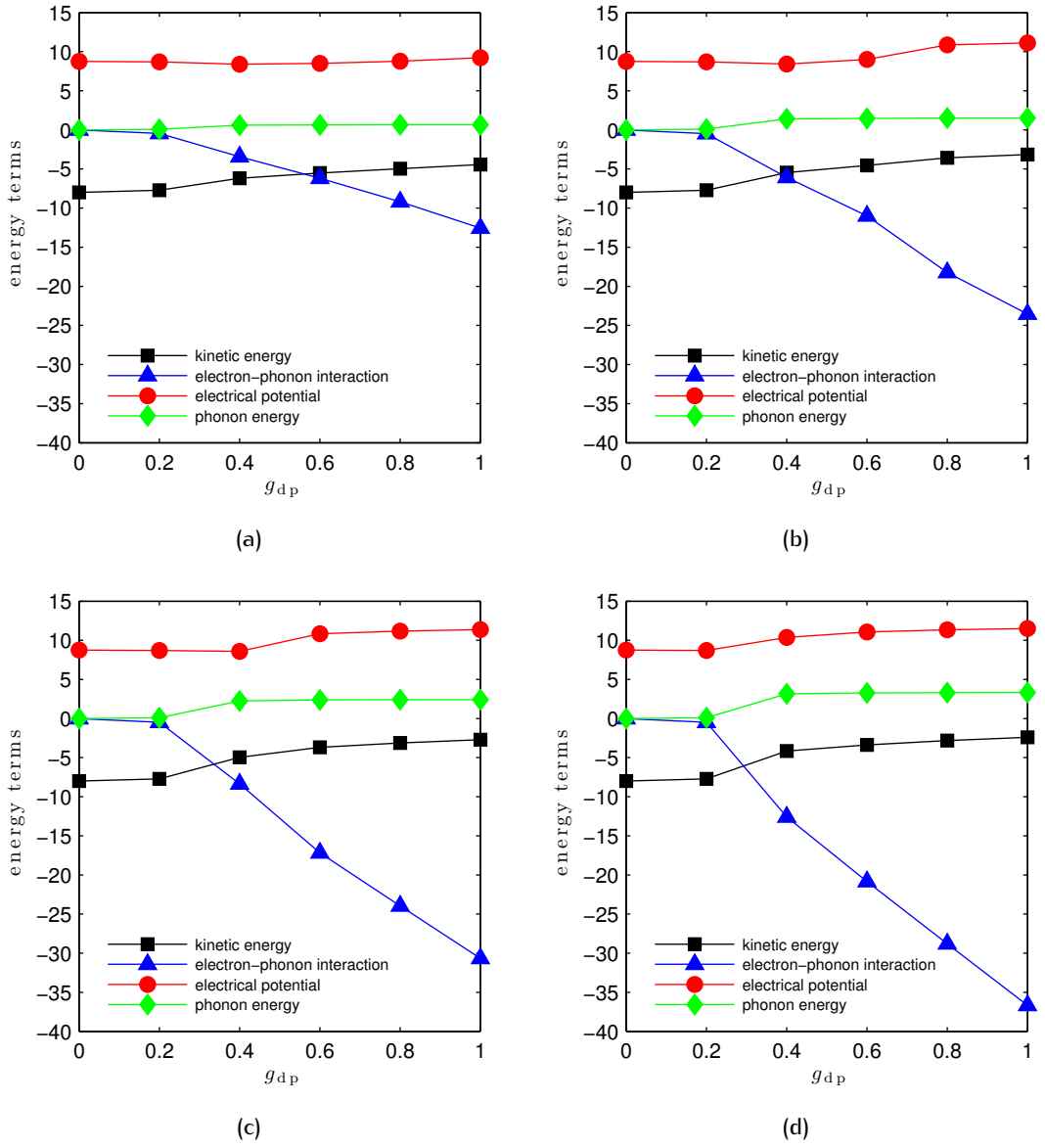

Figure 6.29. Energy terms for different *breathing* phonon numbers at two-holes doping (3 spin ↑ and 3 spin ↓ electrons): **(a)** 5 phonons; **(b)** 10 phonons; **(c)** 15 phonons; **(d)** 20 phonons.

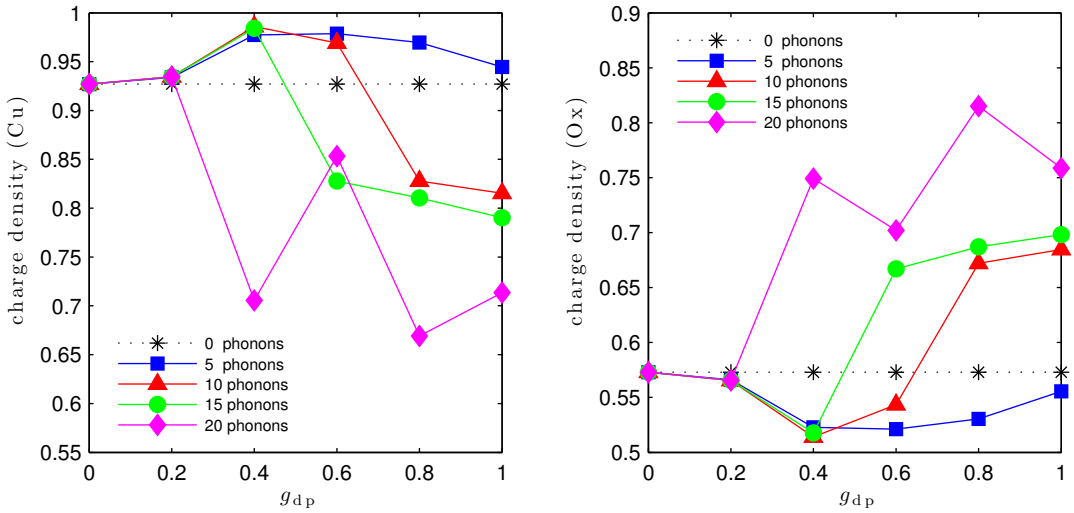

Figure 6.30. Charge densities for different *breathing* phonon numbers at two-holes doping (3 spin ↑ and 3 spin ↓ electrons): **(a)** describes the charge density at the copper site (Cu); and **(b)** describes the charge density at the oxygen site (Ox).

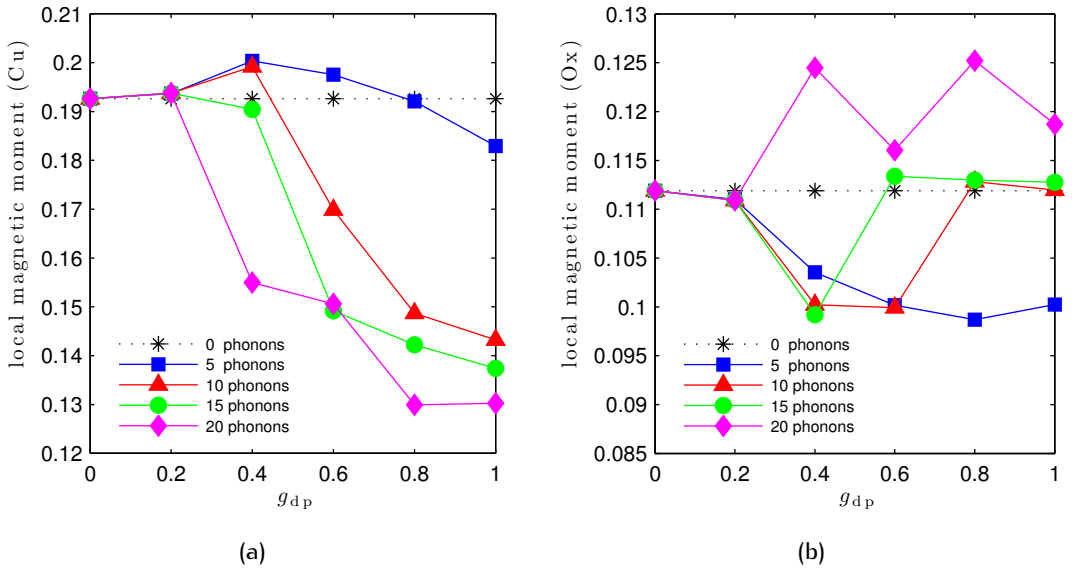

Figure 6.31. Local magnetic momenta for different *breathing* phonon numbers at two-holes doping (3 spin ↑ and 3 spin ↓ electrons): **(a)** describes the local magnetic moment at the copper site (Cu); and **(b)** describes the local magnetic moment at the oxygen site (Ox).

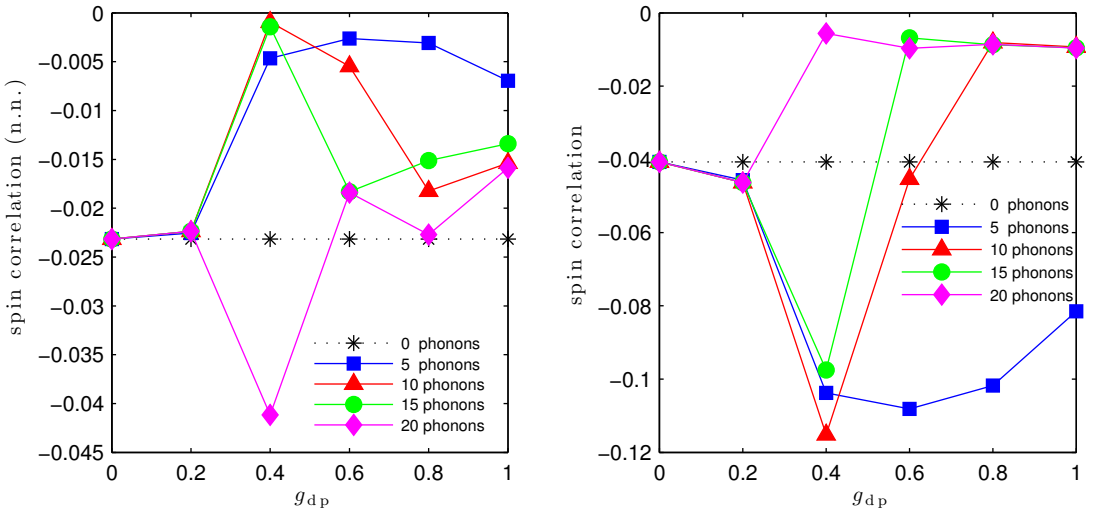

Figure 6.32. Spin correlations for different *breathing* phonon numbers at two-holes doping (3 spin ↑ and 3 spin ↓ electrons): **(a)** describes the nearest neighbor (n.n.) spin correlation between two copper sites; and **(b)** describes the spin correlation between second next copper site neighbors.

6.5 Conclusions

The influence of buckling phonons leads to a charge transfer from oxygen to copper atoms and thus to an increase and decrease of the local magnetic moment on a copper and oxygen site, respectively. With hole doping the local magnetic momenta on copper sites get reduced and we observe the formation of a weak paramagnetic state. By calculating the binding energy in relation to buckling phonons influence [see Fig. 6.33(a)] we observe that pair binding is less favored.

For breathing phonons we observe mainly opposite effects. We observe a charge transfer from copper to oxygen for half-filling and one-hole doping as well as a transition from an antiferromagnetic state towards a paramagnetic one. For two-holes doping we cannot make clear statements due to strong inconsistencies. The binding energy [see Fig. 6.33(b)] is increased at low coupling and strongly decreased at stronger coupling indicating that breathing phonons may cause pair binding.

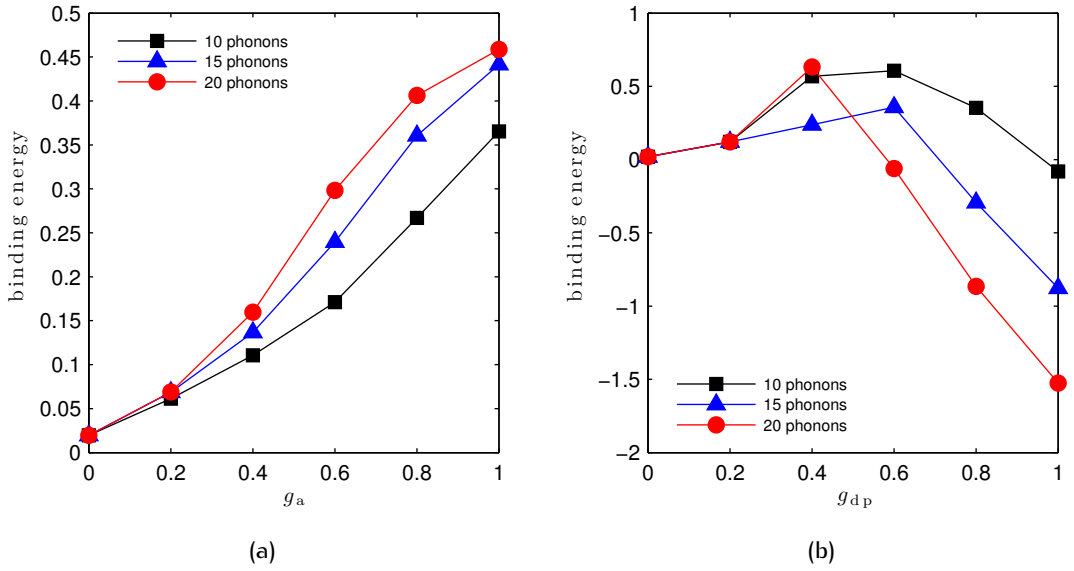

Figure 6.33. Binding energies for various phonon numbers: **(a)** describes binding energies corresponding to different *buckling* phonon numbers; and **(b)** describes binding energies corresponding to different *breathing* phonon numbers.

Chapter 7

Summary

In the underlying work we treated two examples of strongly correlated electron systems and one example of a strongly correlated electron-phonon system using many-body schemes. The study of the first part, namely the case of a simplified 1D problem, was mainly intended to make familiar with the numerical methods used in the present work as well as to obtain a general understanding of many-body quantum theory. The latter two examples, namely the study of magnetic properties of individual carbon clusters and the study of a 1D CuO-chain, represented two contemporary examples associated with recent scientific articles. By treating these, we followed previous studies of the same subjects and conducted further investigations by means of some novel approaches. Thereby it was our aim to make a small contribution to the general understanding of these systems. In the following the most important results are presented with references to the respective sections.

For the one-dimensional eight-site cluster at half-filling we mainly obtained known results typical for the Hubbard model, such as an antiferromagnetic solution with long-range order and a uniform charge distribution with increasing Hubbard-U. The results can be found in Chapter 4 on p. 45 and compared directly with [22].

For the investigated individual carbon clusters with one π-electron per atom we found that the nearest neighbor interaction V in most of the cases "destroys" ferromagnetic solutions (see Sec. 5.3.2 on p. 57). However, for the isomers "iso-g", "iso-h" and "iso-i" the nearest neighbor interaction has no negative effect or even shows an enhancement of the ferromagnetic state. We found that for increasing V-values the ferromagnetic state is maintained if the energy difference ΔE between the ground-state energy E_0 (corresponding to a triplet state) and the first-excited-state energy E_1 (corresponding to a singlet state) is big enough. This can be explained as follows: For all carbon species (except isomer "iso-g") ΔE is reduced if V is increased which means that the triplet ground state becomes less stable. Therefore, only if ΔE is big enough for $V = 0$, the reduction of stability with increasing V is negligible. Moreover, for isomer "iso-g" we observed that with increasing V the triplet ground state becomes even more stable and expands over wider U-regions which implies a

high stability of the triplet ground state. By comparing ground-state energies (see Sec. 5.4 on p. 61) we observed that isomer "iso-i" had the lowest ground-state energy indicating that energetically its configuration may be the most favorable. This, however, only applies if other contributions to the energy (such as lattice) are negligible compared to the electrons contributions. Altogether we can state that the extended Hubbard model approach leads to quite different results and interpretations compared to those in [2] which were obtained by the (simple) Hubbard model approach.

For the one-dimensional eight-atom CuO-chain (see Chapter 6 on p. 63) we found that buckling and breathing phonons cause opposite effects. Buckling phonons lead to a charge transfer from oxygen to copper sites with enhancement of an antiferromagnetic state that turns to a paramagnetic state with hole doping. With increasing phonon numbers and electron-phonon coupling the ground-state energies are lowered, but even for 20 phonons no convergence is reached. Only the charge distribution within the cluster converges towards constant values which means that in fact only a few phonons cause the charge transfer from oxygen to copper atoms. The further increase of the overall phonon number means no significant change in the systems's charge distribution. For breathing phonons we observed a charge transfer from copper to oxygen atoms, however we obtained strong inconsistencies for charge densities, local magnetic momenta and spin correlations which may give reasons to conduct further calculations. Similar to the buckling case, with increasing phonon numbers and electron-phonon coupling the ground-state energies are lowered and again no convergence is reached for 20 phonons. Besides, we observed that only for stronger coupling $g_{\mathrm{dp}} > 0.2$ breathing phonons have physical effects. Finally by comparing binding energies we saw that buckling phonons might prevent pair binding due to a positive (pair) binding energy. Breathing phonons, on the other hand, also exhibit a positive (pair) binding energy at weaker coupling $g_{\mathrm{dp}} < 0.6$, but cause a massive enhancement of pair binding due to a negative (pair) binding energy at stronger coupling. Due to the inconsistencies mentioned above and to a somewhat larger scale of the (pair) binding energy for the breathing case further calculations should be done before drawing reliable physical conclusions.

Finally we want to note that we also made use of [37–44], however not as direct references but for general understanding of many-body problems etc.

Appendix A

Author's Additional Stuff

A.1 Derivation of Phononic Hilbert Space Dimension

As our starting point we take a N_s-site cluster with a *maximum* of N_{ph} phonons. Since the phononic Hilbert space $\mathcal{H}_{ph}$ depends only on these two parameters, it is evident that we can write it as a sum of Hilbert spaces belonging to fixed numbers of sites as well as fixed numbers of phonons reaching from 0 to N_{ph}:

$$\mathcal{H}_{ph} = \mathcal{H}(N_s, N_{ph}) + \mathcal{H}(N_s, N_{ph} - 1) + \ldots + \mathcal{H}(N_s, 0). \tag{A.1}$$

We thus choose a fixed phonon number M and investigate for this particular case. Again, the problem is of *combinatorial* nature, as we need to find all possible combinations for occupation numbers, whereas their sum is equal to M.

Following [28, p. 44-45] we adapt a more descriptive way and consider all particles (phonons) as part of a big "pot." Hence we introduce some kind of "delimiters" dividing this "pot" into many parts (where each part represents a cluster site). Further on we treat "delimiters" and particles equally. Since for a N_s-site cluster we need $N_s - 1$ *delimiters*, our whole "pot" contains now $M + N_s - 1$ particles of two kinds: *phonons* and *delimiters*. In order to obtain all possible combinations for occupation numbers we only have to form all possible *distributions* of *delimiters* within our "pot." We know from before that this number is given by the binomial coefficient

$$\binom{N_s + M - 1}{N_s - 1} = \binom{N_s + M - 1}{M}.$$

By applying this knowledge to Eq. (A.1) we get the dimension of the total Hilbert space by:

$$\mathrm{DIM}\,(\mathcal{H}_{ph}) = \binom{N_s + N_{ph} - 1}{N_s - 1} + \binom{N_s + N_{ph} - 2}{N_s - 1} + \ldots + \binom{N_s + N_{ph} - N_{ph} - 1}{N_s - 1}. \tag{A.2}$$

We now use the identity for binomial coefficients

$$\binom{n}{k} = \binom{n-1}{k-1} + \binom{n-1}{k} \qquad \text{together with} \qquad \binom{n}{n} = 1 = \binom{n-1}{n-1}$$

and collect terms in Eq. (A.2) from right to left by

$$\begin{aligned}\mathrm{DIM}\left(\mathcal{H}_{\mathrm{ph}}\right) = &\binom{N_\mathrm{s}+N_\mathrm{ph}-1}{N_\mathrm{s}-1} + \binom{N_\mathrm{s}+N_\mathrm{ph}-2}{N_\mathrm{s}-1} + \dots \\ &\dots + \underbrace{\binom{N_\mathrm{s}+N_\mathrm{ph}-N_\mathrm{ph}+1}{N_\mathrm{s}-1} + \underbrace{\binom{N_\mathrm{s}+N_\mathrm{ph}-N_\mathrm{ph}-1}{N_\mathrm{s}-1} + \binom{N_\mathrm{s}}{N_\mathrm{s}}}_{\binom{N_\mathrm{s}+1}{N_\mathrm{s}}}}_{\binom{N_\mathrm{s}+2}{N_\mathrm{s}}}.\end{aligned}$$

Since in Eq. (A.2) we have $N_\mathrm{ph}+1$ terms we finally get

$$\mathrm{DIM}\left(\mathcal{H}_{\mathrm{ph}}\right) = \binom{N_\mathrm{s}+N_\mathrm{ph}}{N_\mathrm{s}}$$

describing the total Hilbert space size.

A.2 Algorithm for Creating Phonon Basis States

As described in Sec. 3.2.2 we build a matrix where the rows describe basis states according to second quantization formalism. A maximum number N_ph of phonons is given so that the system can have an arbitrary amount of phonons from zero up to N_ph.

In the following we choose an example with $N_\mathrm{ph} = 2$ for four cluster sites ($N_\mathrm{s} = 4$). The matrix ST containing all basis states has the following form:

$$ST = \begin{pmatrix} 0 & 0 & 0 & 0 \\ 1 & 0 & 0 & 0 \\ 2 & 0 & 0 & 0 \\ 0 & 1 & 0 & 0 \\ 1 & 1 & 0 & 0 \\ 0 & 2 & 0 & 0 \\ 0 & 0 & 1 & 0 \\ 1 & 0 & 1 & 0 \\ 0 & 1 & 1 & 0 \\ 0 & 0 & 2 & 0 \\ \vdots & \vdots & \vdots & \vdots \\ 0 & 0 & 0 & 2 \end{pmatrix}.$$

With this trivial example the principle of the algorithm is already well illustrated: Beginning with the first phonon site (left-most position) the program incrementally increases its occupation number until the maximum phonon number N_{ph} is reached. After that the occupation number of the next phonon site is increased and *all* calculation steps that have been conducted until now are repeated. After every step the program makes sure that the sum of the phonons occupation numbers from all sites is less or equal to N_{ph}. With this method all basis states have an unique order: if an annihilation operator is applied on one of the sites, the new state is located *above* the current state; in the case of a creation operator the new state's position is *below*.

The program is very efficient and creates millions of basis states in just a few seconds on a single PC. The code is listed below in Listing A.1.

Listing A.1. FORTRAN 90/95 recursive subroutine for creating phononic basis states. The input (IN) and output (OUT) parameters are listed below:

ns ..... number of cluster sites (IN)
ns1 ..... number of cluster sites, needed as recursion variable (IN)
nph1 ..... number of phonons (IN)
arr ..... temporary basis state, internal variable (IN/OUT)
ST ..... matrix containing basis states (OUT)
NST ..... number of basis states (OUT).

```
recursive subroutine bosons (ns, ns1, nph1, arr, ST, NST)

implicit none
integer, intent(in)                                  :: ns, ns1, nph1
integer, intent(inout), dimension(0:6000000,0:ns)    :: ST
integer, intent(inout)                               :: NST
integer, dimension(0:ns)                             :: arr

IF (ns1 .EQ. 0) THEN
   DO WHILE (SUM(arr) .LE. nph1)
      ST(NST,:) = arr
      arr(ns1)=arr(ns1)+1
      NST=NST+1
   END DO
   arr(0) = 0
ELSE
   DO WHILE (arr(ns1) .LE. nph1)
      CALL bosons(ns, ns1-1,nph1,arr, ST, NST)
      arr(ns1)=arr(ns1)+1
      arr(0:(ns1-1)) = 0
   END DO
END IF

end subroutine bosons
```

A.3 Algorithm for Loading Binary Files

When exporting an array (e. g. matrix or vector) into a binary file with FORTRAN 90/95 it is saved into a "data block" whereas during this process two "length fields" are added, one at the beginning and one at the end (as depicted in Fig. A.1). The length fields are integer numbers that contain the size of the array (i. e. the amount of bits). In our programs, when exporting an arbitrary array, we save three values: number of rows (*integer*), number of columns (*integer*) and the particular array (e. g. *double*). In this way we can export any kind of array automatically and load the array with corresponding dimensions in MATLAB (otherwise MATLAB doesn't know the array's dimensions). Therefore the MATLAB routine first loads three integers and then builds the array from the binary file. Since we mostly save many arrays into one file, the file contains many data blocks and the same procedure is repeated in MATLAB many times. In Listing A.2 the code for the MATLAB routine is listed.

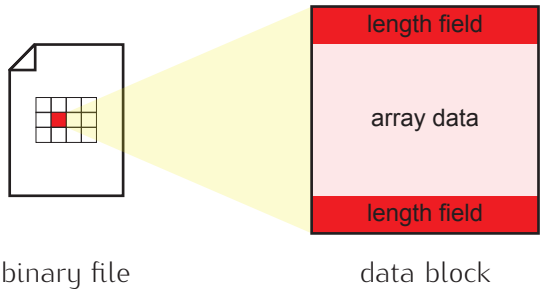

Figure A.1. Illustration of a FORTRAN 90/95 binary file. All arrays are saved in data blocks whose "length fields" contain the length (integer number) of the array elements.

Listing A.2. MATLAB routine for loading binary files created with FORTRAN 90/95 .

```
% program for loading fortran data files and plotting
% date: 05.03.2010
% author: goran lovric
% ------------------------------------------------------------------------

% ------------------------------------------------------------------------
% names AND types for loaded arrays
% ------------------------------------------------------------------------
names = {'A' 'B' 'C' 'D' 'E' 'F'};
types = {'double' 'double' 'double' 'double' 'double' 'float' 'float'};
n_a = 5;                                        % number of loaded arrays

% ------------------------------------------------------------------------
% open and load from fortran data file
% ------------------------------------------------------------------------
fid = fopen ('fort.10', 'r' );                  % open data file
for kk = 1:n_a
    mn = fread ( fid, [ 1, 3 ], 'int' );
    ii = mn(2);
```

```
    jj = mn(3);
    x_tmp = fread ( fid, [ii, jj], types{kk} );
    eval ( [ names{kk} ' = x_tmp' ] );
    lf = fread ( fid, [ 1, 1 ], 'int' );
    if lf ~= mn(1)                                  % error check
        error(['invalid record structure at data point: ', num2str(kk)]);
    end
end
st = fclose( fid );

% ------------------------------------------------------------------------
% plotting part
% ------------------------------------------------------------------------

[...]
```

A.4 Exact Numerical Results

The numerical results of a simplified 1D CuO chain are given. The system consists of four atoms (2×Cu and 2×O) with a periodic boundary condition and is filled with one electron. The numerical results, obtained by semi-analytical calculations, are presented below: the results for the "buckling Hamiltonian" [Eq. (2.32)] are listed in Tab. A.1 for one and two phonons, whereas the results for the breathing Hamiltonian [Eq. (2.33)] are listed in Tab. A.2.

Table A.1. Ground-state energies of a four-site cluster in dependency on various parameters for one and two *buckling* phonons coupled to one electron:
ω_a ..... phonon frequency
g_a ..... coupling constant
ε ..... $\varepsilon := \varepsilon_p - \varepsilon_d$
E_0 ..... ground-state energy .

phonons	ω_a	g_a	ε	E_0
1	0.2	0.4	3.0	−1.3730
	0.2	0.2	3.0	−1.1498
	0.2	0.4	2.0	−1.3673
	0.4	0.4	3.0	−1.1044
	0.5	0.4	1.5	−1.6076
2	0.2	0.4	3.0	−1.6020
	0.2	0.2	3.0	−1.2169
	0.2	0.4	2.0	−1.7767
	0.4	0.4	3.0	−1.4448
	0.5	0.4	1.5	−1.6891

Table A.2. Ground-state energies of a four-site cluster in dependency on various parameters for one and two *breathing* phonons coupled to one electron:
ω_b ..... phonon frequency
g_{dp} ..... coupling constant
ε ..... $\varepsilon := \varepsilon_p - \varepsilon_d$
E_0 ..... ground-state energy .

phonons	ω_b	g_{dp}	ε	E_0
1	0.2	0.4	3.0	−1.0532
	0.2	0.2	3.0	−1.0133
	0.2	0.2	2.0	−1.2514
	0.4	0.2	3.0	−1.0114
	0.5	0.4	1.5	−1.4409
2	0.2	0.4	3.0	−1.0802
	0.2	0.2	3.0	−1.0148
	0.2	0.4	2.0	−1.3300
	0.4	0.4	3.0	−1.0579
	0.5	0.4	1.5	−1.4531

A.5 Project's Timetable

For personal reasons the author documented all working steps (day by day) which are summarized in the following. For eventual future projects this time table may be helpful since it can serve as a "time management reference" in order to know *what* amount of work can be done in *what* period of time.

January

theory reading (many-body quantum mechanics, numerical methods, Green's functions, linear response theory, etc.)	▶ 1 week
learning FORTRAN 90/95	▶ 1 week
studying FORTRAN 90/95 code for Lanczos method	▶ 1-2 weeks

February

holidays (visit to Zhengzhou)	▶ 4 days
studying FORTRAN 90/95 code for Lanczos method, theory (ED)	▶ 2 weeks
LaTeX layout for master thesis, all package configurations	▶ 1-2 weeks
theory writing (*Lanczos Method*)	▶ 3 days
studying theory about Hubbard model, methods (papers, books)	▶ 3 days

March

analytical calculations (correlation functions etc.)	▶ 2-4 days
MATLAB routine for opening binary files	▶ 1-2 days
calculation of 1D problems from Chapter 4	▶ 2-4 days
concept for master thesis	▶ 1 day
beginning calculations for 3D clusters in Chapter 5	▶ 3 days
holidays (visit to Maoping, Xian, Beijing, Tianjin, Shanghai)	▶ 16 days

April

theory writing (*Introduction to Many-Body Physics*)	▶ 1-2 days
reproducing results for individual carbon clusters (Chapter 5)	▶ 2-3 days
calculations with extended Hubbard model, failure corrections, figures	▶ 2 weeks
theory reading and writing	▶ 1 week

May

studying all papers about electron-phonon coupling etc.	▶ 3-5 days
phonon implementation and optimization	▶ 1-2 weeks
reproducing paper results (*Exact Numerical Solutions*)	▶ 1 week
writing theory (various chapters)	▶ 1 week
studying AIP style manual for figures, tables, etc. and LaTeX coding	▶ 1-2 days

June

buckling phonons implementation, figures	▶ 1 week
breathing phonons implementation, figures	▶ 1 week
theory writing (most parts finished)	▶ 1-2 weeks
holidays	▶ 5 days

July, September, October

final corrections, discussion etc.	▶ 5 weeks
proofreading (by Dr. Renate Belaj) and correction	▶ 1 week

Bibliography

[1] L. A. Openov and V. F. Elesin, Soviet Journal of Experimental and Theoretical Physics Letters **68**, 726 (1998), arXiv:physics/9811023.

[2] F. Lopez-Urias, E. Cruz-Silva, E. Munoz-Sandoval, M. Terrones, and H. Terrones, Journal of Materials Chemistry **18**, 1535 (2008).

[3] P. Piekarz, J. Konior, and J. H. Jefferson, Phys. Rev. B **59**, 14697 (1999).

[4] P. Piekarz and T. Egami, Phys. Rev. B **72**, 054530 (2005).

[5] O. Gunnarsson and O. Rösch, Journal of Physics: Condensed Matter **20**, 043201 (2008).

[6] W. Nolting, *Grundkurs Theoretische Physik 7: Viel-Teilchen-Theorie (Springer-Lehrbuch) (German Edition)*, 7., aktualisierte ed. (Springer, 2009).

[7] H. Bruus and K. Flensberg, *Many-Body Quantum Theory in Condensed Matter Physics: An Introduction (Oxford Graduate Texts)*, illustrated ed. (Oxford University Press, USA, 2004).

[8] G. Czycholl, *Theoretische Festkörperphysik: Von den klassischen Modellen zu modernen Forschungsthemen (Springer-Lehrbuch) (German Edition)*, 3., aktualisierte ed. (Springer, 2007).

[9] C. Cohen-Tannoudji, B. Diu, and F. Laloe, *Quantenmechanik (German Edition)*, 4 revised ed. (SLR, 2009).

[10] F. Schwabl, *Quantenmechanik für Fortgeschrittene (QM II) (Springer-Lehrbuch) (German Edition)*, 5., erw. u. aktualisierte ed. (Springer, 2008).

[11] V. Fock, Zeitschrift für Physik A Hadrons and Nuclei **75**, 622 (1932).

[12] G. F. Giuliani and G. Vignale, *Quantum Theory Of The Electron Liquid* (Cambridge University Press, 2006).

[13] C. Weissmantel and C. Hamann, *Grundlagen der Festkörperphysik (German Edition)*, 1 ed. (Springer, 1979).

[14] J. Hubbard, Proceedings of the Royal Society of London. Series A, Mathematical and Physical Sciences **276**, 238 (1963).

[15] P. G. J. van Dongen, Phys. Rev. B **49**, 7904 (1994).

[16] G. Beni and P. Pincus, Phys. Rev. B **9**, 2963 (1974).

[17] T. Sakamoto, M. Wakeshima, Y. Hinatsu, and K. Matsuhira, Phys. Rev. B **75**, 060503 (2007).

[18] N. Tomita, Phys. Rev. B **73**, 115105 (2006).

[19] T. Paiva and R. R. dos Santos, Phys. Rev. B **65**, 153101 (2002).

[20] D. Reiter, M. Glanemann, V. M. Axt, and T. Kuhn, Phys. Rev. B **75**, 205327 (2007).

[21] M. Saubanère and G. M. Pastor, Phys. Rev. B **79**, 235101 (2009).

[22] S. R. White *et al.*, Phys. Rev. B **40**, 506 (1989).

[23] F. Marsiglio, Phys. Rev. B **55**, 575 (1997).

[24] W. M. C. Foulkes, L. Mitas, R. J. Needs, and G. Rajagopal, Rev. Mod. Phys. **73**, 33 (2001).

[25] W. von der Linden, Physics Reports **220**, 53 (1992).

[26] T. Maier, M. Jarrell, T. Pruschke, and M. H. Hettler, Rev. Mod. Phys. **77**, 1027 (2005).

[27] D. Sénéchal, ArXiv e-prints (2008), 0806.2690.

[28] W. von der Linden and A. Prüll, Wahrscheinlichkeitstheorie, Statistik und Datenanalyse, 2002.

[29] G. Wellein, H. Röder, and H. Fehske, Phys. Rev. B **53**, 9666 (1996).

[30] C. Lanczos, Journal of Research of the National Bureau of Standards **45**, 255 (1950).

[31] L. Komzsik, *The Lanczos Method: Evolution and Application (Software, Environments and Tools)* (Society for Industrial Mathematics, 1987).

[32] M. Hanke-Bourgeois, *Grundlagen der Numerischen Mathematik und des Wissenschaftlichen Rechnens* (Vieweg+Teubner Verlag, 2008).

[33] G. H. Golub and C. F. V. Loan, *Matrix Computations (Johns Hopkins Studies in Mathematical Sciences)(3rd Edition)*, 3rd ed. (The Johns Hopkins University Press, 1996).

[34] D. Calvetti, L. Reichel, and D. C. Sorensen, ETNA **2**, 1 (1994).

[35] A. Ruhe and T. Wiberg, BIT Numerical Mathematics **12**, 543 (1972).

[36] A. S. Alexandrov, V. V. Kabanov, and D. K. Ray, Phys. Rev. B **49**, 9915 (1994).

[37] W. von der Linden, Lecture Notes on Numerical Treatment of Many-Body Problems, Technische Universität Graz, 2009.

[38] A. Mielke, Starke Korrelationen und Magnetismus, Universität Heidelberg, 2006.

[39] H. Kolinsky, Programmieren in Fortran 90/95, Universität Bayreuth, 2007.

[40] G. Opfer, FORTRAN und MATLAB, Universität Hamburg, 2002.

[41] E. Elbrächter, Einführung in Matlab, Technische Universität Kaiserslautern, 2004.

[42] T. Nishino, *Electron Correlation Effects in Low Dimensional Periodic Systems*, PhD thesis, Osaka University, 1992 (uncertain).

[43] M. Hohenadler, *Numerical investigations of strongly correlated electron-phonon models*, PhD thesis, Technische Universität Graz, 2004.

[44] AIP Publication Board, AIP STYLE MANUAL Fourth Edition, American Institute of Physics, 1990.

Deutsche Fassung:
Beschluss der Curricula-Kommission für Bachelor-, Master- und Diplomstudien vom 10.11.2008
Genehmigung des Senates am 1.12.2008

EIDESSTATTLICHE ERKLÄRUNG

Ich erkläre an Eides statt, dass ich die vorliegende Arbeit selbstständig verfasst, andere als die angegebenen Quellen/Hilfsmittel nicht benutzt, und die den benutzten Quellen wörtlich und inhaltlich entnommene Stellen als solche kenntlich gemacht habe.

Graz, am ……. ……..
(Unterschrift)

Englische Fassung:

STATUTORY DECLARATION

I declare that I have authored this thesis independently, that I have not used other than the declared sources / resources, and that I have explicitly marked all material which has been quoted either literally or by content from the used sources.

……. ……..
date (signature)